

no glory  
no glory

# Hot-Air Balloon Wind Sensing

Evert Izaac Franciscus de Bruijn



## Propositions

1. Hot-air balloon-derived wind observations are a valuable asset for our understanding of atmospheric boundary layer wind regimes.  
(this thesis)
2. Hot-air balloon observations have a positive impact on data assimilation for local weather prediction.  
(this thesis)
3. Higher investments in taxonomy are urgently needed for better describing and understanding biodiversity.
4. The increase in lift that a sailing boat experiences in a wind gust is explained more effectively by the law of momentum conservation than the law of Bernoulli.
5. Open offices are a nuisance and frustrate the production and well-being of employees.
6. Churches do not prioritize environmental issues as much as they should.
7. The difference in status between Schubert's 8th symphony and this PhD dissertation boils down to "un".

Propositions belonging to the PhD thesis, entitled

Hot-air Balloon Wind Sensing

Evert Izaak Franciscus de Bruijn

Wageningen, 25 April 2023

# Hot-Air Balloon Wind Sensing

Evert Izaak Franciscus de Bruijn

## **Thesis committee**

### **Promotor**

Prof. Dr A.A.M. Holtslag  
Professor of Meteorology  
Wageningen University & Research

### **Co-promotors**

Dr F.C. Bosveld  
Senior research scientist  
KNMI De Bilt

Dr S. de Haan  
Senior research scientist  
KNMI De Bilt

### **Other members:**

Prof. Dr B.J.H. van de Wiel, Delft University of Technology  
Prof. Dr A.K. Bregt, Wageningen University & Research  
Prof. Dr M.W. Rotach, University of Innsbruck, Austria  
Dr A.B.C. Tijm, KNMI, De Bilt

This research was conducted under the auspices of WIMEK

# Hot-Air Balloon Wind Sensing

Evert Izaak Franciscus de Bruijn

## **Thesis**

submitted in fulfilment of the requirements for the degree of doctor  
at Wageningen University

by the authority of the Rector Magnificus

Prof. Dr A.P.J. Mol,

in the presence of the

Thesis Committee appointed by the Academic Board

to be defended in public

on Tuesday 25 April 2023

at 4 p.m. in the Omnia Auditorium.

Evert Izaak Franciscus de Bruijn  
Hot-Air Balloon Wind Sensing  
120 and xi pages.

PhD thesis, Wageningen University, Wageningen, the Netherlands (2023)  
With references, with summary in English

ISBN 978-94-6447-625-5  
DOI <https://doi.org/10.18174/589639>

*No guts, no glory*  
*Wie niet waagt, wie niet wint*

*For my parents*

# Preface (Voorwoord)

Er zijn twee gebeurtenissen die mij ertoe gebracht hebben om dit onderzoek te gaan doen namelijk een ballonvaart die ik cadeau kreeg voor mijn vijftigste verjaardag en een project van de Volkskrant genaamd Ware Wetenschap, waarin wetenschappers gevolgd werden tijdens hun onderzoek. De ballonvaart was een avontuur, die ik samen met mijn familie heb beleefd. Tijdens de vaart zag ik hele interessante windverschijnselen, die horen bij een stabiele grenslaag. Het idee om heteluchtballon vaarten te gebruiken als wind informatie ontstond in de wandelgangen van het KNMI. Ik sprak met Siebren de Haan over mijn ervaringen en hij stimuleerde mij om een voorstel te schrijven voor het project Ware Wetenschap van de Volkskrant. Het was de bedoeling dat een journalist in de keuken van het onderzoek zou mee lopen om te zien hoe er gewerkt wordt en waar het fout kan gaan en wat mogelijke valkuilen kunnen zijn. Een wetenschapper behoort integer te zijn, maar door de toegenomen publicatie druk, komt de integriteit in de verdrinking en soms worden de data mooier gemaakt dan ze zijn. Mijn voorstel kwam op de shortlist, maar werd uiteindelijk afgeblazen. Het onderzoek heeft echter wel doorgang kunnen vinden en de weerslag is dit proefschrift geworden.

Tijdens een ballonvlucht met mijn familie ervoer ik dat, hoewel de ballon bewoog, ik helemaal geen wind voelde. Natuurlijk, ook als zeiler wist ik al dat je voor de wind weinig van de wind merkt. Een ballon wordt met de wind meegevoerd en drijft in een stromend medium. Later op het KNMI realiseerde ik mij dat een luchtballon indien uitgerust met GPS in feite een windmeting doet. Immers de gemiddelde snelheid kan worden bepaald door de afstand tussen twee opeenvolgende posities te delen door het tijdsverloop.

In dit proefschrift laat ik zien dat de verplaatsing van een heteluchtballon een bruikbare windsnelheid oplevert die toepasbaar is als waarneming op zich en die bovendien toegepast kan worden in een weermodel. Standard smartphones (met de juiste app) kunnen gebruikt worden om de data in te zamelen. De wind data

zijn afkomstig uit de onderste kilometer van de atmosfeer en zijn meteorologisch gezien interessant omdat ze vaak de stabiliteits overgangen (stabiel  $< - >$  onstabiel) bevatten. Weermodellen hebben hier moeite mee. De waarnemingen geven meer inzicht in de processen en deze kennis kan gebruikt worden om het model te verbeteren.

# Summary

High resolution upper air wind observations are sparse and additional observations are a welcome source of meteorological information. In this thesis, it is shown that Hot-air Balloon (HAB) tracks can be processed into useful wind data.

In **Chapter one**, upper air wind measurements and HABs are introduced and viewed from a historic perspective. Some meteorological features which affect Hot-air Ballooning are discussed and at the end of this chapter, research questions are posed.

In **Chapter two**, we explore the potential of utilizing balloon flights for upper air wind measurements and investigate the meteorological content of this information. The displacement of a HAB is a measure for the wind speed and direction and thus, is a potential source for wind observations in the lower part of the troposphere. The balloon's response time to changing wind is fast in the beginning and levels off for smaller relative wind speeds. Four case studies are presented and we compare the balloon-derived winds with other wind observations and with the HARMONIE-AROME model. It turns out that hot-air balloon tracks can indeed produce useful wind observations just above and in the Atmospheric Boundary Layer (ABL).

In **Chapter three**, a field experiment with a HAB was conducted in the vicinity of the meteorological observatory of Cabauw in the Netherlands. An application (app) for smartphones has been developed to collect location data. We report about a feasibility study of a HAB experiment where we investigated the accuracy of the smartphone's Global Navigation Satellite System (GNSS)-receiver using an accurate geodetic GNSS-receiver as a reference. Further, we study the dynamic response of the HAB to variations in the wind by measuring the relative wind with a sonic anemometer which is mounted below the gondola. The GNSS comparison reveals that smartphones equipped with a GNSS-chip, have an absolute position error standard deviation of 5 *m* in the horizontal plane, but their relative position

error standard deviation is smaller. Therefore, the horizontal speeds, which are based on relative positions and a time step of 1 s, have standard deviations of  $\sigma_u = 0.8 \text{ ms}^{-1}$ ,  $\sigma_v = 0.6 \text{ ms}^{-1}$ . The standard deviation in altitude is 12 m. We have validated the hot-air balloon-derived wind data with observations from the Cabauw tower and the results are encouraging. We have studied the dynamics of a hot-air balloon. An empirical value of the response length has been found which accounts for the balloon's inertia after a wind change, and which compared favorably with the theoretically derived value. We have found a small, but systematic movement of the HAB relative to the surrounding air. The model for the balloon dynamics has been refined to account for this so-called inertial drift.

In **Chapter four**, we compare the HAB winds with wind measurements from a meteorological tower and a radio acoustic wind profiler, both situated at the topographically flat Cabauw observatory in the Netherlands. To explore the potential of this type of wind observation in other topographies, we present an intriguing HAB flight in Austria with a spectacular mountain-valley circulation. Subsequently, we compare the HAB data with the HIRLAM model during 2011-2013 and the standard deviation of the wind speed is  $2.3 \text{ ms}^{-1}$ . Finally, we show results from a data-assimilation feasibility experiment that reveals that HAB wind information can have a positive impact on a hindcasted NWP trajectory.

In **Chapter five**, a quality assessment is carried out by comparing HAB winds against wind observations at the meteorological tower of Cabauw in the Netherlands over a long time period (May-September 2018). We have found error standard deviations of  $\sigma_u = 0.65 \text{ ms}^{-1}$  and  $\sigma_v = 0.69 \text{ ms}^{-1}$  for the measured zonal and meridional wind components respectively. Subsequent comparison against short-term model forecasts of the HARMONIE-AROME model reveals a standard deviation of  $2.5 \text{ ms}^{-1}$  for the wind vector difference. From the HAB observation set, a case is selected with a rapidly changing wind field belonging to a small intensifying depression. The HAB wind observation is applied in data assimilation using a single observation experiment and it is shown that in a complex baroclinic situation, the model state can be improved.

In **Chapter six**, we collect findings, draw conclusions and answer the research questions and we envision how this research can be continued in the future.

# Contents

	Page
Preface	vii
Summary	ix
Contents	xi
Chapter 1 Introduction	1
Chapter 2 Observing Boundary Layer Winds from Hot-air Balloon Flights	19
Chapter 3 Measuring Low Altitude Winds with a Hot-air Balloon and their validation with Cabauw Tower observations	39
Chapter 4 Opportunistic Sensing with Recreational Hot-air Balloon Flights	67
Chapter 5 Wind observations from Hot-air Balloons and their application in NWP models	77
Chapter 6 Synthesis	99
References	105
About the author	113
Acknowledgments	119



# Chapter 1

## Introduction

## 1.1 Introduction

This thesis is about wind measurements based on the displacement of Hot-air Balloons (HAB). Hot-air ballooning is a leisure activity which takes place in the atmospheric boundary layer below altitudes of 2000 *m*. We explain in this thesis that HAB flights can be processed to valuable wind observations. Upper air wind observations in the Atmospheric Boundary Layer (ABL) are sparse and additional in-situ observations are a welcome source of meteorological information. These observations are useful for application in Numerical Weather Prediction (NWP) models, because with decreasing model grid distances more detailed observations in space and time are necessary.

Most HAB launches are made during the cooler hours of the day in the early morning and late afternoon. At these times of day, the winds are typically light and stationery, making it easier for launch and landing of the balloon. Flying at these times also avoids thermals, which are vertical air currents caused by ground heating, cold air advection or falling raindrops that make it more difficult to control the balloon. In extreme conditions, the up- and downdrafts associated with these processes can exceed the ability of a balloon to climb and can thus force a balloon onto the ground (FAA, 2008). Weather predictions are important for ballooning and we will show that these predictions can be improved, benefiting pilots, if they provide their flight data to meteorological weather centres. In this thesis, we will elaborate on how the data can be collected.

## 1.2 Historic background on the wind and its sensing

In the ancient past, the Greeks were quite interested in wind. In Athens the Tower of Winds, also named Aerides, was built near a marketplace and it showed the wind direction by a wind vane in the shape of Triton. On the frieze, just below the roof, wind gods were depicted which corresponded to the wind directions. The vane pointed to Boreas in case of northerly winds, to Eurus in case of easterly winds, Notus to southerly winds and Zephyrus to westerly winds. By knowing the wind direction a basic weather forecast could be made, depending from which quadrant the wind came from. Northerly wind would give chilly weather, easterly and southerly winds would bring heat, and westerly wind would give unstable weather, with a higher probability of rain. In the tower there was also a timepiece, but the wind force was not measured.



**Figure 1.1:** The tower of the winds at the Roman Agora (market) in Athens, source: Wikipedia

Centuries after the Greeks, a British admiral, Francis Beaufort, invented a practical scale for wind speed measurements. The scale consisted of thirteen classes (zero to twelve) that did not reference wind speed numbers but related qualitative wind conditions to effects on the sails of a frigate, at that time the main ship of the British Royal Navy, from "just sufficient to give steerage" to "that which no canvas sails could withstand". The Beaufort scale was easy to use and could be applied by any navigation officer. Beaufort was a contemporary of Charles Darwin and during the expedition with the HMS Beagle to the Galapagos Islands wind speed observations were recorded applying the Beaufort scale. The scale was made a standard for ship's log entries on Royal Navy vessels in the late 1830s and was adapted to non-naval use from the 1850s, with scale numbers corresponding to cup anemometer rotations. In 1853, the Beaufort scale was accepted as generally applicable at the First International Meteorological Conference in Brussels. It should be noted that the Beaufort scale did not address the wind direction.

The wind is a vector and is regarded differently by forecasters and by scientists in fluid dynamics. In meteorology, the wind direction corresponds with bearing over a compass. In fluid dynamics the wind is represented by two components in a Cartesian coordinate system.

Wind barbs are a convenient way to represent both wind direction and speed on maps and diagrams. Wind barbs have three parts: a dot, a staff, and a feather. The staff part of a wind barb shows the wind direction. The dot end of the staff is where the wind is blowing to, while the top of the staff shows the direction from which the wind is coming. The wind direction is reported as a compass degree.

There are 360 degrees on a compass, with north being 0 or 360 degrees and south 180 degrees. The wind speed is indicated by feathers added to the top of the staff. A short feather represents a low wind speed, a long feather equals a higher wind speed. Usually, wind speeds are given in knots or in  $ms^{-1}$ , depending on the application. Very low wind speeds are represented by open circles.

The World Meteorological Organization (WMO) has established a network of meteorological measurement instruments all over the world. Weather parameters can be easily interchanged and the measurements should comply with standards. Nowadays many instruments are available for wind sensing and can be ground based, airborne or space based.

A typical surface observation comes from wind masts and ground based wind profilers. They sense the ABL at one location, but the measurements are continuous in time. Wind lidars provide also wind information and they are easy to deploy, while wind mast observations require more effort.

Weather balloons are airborne observations and measure the troposphere and lower stratosphere. The wind measurement principle is based on Global Navigation Satellite System (GNSS) locations. Two locations and the elapsed time deliver the wind components. For the vertical coordinate also the pressure is used to calculate the altitude. Weather balloons measure not only vertical profiles of the wind components, but also of temperature and humidity. Nowadays effort is put into collecting and applying the descent phase of the radiosonde in NWP models and the results are promising (Ingleby & Edwards, 2018). In the troposphere and lower stratosphere, air traffic (AMDAR) provides a huge amount of wind data (Petersen, 2016). The data have a good time resolution, but they are concentrated in flight corridors; only profiles in the vicinity of airports can be obtained. At the top of the atmosphere, satellites (a typical space-born device) obtain important observations, e.g. Atmospheric Motion Vectors to measure the wind (Lean et al., 2015). Clouds are detected by measuring their radiative properties. They can be identified and tracked and a wind vector can be subsequently derived. A drawback of this method is that clouds are not always present and their occurrence varies with height, but in general a cloudless sky will seldom occur.

Additional wind measurements are provided from the Aeolus satellite (Rennie et al., 2021). This satellite is in a polar orbit and provides transects of wind information along a swath. The measurement principle is based on measuring the Doppler shifted laser frequency from Rayleigh and Mie scattering by atmospheric particulates and molecules which move with the ambient wind. The Aeolus laser beam can not penetrate optically thick cloud layers which reduces data coverage near

the surface. To overcome this problem, metedrones (Sziroczak et al., 2022) can be applied. They fly from the surface layer to the free atmosphere up to altitudes beyond 6 km and in virtually all weather situations. Apart from profiles of wind components they measure also profiles of temperature and humidity, just like a weather balloon.

Third party observations are data collected by other organizations using meteorological sensors. Examples are wind observations from ground based wind turbines (Sun et al., 2022) and data from Air Traffic Control (ATC). A surveillance radar interrogates aircraft and in case of Enhanced Surveillance (EHS) position, identity, airspeed, Mach number are exchanged (De Haan, 2011), in case of Meteorological Routine Airport Report (MRAR) wind speed and temperature are directly transferred (Strajnar et al., 2015). MRAR is applied for small business planes in less busy airports. EHS is used in busy airports with many airplanes. Additional third party observations can be derived from the airborne gliders.

Personal weather stations provide wind information from amateurs (Garcia-Marti et al., 2022), but the representativity and quality control are topics that need to be addressed. The data are available on the Weather Observations Website (WOW) platform (<https://wow.knmi.nl>) and wind surface maps give detailed wind information, especially about wind gusts, which is very useful for balloon pilots. Wind gusts can display a large variability in space and time. Extreme wind gusts are typically very small scale and so the measurements taken only at official weather stations leave vast distances unobserved. So, these third party wind data can improve the spatial-temporal resolution of the regular observational network.

## 1.3 History and some interesting facts of Hot-air Balloons

Unmanned HABs are already mentioned in Chinese history. Zhuge Liang in the Three Kingdoms era, Shu Kingdom, used airborne lanterns for military signaling. These lanterns are known as Kongming lanterns. There is also some speculation that HABs were used by the Nazca Indians of Peru some 1500 years ago as a tool for designing vast drawings on the Nazca plain.

The first clearly recorded instances of balloons capable of carrying passengers used hot air to obtain buoyancy and were built by the brothers Josef and Etienne Montgolfier in Annonay, France. This happened during the era of the Enlightenment at the end of the 18th century when there was a revival of interest in nature, physics and experimentation. The Montgolfier brothers were from a family of pa-



**Figure 1.2:** First ascent with a hot-air balloon in 1783 Versailles, source: Wikipedia.

per manufacturers who had noticed the ash rising in fires. After experimenting with unmanned balloons and flights with animals, the first balloon flight with humans on board took place on 19 October 1783 with the physician Pilâtre de Rozier, the manufacture manager, Jean-Baptiste Réveillon and Giroud de Villette, at the Folie Titon in nowadays Paris.

Officially, the first flight was one month later, 21 November 1783. King Louis XVI had originally decreed that condemned criminals would be the first pilots, but a young physicist named Pilâtre de Rozier and the Marquis Francois d'Arlandes successfully petitioned for the honor. The first hot air balloons were basically cloth bags (sometimes lined with paper) with a smoky fire built on a grill attached to the bottom. They had a tendency to catch fire and be destroyed upon landing.

Ventotene is one of the Pontine Islands in the Tyrrhenian Sea, 46 kilometres off the coast of Gaeta right at the border between Lazio and Campania, Italy. On 19 September Ventotene celebrates the saint's day of Santa Candida, the patron saint of the island. There is a procession with a statue of Santa Candida crossing the island and there is a festivity with paper HABs. There is a traditional, colorful and extremely popular competition of paper HABs with various schools of the island that compete with their own creations of different shapes, decorations and sizes.

HABs travel with the wind and it is uncertain where they will land. Trajectories



**Figure 1.3:** Ventotene, paper hot-air balloons, 19 September saint's day Santa Candida, source: Agenzia di Viaggi e Turismo di Ventotene.

can be used to calculate the landing place. Trajectory models are based on moving air parcels and a HAB will slightly divert from the meteorological trajectories. A relevant constraint is the amount of fuel they have on board and obviously their weight. When the fuel runs out, landing is imminent. Juridically speaking every landing is an emergency landing and can be made in principle everywhere.

This thesis explores wind sensing using the HABs in which the air is heated up with gas burners. But it is also possible to heat the air inside the envelope with solar energy. If the envelope is black, it can absorb the incoming solar radiation resulting in a positive buoyancy. Solar balloons can reach altitudes of more than 20 *km*. If they are equipped with light weight sensors they can sample the atmosphere for a couple of hours (Bowman et al., 2020). This solar-powered balloon is attractive concept for exploring atmospheres of other planets like Mars (Fathpour et al., 2014) and Venus (Schuler et al., 2022).



**Figure 1.4:** The Aeronauts, Amelia tries to reach the frozen valve on top of the balloon, source: Amazon Prime.

## 1.4 Balloon movies

### 1.4.1 The Aeronauts (2019)

This film is about the history of meteorology and underlines the need of conducting experiments in scientific research. It should be noted that in this film a gas balloon is used, which has its own characteristics. For instance, a burner with fuel is not required, but instead, a lighter-than-air gas and some redundant weight are used to obtain and control the buoyancy of the balloon. In the Victorian Age in London, James Glaisher (meteorologist) posed a theory that the weather could be predicted if you would know the state of the upper air. The Royal Society did not want to fund an expedition, because they were skeptical about his theory.

James had to rely on his family to find the funding for a balloon excursion to explore the upper air. James and his wife Amelia, who were both pilots, left with a gas balloon from a fun fair somewhere in London. With a cheering crowd they started ascending and James commenced to measure pressure, temperature and humidity. At some stage he released pigeons carrying scientific readings in case they did not survive. They discovered an air current which was home to a group of butterflies which confirmed James' theory of convection. Updrafts could transport air from the surface to high altitudes and the insects proved that the air originated from below. They acted as a passive tracer of the air mass.

The gas balloon went higher and higher and it started snowing. Then James became unconscious and Amelia decided to descend immediately. Unfortunately

the valve was frozen and she had to go to top of the balloon to open the valve. They managed to descend, but too much gas had been released and the balloon descended too fast. To reduce the weight all redundant payload was dropped and at last even the gondola was dropped. Eventually, they used the balloon as a parachute and the falling speed was reduced. They managed to land safely, albeit with minor injuries. James' findings eventually paved the road for the first weather forecasts.

#### 1.4.2 Night crossing (1982) and Balloon (2018)

In 1979 two families, with eight members in total, escaped East Germany by crossing the border to West Germany in a homemade HAB and they were inspired by a HAB festival in the USA. The escape took place around 02:00 LT on 16 September 1979. The plan to accomplish this was carried out over a period of one and a half years (including an unsuccessful attempt), the construction of three different balloons, and various modifications until the successful escape occurred. One failed crossing alerted the government, but the police (Stasi) were not able to identify the suspects before their flight to West Germany. The second attempt began in a remote place in Oberlemnitz (Thüringen) close to the border. The launch place was concealed in the middle of the woods and the ABL was stable and a ground inversion developed. The synoptic situation showed a high pressure area over Poland which resulted in a northern flow. During the take-off, there was considerable wind shear. The balloon even caught fire during the ascending phase, but the brave crew managed to extinguish it quickly. They went up to 2500 *m* and were drifted by a northerly wind at a speed of 30 *km/h* to freedom in Bavaria near the city of Naila. The adventurous escape was the basis of two movies namely: Night crossing (1982) and Balloon (2018).

## 1.5 Buoyancy principle of Archimedes

A HAB is floating in the atmosphere and the fact that lower density objects float in a more dense medium is described by the law of Archimedes. Here we give some background on how this law was established. Archimedes was confronted with the following problem: namely checking the constituency of a golden object.

The king of Syracuse on the island of Sicily had a golden crown and wanted to know if the crown was made of pure gold. There was a suspicion that the crown was mixed with silver because of its light color. Archimedes had to prove that the crown consisted of pure gold and was not polluted with another constituent. When he took a bath to think for a moment, he noticed that he was feeling lighter. Then



**Figure 1.5:** 16 September 1979 02:00 LT Escape from East Germany with a hot-air balloon, source: StudioCanal.

he remembered that gold had a higher density than silver and that gold therefore had a smaller volume with the same weight. So, if you have the original weight of gold from the crown in a container with water that is filled to the brim, the water will overflow. At the moment that less water overflows than at the crown with the original weight (given from the craftsman), this will not be the same amount of gold. This would therefore mean that the manufacturer has mixed gold with a metal with a lower density, for example silver.

Archimedes' principle is the statement that the buoyant force on an object is equal to the weight of the fluid displaced by the object. The formula is concise and straightforward:

$$F_b = \rho g V_f \quad (1.1)$$

$$= m_f g \quad (1.2)$$

where  $F_b$  is the buoyant force and  $\rho$ ,  $V_f$ ,  $m_f$  are respectively the density, volume and mass of the displaced fluid or gas,  $g$  is the acceleration of gravity.

## 1.6 Atmospheric Boundary Layer

HAB flights take place in the lower troposphere where the wind is affected by the surface due to friction, heating and cooling. This lower part of the troposphere is called Atmospheric Boundary Layer (ABL) and the wind is governed by:

$$\frac{\partial u}{\partial t} = +f_c(v_a - v_g) - \frac{\partial \overline{u'w'}}{\partial z} \quad (1.3)$$

$$\frac{\partial v}{\partial t} = -f_c(u_a - u_g) - \frac{\partial \overline{v'w'}}{\partial z} \quad (1.4)$$

Here  $f_c$  is Coriolis force,  $u_a, v_a$  zonal and meridional wind in the ABL,  $u_g, v_g$  zonal and meridional geostrophic wind,  $\overline{u'w'}, \overline{v'w'}$  are the stress terms in respectively zonal and meridional direction. Above the ABL, in the so-called free troposphere, the stress terms become zero. At that height, the geostrophic balance holds in stationary conditions. The geostrophic wind is then parallel to the isobars and the pressure gradient force is in balance with the Coriolis force. This geostrophic balance was discovered theoretically by the American meteorologists J.H. Coffin and W. Ferrel. But Buys-Ballot, a Dutch meteorologist and founder of the Royal Netherlands Meteorological Institute (KNMI) was the first to provide an empirical validation of this finding (Buys-Ballot, 1857). He also applied the law in the planning and the safe navigation of ships at sea.

The ABL height depends on the vertical distributions of temperature, humidity and momentum. During daytime, the depth of the ABL can rise to typically 1 km over land in summertime, but can be much larger in dry conditions. At the surface, the momentum is zero and at the top of the ABL the geostrophic wind determines the momentum. The momentum varies with height, resulting in a momentum flux and wind shear. Temperature and humidity are the driving factors behind the buoyancy of the air. Relatively warm and dry air bubbles are lighter than the environment and have the tendency to rise. The ABL can be subdivided in zones, close to the surface the so-called surface layer is found.

Here in neutral conditions, with sufficient wind, the logarithmic wind profile applies:

$$u(z) = \frac{u_*}{\kappa} \ln \left( \frac{z}{z_0} \right) \quad (1.5)$$

where  $u_*$  is friction velocity,  $\kappa = 0.4$  is the Von Kármán constant,  $z$  is the height and  $z_0$  is roughness length. In the surface layer the stress varies very little with height. As a result, there is hardly stress divergence and the wind direction remains almost constant with height.

But if we consider the whole ABL, the wind direction changes with height, which is a well-known principle by balloon pilots. They know that normally the wind veers with height and we will explain this phenomenon in more detail. We recall equations (1.3), (1.4) and use first-order closure with local K-theory to estimate the stress terms (Monin & Obukhov, 1954). Hence  $\overline{u'w'} = -K_m \frac{\partial u}{\partial z}$  and  $\overline{v'w'} = -K_m \frac{\partial v}{\partial z}$ .

$$f_c(u - u_g) = K_m \frac{\partial^2 v}{\partial z^2} \quad (1.6)$$

$$f_c(v - v_g) = -K_m \frac{\partial^2 u}{\partial z^2} \quad (1.7)$$

The boundary conditions are very important in solving these equations. We choose at  $z = 0, u = 0, v = 0$  and at  $z = \infty, u = u_g, v = 0$  and also a new coordinate system is defined, where the x-axis is lined up with the geostrophic wind (Stull, 1988). This gives the following solution:

$$u(z) = \vec{G}[(1 - e^{-\gamma z} \cos(\gamma z))] \quad \text{and} \quad (1.8)$$

$$v(z) = \vec{G}[e^{-\gamma z} \sin(\gamma z)], \quad (1.9)$$

where  $\vec{G}$  is the geostrophic wind vector defined as  $|\vec{G}| = \sqrt{u_G^2 + v_G^2}$  and  $\gamma = \sqrt{\frac{f_c}{2K_m}}$  which can be recognized as an Ekman spiral. In reality, it is difficult to establish a full Ekman spiral, because stationarity is a hard constraint and  $K_m$ , the turbulent diffusion coefficient, is not constant in the ABL. But there are more mechanisms which are responsible for the wind vector turning with height.

### 1.6.1 Baroclinic effects

Baroclinicity is a synoptic scale effect and can result in wind turning with height. Sometimes this effect is so strong that it can overrule the ABL regime. The term baroclinic is derived from the Greek *baro* relating to pressure, and *klines*, meaning inclining or intersection. In a baroclinic atmosphere, surfaces of constant pressure intersect surfaces of constant temperature (or density) so that, in general  $\nabla T \neq 0$  on constant pressure surfaces. An equivalent barotropic atmosphere may be regarded as a special kind of baroclinic atmosphere in which  $\nabla T$  and  $\nabla \phi$  on pressure surfaces are linearly related. If we consider the wind as function of height, then cold air advection leads to a backing wind, while warm air advection results a veering wind with height. Note that veering is clockwise turning, and backing is

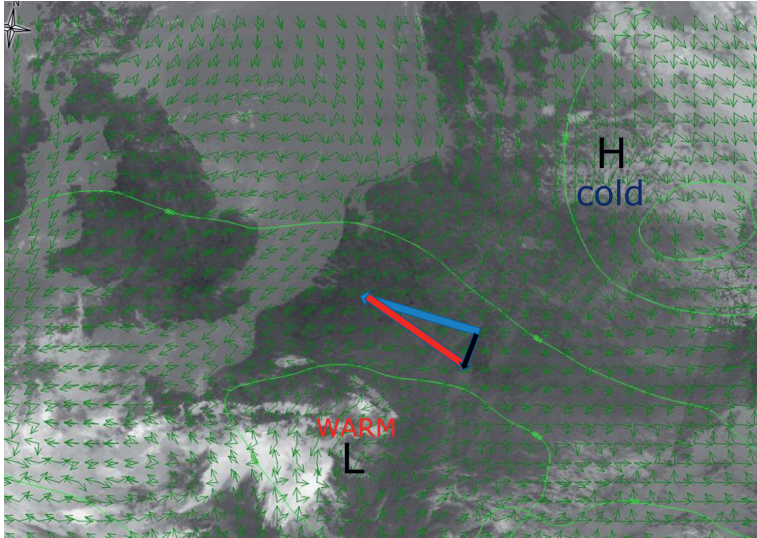


**Figure 1.6:** 02 July 2018 12:00 UTC, geostrophic wind 1000  $hPa$  (blue) 850 (red), thermal wind (black), pressure and temperature gradient are not lined-up.

anti-clockwise turning.

$$U_T = -\frac{R}{f} \left( \frac{d\bar{T}}{dp} \right) \ln \left( \frac{p_0}{p_1} \right) \quad (1.10)$$

$$V_T = +\frac{R}{f} \left( \frac{d\bar{T}}{dp} \right) \ln \left( \frac{p_0}{p_1} \right) \quad (1.11)$$

Here  $\bar{T}$  is the mean temperature in the layer between pressures  $p_0$  and  $p_1$ . Baroclinicity causes the wind turning with height which allows the balloon pilots to change their course. But sometimes the thermal wind frustrates the take-off of HABs, because the wind does not slow down when the ABL stabilizes. The temperature drops in the evening, while the wind remains constant with an enhanced gustiness. In the Netherlands this usually happens when there is an eastern flow of dry air and no clouds. In this special case the pressure gradient and temperature are opposite to each other: high pressure with cold air in the Northeast and low pressure and warm air in Southwest (Figure 1.6). This induces extra mixing which will overrun the stabilizing effect of disappearing buoyancy.

### 1.6.2 Convection in the ABL

Most HAB launches are made just after dawn or two to three hours before sunset (FAA, 2008). At these times of day, the winds are typically light, for easier launch and landing of the balloon. Flying at these times also avoids thermals, which are vertical air currents caused by ground heating that make it more difficult to control the balloon. In the extreme case scenario, the downdrafts associated with strong thermals can exceed the ability of a balloon to climb and can thus force a balloon into the ground.

Hot-air ballooning can not take place in random meteorological circumstances. In general, calm conditions with good visibility are required without strong convective activity. Convection is ideal for birds and gliders, because they can gain height with a minimum of effort. A thermal is simply the updraft in a small-scale convective current. Convective currents (vertical or horizontal air movements) develop in air, which is heated by contact with a warm surface. This heating from below occurs when either cold air is advected (moved horizontally) over a warmer surface or the ground is strongly heated by solar radiation. The strength of convective currents depends on the extent to which the Earth's surface has been heated, which depends upon the nature of the surface. Barren surfaces, such as sandy or rocky wasteland and plowed fields, are heated more rapidly than surfaces covered in vegetation. Thus, barren surfaces generally cause stronger convection currents. In comparison, water surfaces are heated more slowly. When the air is very dry, convective currents may be present although convective-type clouds (cumulus) are absent. The general upper limits of the convective currents are often marked by the tops of cumulus clouds, which form in them when the air is moist, or by haze lines. However, turbulence may extend beyond this boundary. Varying types of surfaces, and the resultant thermal conditions, can affect a balloon to a considerable extent.

In Figure 1.7, an example of a balloon caught in thermal is given. The balloon pilot will recognize the condition by an increase in altitude without the application of heat from the balloon's heater. This ascent can be rapid and may exceed the maximum rate of climb limitations. Since the air mass is also rising with the balloon, there is no significant pressure against the top of the balloon. Thus, the top cap will not be pushed open (commonly referred to as "floating the top"). Depending on their size, some thermals may have a rotating motion similar to a small low pressure system. This motion draws the balloon in and forces it to fly in an uncontrolled circle.

A balloon, that is caught in a thermal, is a rather scary experience. The pilot loses control of altitude. Therefore, the pilot should insure there is sufficient altitude

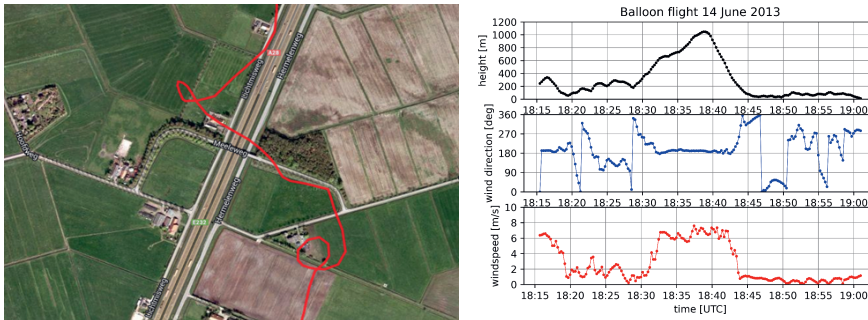


**Figure 1.7:** Example of a hot-air balloon which is caught twice in a thermal up-draft (De Bruijn et al., 2016)

to clear potential obstacles. Secondly, the pilot should maintain the temperature in the balloon appropriate for level flight. Many pilots attempt to descend immediately, but this may put the balloon, as well as the passengers, at risk of an uncontrolled descent with possible injury. Most thermals have a short life span. In the depicted case, the first thermal takes 5 minutes and the second thermal even less. At the end the thermal will “spit” the balloon out the top after a short time, and the pilot is in control again and may descend and land as necessary. Convection plays also a role on a smaller scale, namely in the balloon itself. Hot air from the gas burner ascends, goes to the top, and then descends along the canvas of the balloon and is then heated again. The hottest air is located at the top of the balloon. Some balloonists prepare meals using the hot air in the balloon, see Figure 1.8. They hang a basket on a rope from the top of the balloon to cook the vegetables and the meat. The temperature at the top of the balloon is around 80 degrees Celsius.

### 1.6.3 Inversions

In stable atmospheric conditions, especially early in the morning after a radiation night, strong winds may be encountered in the near-surface layer. A low-level jet is likely to be present whenever there is a marked ground-based inversion (Galvin, 1999). To give some guidance on the occurrence of such nocturnal jets, radiosonde profiles could be studied. Also the output of a mesoscale NWP could give pilots insight into which altitudes are suitable for a balloon flight and in which layer fast winds can be expected. Forecasters using a thermodynamic diagram can examine a temperature inversion and the temperature to which the surface must warm in order for the winds to mix down to the surface. This information is useful for pilots,



**Figure 1.8:** High altitude cooking using the warm air in the top of hot-air balloon, source: CuliAir.

because then they know the time they should be on the ground (FAA, 2008). A day can start with unsuspecting light winds. However, as soon as the inversion weakens and more momentum is mixed to the surface, higher wind speeds will occur, which might cause a rough drag-out landing.

## 1.7 Scope of this thesis and research questions

As stated before, this thesis is about a novel method to measure the wind in the ABL. We will describe a wind retrieval method based on tracking a HAB with GNSS sensors (see chapter 3). These sensors are built-in navigational devices from balloonists and cell phones from passengers. A HAB is an object suspended in the air due to its buoyancy and is unable to resist the wind, thus a HAB can be considered as a Lagrangian drifter. However, balloon motion and the wind are not necessarily similar, especially in case of a wind change due to wind shear or wind gusts. Due to its inertia, the balloon needs some time to adapt and to become in equilibrium with its driving force. During this adapting process, passengers will feel the wind.

In this thesis we would like to address the following research questions:

1. Are HAB-winds a pie-in-the-sky conjecture or a novel method for ABL wind retrieval?
2. What makes HAB wind measurements so unique?
3. What correction is necessary to account for the balloon's inertia?
4. Can smartphones be used to collect the data?
5. What is a typical error in the wind of a HAB?
6. What kind of devices do you need to obtain the measurements?
7. Can HAB observations be applied in NWP models?
8. What are typical circulations that are caught by HABs?
9. What is the recommended application of HAB winds?



## Chapter 2

# Observing Boundary Layer Winds from Hot-air Balloon Flights

This chapter is based on:

Evert I.F. de Bruijn, Fred C. Bosveld, Siebren de Haan, Ben Wichers Schreur, Albert A.M. Holtslag: Observing Boundary Layer Wind from Hot-air Balloon Flights, *Wea. Forecasting*, **2016**, 31, 1451-1463, doi:10.1175/WAF-D-16-0028.1

## Abstract

High resolution upper air wind observations are sparse and additional observations are a welcome source of meteorological information. In this paper we explore the potential of applying balloon flights for upper air wind measurements and investigate the meteorological content of this information. The displacement of a hot-air balloon is a measure for the wind speed and direction and thus a potential source for wind observations in the lower part of the troposphere. The response time of the balloon on the changing wind is fast in the beginning and levels off for smaller relative wind speeds. Four case studies are presented and we compare the balloon derived winds with other wind observations and with the HARMONIE model. It turns out that hot-air balloon tracks can indeed produce useful wind observations just above and in the Atmospheric Boundary Layer (ABL).

## 2.1 Introduction

Hot-air balloons float in the air and travel with the wind. Global Navigation Satellite System (GNSS) navigation data acquired during the flight, provides a displacement during a time interval which is a measure of the airspeed. This wind information is obtained in the Atmospheric Boundary Layer (ABL) where in general few observations are present.

In the Netherlands there are approximately 500 registered balloons and on yearly basis between 8,000 and 9,000 flights are made. The measurements consist of recorded GNSS positions by courtesy of professional balloonists. A hot-air balloon is a passive moving platform and in meteorology moving platforms are used for collecting data like for example radiosondes. These balloons are filled with Helium gas and have an ascend speed of approximately  $5 [m.s^{-1}]$ , because they have to sample the troposphere and a part of the stratosphere in a certain time slot. Further controlled meteorological balloons (Voss et al., 2013) can do repeatedly soundings and are also an attractive possibility for upper air observations. Other observations from moving platforms are obtained from commercial aircraft like Aircraft Meteorological Data Relay (AMDAR) (World Meteorological Organization, 2003) and Mode-S Enhanced Surveillance (De Haan, 2011). In addition research aircraft collect also a lot of atmospheric data. For example Unmanned Aerial Vehicles (UAV) are applied for vertical profiling of the ABL e.g. Jonassen et al. (2015) and even for continental-scale observations (Intrieri et al., 2014). These data are received from moving platforms which have their own propulsion. The wind speed is calculated by subtracting the airspeed from the ground speed and therefore the airspeed has to be measured accurately. For hot-air balloons it is simpler, because they travel with the wind in a Lagrangian framework and therefore the displacement is closely related to the wind. So only positions (longitude,latitude,altitude) and an accurate time stamp are needed to obtain the wind components.

Balloon flights usually last about two hours and take generally place after sunrise and before sunset. During the day when thermals develop, ballooning can become dangerous, because the up- and down drafts can deform the shape of the balloon which affects the buoyancy, resulting in dangerous drops.

The transition from stable to neutral and then unstable conditions and vice versa are a research field of interest. In the morning there is an increasing turbulence and in the evening the turbulence dies out. In the BLASST campaign (Lothon et al., 2014) the evening transition was studied in Southern France. Observations from a wide range of platforms have been applied to record this typical ABL regime during several days in late June 2011. Beare et al. (2006) studied the same phe-

nomenon, but then from the Large Eddy Simulation (LES) model's perspective and in Beare (2008) the focus was on the morning transition. In the model comparison study GABLS3 (Bosveld et al., 2014) a diurnal cycle with an evening- and morning transition was studied in one location, namely Cabauw.

The trajectories of hot-air balloons can be regarded as airborne wind observations which sample the ABL in the above-mentioned regimes on different locations. Balloons have been widely applied in atmospheric research, for example Businger et al. (2006) conducted experiments with balloons which sampled at low altitudes the marine boundary layer with advanced instruments. These balloons were filled with helium and designed to operate autonomously. Laakso et al. (2007) used a hot-air balloon as a measuring platform. They studied particle and cluster formation and measured profiles of aerosols. In a Lagrangian perspective, they benefited from the effect that the balloon was carried along by the wind and thus the effects of advection and heterogeneity did not play a big role in the measurements.

In this study the focus is on the wind in the ABL over land and instead of data from a measuring campaign we use data from a leisure activity. The data can be applied for process studies and model validation. Furthermore they can be useful as an extra wind observation in the lower troposphere for the operational forecaster.

In this paper, we start with pointing out the principle of measuring wind from hot-air balloon flight tracks. We address the dynamics of the hot-air balloon and the interaction with the drag forces. In the next section we describe briefly the observations which have been used for inter comparison. We also introduce the HARMONIE model which provides model winds that have been used for comparison. Further HARMONIE is also necessary to get insight of the meteorological background. Subsequently, in section 3 we present four case-studies during 2013 with interesting meteorological features on different scales. In the final sections we discuss the results followed by conclusions and outlook.

## 2.2 Characteristics of a hot-air balloon

### 2.2.1 Hot-air balloons as wind measuring device

In meteorology radiosonde balloon observations are a well known measuring method that is used for determining wind, temperature, humidity at various altitudes. The radiosonde balloon is tracked with GNSS and from two consecutive positions the wind speed and -direction can be derived using the time delay between these points. The radiosonde or sounding balloon has an initial content of  $1.5 [m^3]$  and its purpose



**Figure 2.1:** Photograph of a hot-air balloon.

is to measure profiles of wind, temperature and humidity. A sounding balloon has an elastic envelope, is filled with helium gas and ascends until it bursts in the stratosphere.

A hot-air balloon (Fig.2.1) has a non-elastic envelope and the content varies from 3,000 to 8,000  $[m^3]$ . In contrast to the sounding balloon, a hot-air balloon remains on a more or less constant level and stays in the lower troposphere. The ceiling of a flight is usually not higher than 2,000 [m]. The energy to heat the air in the balloon is supplied from a propane heating device. The buoyancy is dependent on the temperature excess between the balloon and the surrounding air. To determine the wind speed and direction, we make use of the movement of the hot-air balloon. A hot-air balloon is about 30 [m] high and the payload has a mass of about 500 [kg]. The total mass of the balloon varies between 4,000 and 10,000 [kg]. For the navigation the balloonist uses a GNSS-receiver. In this paper the three dimensional positions were recorded at a maximum rate of 4 [Hz]. Two successive positions in combination with the time interval deliver the velocity of the air in which the balloon is submerged. The flying height is determined by the balloonist, while the vertical displacement is influenced by buoyancy, turbulence and other

external factors. The accuracy of the measured position depends mainly on the constellation of the satellites. Typical values for the standard deviation in the horizontal and vertical plane are 2.5 [m] and 30 [m], respectively. In the vertical this is quite inaccurate and therefore some dedicated GNSS-receivers are equipped with a barometer which reduces the error. The balloon flight is a leisure activity, but the recorded GNSS data conceal useful meteorological information. In fact the data are a kind of byproduct and it requires some organization to obtain them, but there are no substantial costs involved. Finally, it should be noted that a hot-air balloon is not a rigid body and that it will deform easily. For this reason hot-air ballooning takes only place in light wind conditions with moderate turbulence and without intense up and down drafts. Practically speaking, the wind speed should be less than 6 [ $m \cdot s^{-1}$ ] and during the take-off the gustiness should not be excessive.

### 2.2.2 Drag and response time

During the launch the balloon experience a certain drag force, but as soon as it takes off the drag force decreases. During the flight the balloon feels the drag as soon as the relative speed is not zero anymore, for instance when the balloon enters a layer with vertical wind shear.

For large objects moving through the air, the air resistance is approximately proportional to the square of the velocity difference. The form of the resistance (Johnson, 1954) is

$$F_d = -\frac{1}{2}c_d\rho\pi R^2|v| \cdot v \quad (2.1)$$

where  $v = v_{bal} - v_{air}$ , the relative velocity between the speed of the balloon ( $v_{bal}$ ) and the air velocity ( $v_{air}$ ),  $c_d$  is the dimensionless drag coefficient,  $\rho$  is the air density [ $kgm^{-3}$ ] and  $\pi R^2$  is the cross sectional area [ $m^2$ ] of the hot-air balloon. Note that the drag force has an opposite sign compared to the relative velocity. The drag coefficient  $c_d$  is 0.4 for a spherical object in a laminar flow (Munson et al., 1990) and can become larger for irregularly shaped objects. For small relative speeds the viscous friction gives an extra term, namely the Stokes' drag force (Johnson, 1954):

$$F_{Stokes} = -6\pi\mu Rv \quad (2.2)$$

where  $\mu$  is the dynamic viscosity of air,  $1.9983 \cdot 10^{-5}$  [Pa·s], and  $R$  is the radius of the balloon [m]. Because the balloon is going to be used as a wind measuring device, we study the balloon's response time on a changing wind.

Applying Newton's second law the following differential equation is obtained:

$$\frac{1}{2}c_d\rho\pi R^2|v| \cdot v + 6\pi\mu Rv + m_{bal} \frac{dv}{dt} = 0 \quad (2.3)$$

where  $m_{bal}$  is the mass [kg] of the balloon including the payload. If we divide the linear term by the quadratic term, the following ratio can be composed:  $\frac{12}{c_d Re}$  where  $Re$  is the Reynolds number ( $Re = \frac{\rho v R}{\mu}$ ). The linear term becomes relevant if  $Re \leq 30$  and given the dimensions of the balloon ( $R=10$  [m]) the velocities should be smaller than  $10^{-5}[ms^{-1}]$ . Alternatively we can interpret  $\frac{6\pi\mu R}{m_{bal}}$  as the time constant related to the frictional effect and we arrive at values of  $10^6[s]$ . Conclusively the viscous friction term in equation 2.3 is very small and can be neglected. The equation is rewritten as follows:

$$\frac{c_d \rho \pi R^2}{2m_{bal}} |v| \cdot v + \frac{dv}{dt} = 0 \quad (2.4)$$

and we solve this equation with respect to time to get an expression for  $v$ :

$$v(t) = \frac{1}{at + \frac{1}{v_0}} \quad (2.5)$$

where  $a = \frac{c_d \rho \pi R^2}{2m_{bal}}$  and  $v_0$  is the relative wind speed at  $t = 0$ . By applying Archimedes' law we obtain  $m_{bal} = \rho \frac{4}{3} \pi R^3$ , where  $\rho$  is the density of the air in the environment. Subsequently  $a$  can be simplified to  $a = \frac{3}{8} \frac{c_d}{R}$ , which can be recognized as an inverse length scale. Equation 2.5 reveals that the balloon does not respond with a response time in terms of a e-power decay, but with a response length, just like a cup-anemometer (Kristensen, 1998). The difference between the hot-air balloon and a cup-anemometer is that the latter has a fixed position and in moderate wind speeds an equilibrium state is quickly reached. In our case, the balloon moves with the wind and the relative speed becomes smaller. This implies that its response time grows. The concept of the response length (being  $\frac{8}{3} \frac{R}{c_d}$ ) shows us that the balloon's response time to a certain wind jump corresponds to the time it takes for the relative velocity to travel a distance of  $10R$ .

In Figure 2.2 we present the relative wind speed as a function of time. It is seen that it takes 300 [s] before the initial speed difference of 2 [ $ms^{-1}$ ] is reduced to 10 percent. In the beginning the response is fast and levels off as the speed difference becomes less. So it takes a couple of minutes before the hot-air balloon eventually travels with the ambient air velocity. This makes sense because a hot-air balloon is a large body with a substantial weight. Due to the inertia of the hot-air balloon, its displacement does not capture the small scale variations in the wind pattern. The wind observations represent an average in space and time.

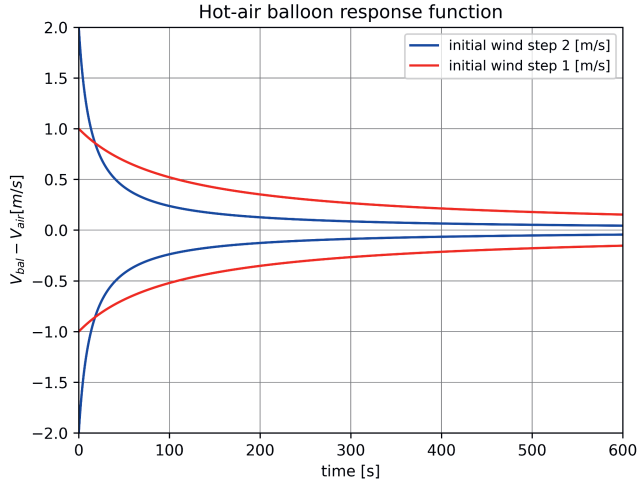


**Figure 2.2:** Response time of a hot-air balloon due to a step-wise changing wind.

## 2.3 Inter comparison data

In this study we have applied data from the KNMI observation network. It should be noted that some of the balloon flights (see Fig. 2.3b) took place in areas where wind observations in the lower atmosphere were not present and therefore we also used a numerical weather prediction (NWP) model for comparison (see Fig. 2.3a). Further we have used the model to study the meteorological circumstances of the balloon flights. We have chosen the HARMONIE model because this NWP represents the wind quite well, especially in the ABL (Baas et al., 2015).

### 2.3.1 Routine observational network

The KNMI network consists of 33 automatic weather stations on land, 15 wind poles in coastal areas and 13 automatic weather stations on North Sea platforms. In this study the focus was on the wind which is sampled every 12 [s] and becomes available as 10 minutes averages. For the upper air a radiosonde launch is available, but that is only launched at midnight. Other upper air observations are supplied by a RASS wind profiler and tower observations. Each observation has its own characteristics, i.e. radiosondes deliver profiles of wind, temperature and humidity but they are not frequently sampled, aircraft observations deliver wind and temperature information with a high sampling rate but their locations are in small corridors above the

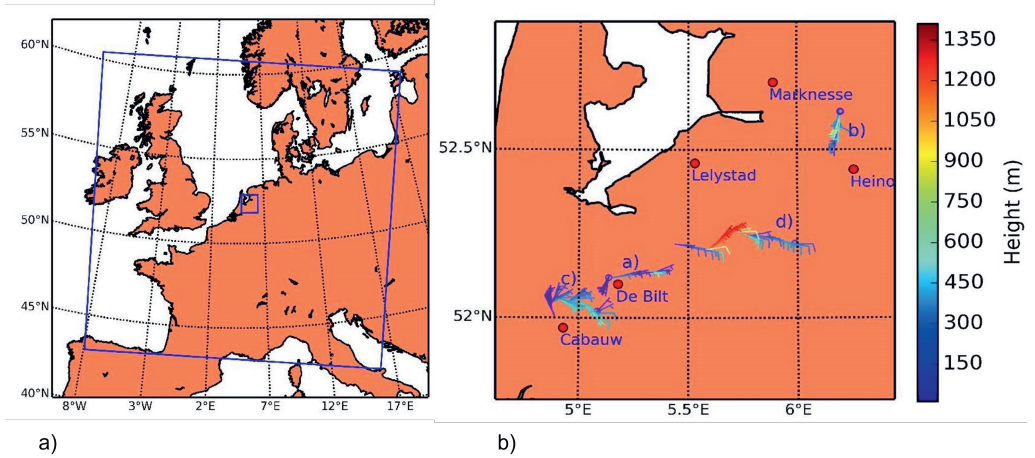


**Figure 2.3:** a) HARMONIE domain (2.5 km grid resolution, 800 by 800 grid points) b) Hot-air balloon tracks and the nearby observations which are used for the inter-comparison. The balloon tracks are presented as wind flags; a full barb corresponds with  $5 [m s^{-1}]$ , the color is a measure of the height.

tropopause. Further, they measure also vertical profile data from the take-off and landing areas. Recently new aircraft sensors also deliver humidity observations, albeit in small numbers. Synops give observations on surface level every hour, but they are representative for the local scale. In our study we also use Cabauw data, because two of the flights took place in surroundings of the KNMI observatory at Cabauw, the Netherlands. This observational site is located in a rural area, 20 km southwest of the city of Utrecht. There is a 213 [m] high tower with wind sensors at 10, 20, 40, 80, 140 and 200 [m] and the data are available as 12 [s] and 600 [s] averages. At the site a whole range of instruments is deployed and amongst them there is a RASS wind profiler. The wind profiler measures wind profiles up to 4000 [m], dependent on the concentration of small particles.

### 2.3.2 NWP

In this study we have used data from HARMONIE (Cycle 38) (see Fig. 2.3a) which has been implemented at the computer system of the ECMWF. HARMONIE is a non-hydrostatic model (Seity et al., 2011). which has a horizontal resolution of 2.5 km. In the vertical, there are 65 layers defined and 10 layers are positioned in the lower 2 km. HARMONIE covers an area as large as Western Europe and receives lateral boundary layer (LBC) information from the global ECMWF model. HAR-

MONIE runs every three hours and a 3D-VAR Data-assimilation scheme is used with time window of 1.5 hours. The following surface observations are assimilated: synops, buoy and ship for ground level, in the upper air radiosondes and aircraft observations are used. The analysis tries to optimally combine the information based on the previous model run (first guess) and the observations.

Relevant parts of the model for the ABL processes are the turbulence- and the land surface scheme. The turbulence scheme describes the transport of momentum, heat, humidity from the earth's surface to the atmosphere and vice versa on the basis of the Turbulent Kinetic Energy (TKE) equation. The turbulence and convection schemes work together in the framework of an Eddy Diffusivity Mass Flux (EDMF)-scheme (Siebesma et al., 2007) which adequately describes up- and down-drafts. In the land surface scheme the energy balance is solved. The soil moisture content, air temperature, humidity and wind speed as well as the surface albedo, roughness lengths, soil temperature profile and the heat conductivity of dry soil affect how the net amount of radiation is distributed over sensible -, latent - and soil heat flux. The roughness lengths, vegetation and land-use are important parameters which have a clear impact on the wind profile. The surface data are derived from the ECOCLIMAP database.

## 2.4 Case-studies

Now we present four case-studies of hot-air balloon flights during the summer of 2013. The first case is about a large scale baroclinic phenomenon which is well captured by KNMI's observation network.

### 2.4.1 Occluded front, 28 May 2013

Although balloon flights usually took place in fair weather conditions, this flight from Amersfoort to Utrecht (see Fig. 2.4a ) commenced when thunderstorms were developing in the southern part of the Netherlands. These thunderstorms belonged to an occluded front which moved slowly in North easterly direction and approached the area where the balloon flight took place. Just before the occluded front a convergence line in the wind field could be recognized (see Fig. 2.4b). This was the area where two air masses collided. Despite the adverse weather forecast the balloonist decided to take off and during the flight the wind direction was steady around 90 degrees, the wind speed was more variable and increased slightly when the balloon went up to higher levels (see Fig. 2.5a). When the balloonist approached the city of Utrecht he realized that he would fly over an urban area with limited possibilities to land. Therefore he decided to land in the outskirts of

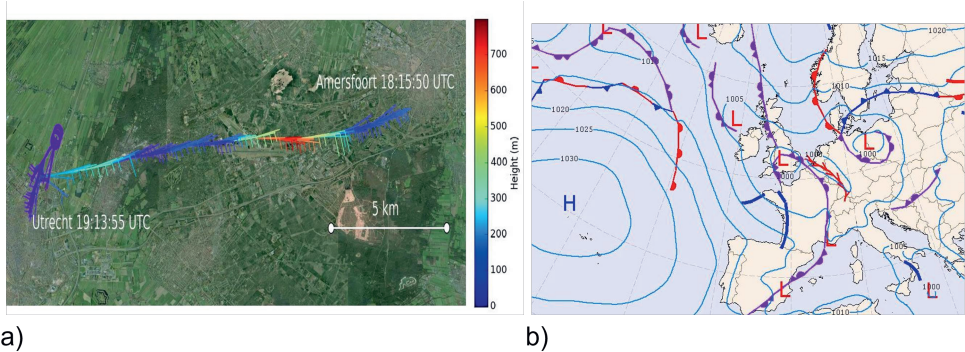


**Figure 2.4:** a) Wind data based upon a hot-air balloon flight from Amersfoort to Utrecht in the evening of 28 May 2013. b) Weather map of 28 May 2013 18:00 UTC with an occluded front (magenta) and a convergence line (red).

Utrecht which was still rural area. During the descend, the passage of the frontal system set in, resulting in a wind direction change of 120 degrees. The balloon was pushed in a more favorable area to land, but the gustiness as reported by the balloonist increased which hindered the landing. The balloonist lost control and was forced to land in a ditch. This sudden wind change was also recognized at the nearby KNMI stations De Bilt (5 km) and Cabauw (30 km) as depicted in Figure 2.5b. Note that this frontal system arrived one hour earlier at Cabauw and was also recognized at 200 m. All in all, the wind information from this balloon track confirmed the passage of the frontal zone and provided extra vertical wind information. In the next case we present a very small phenomenon which is hardly visible in the KNMI observational network.

### 2.4.2 Major wind-shifts, 14 June 2013

In this case a sea breeze circulation develops and at the same time a depression on the Atlantic ocean deepens and moves slowly eastwards. The pressure gradient is small and there is a gradual transition from a southerly to a westerly flow. In this transition zone substantial wind-shifts develop which have impact on the balloon's track. From the Figures 2.6a and 2.7a it is seen that the balloon remains more or less at the same altitude and describes two circles in a time span less than 300 [s]. These features are not artifacts from the GNSS system, because the balloonist has confirmed (personal communication) that two circular tracks were flown. The balloonist managed to escape from the unsettled conditions by ascending to a higher altitude where the flow is less variable.

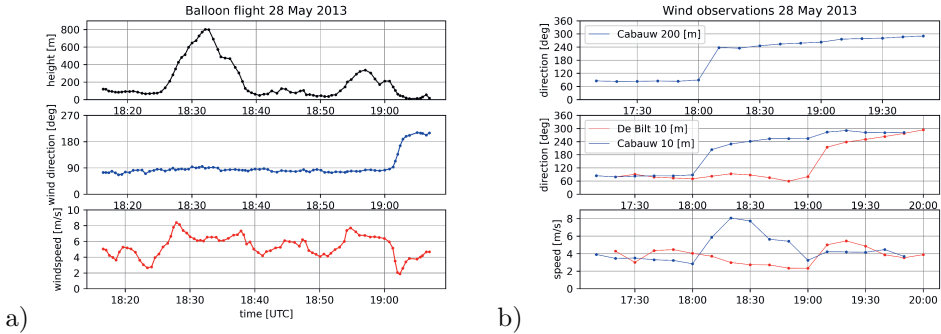


**Figure 2.5:** a) Height, wind direction and -speed during 28 May 2013 along the trajectory of the hot-air balloon b) Wind observations at Cabauw and De Bilt during 28 May 2013, Note that the wind shift arrives 1 hour later at De Bilt.

Interestingly, the observations in Lelystad and Marknesse in Figure 2.7b show a significant wind change during the flight of the hot-air balloon. This change arrives later in Marknesse which indicates that a convergence zone is passing over. The NWP output confirms this. The observations are measured at 10 [m] height and are averaged over 600 [s]. The first circle takes 300 [s], the second one takes only 180 [s] with diameters of few hundred meters. Note that the height slightly varies. The sampling rate of the KNMI network can not represent this small scale phenomenon. A higher sampling rate is required to capture the details of this wind shift. Moreover the measurements are taken at 10 [m] height while the wind shifts are observed at approximately 200 [m] height.

The small scale phenomena are for the same reasons not represented by the NWP model (see Fig. 2.6b), because the horizontal and the temporal resolution are too coarse i.e., the grid size is 2.5 km and the output frequency is 1 hour. It is evident that the wind shifts are a sub grid scale feature which are not resolved by the model. Possibly a nested run with a very high resolution or a LES-model simulation might reveal these wind patterns. On the other hand due to the balloon's inertia (see section 2.2.2) not all variations in the wind are captured, so the accuracy of the balloon based wind measurement is questionable especially in this case. At the end of the flight at heights below 200 m, the balloon meets again variable winds, resulting in a curved trajectory (not shown). Without further experiments an explanation of this event is rather speculative, but it is possible that a convergence line with embedded updrafts has passed over the area where the hot-air balloon flight took place.

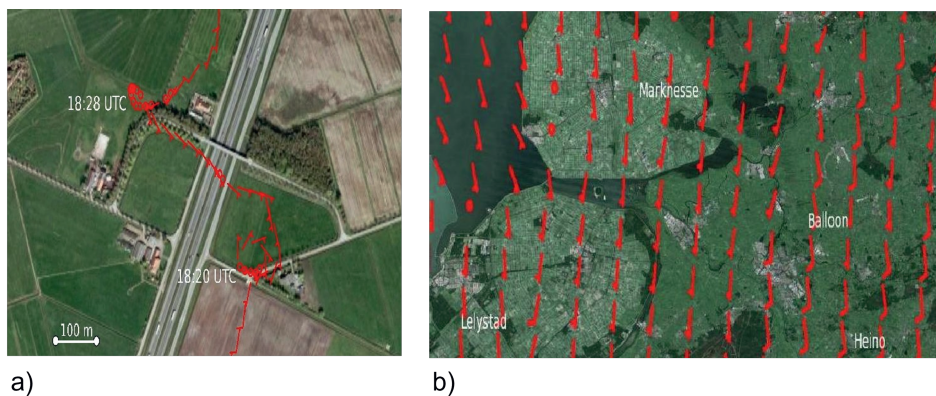


**Figure 2.6:** a) Circular wind patterns recorded from a balloon's track between 18:20 and 18:30 UTC during 14 June 2013, Note that the wind data are multiplied by a factor 2. b) HARMONIE +03h forecast at model level 55 valid at 18:00 UTC 14 June 2013. Distance between two wind flags is 5 [km]. Note that model level 55 corresponds with 200 [m] AGL, which is the altitude of the balloon at the beginning of the flight.

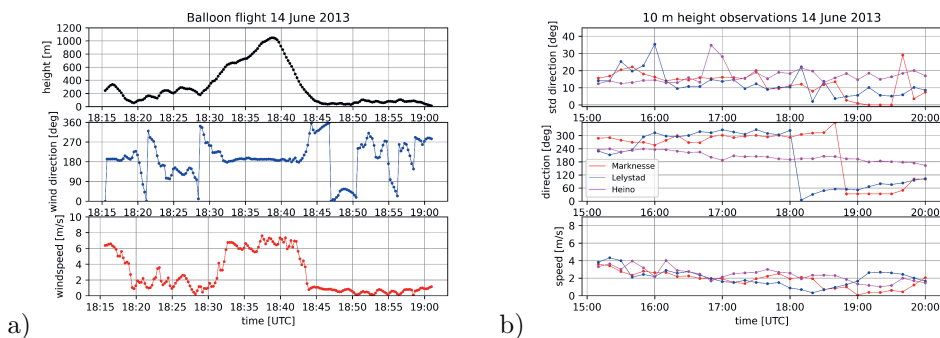


**Figure 2.7:** a) Height, wind direction and -speed during 14 June 2013 along the trajectory of a hot-air balloon. b) Wind observations (10 [m] height) at nearby stations during 14 June 2013.

### 2.4.3 Wind shear during a hot summer day, 18 June 2013

During this case the trajectory of the balloon is curved because the balloon goes up and down in an ABL with a lot of wind shear (Fig. 2.8a ). It is a hot summer day with northeasterly winds and there is a distinct temperature contrast over the Netherlands. In a barotropic atmosphere the wind changes with height due the vertical gradient in stress between the top of the surface-layer and the free atmosphere. As a result the wind veers with height (clockwise turning), which is the so-called Ekman spiral. However the wind can also change with height because of baroclinic effects. If the horizontal temperature gradient in a certain layer is positive, the wind veers with height, conversely if the horizontal temperature gradient is negative, the wind backs (anti-clockwise turning) with height. Using NWP output we have calculated the geostrophic wind based on the pressure gradient and the Coriolis force and found that the geostrophic wind changes with height which confirms the presence of the thermal wind.

The balloon takes off from a city park and goes in southerly direction. During the ascent the balloon's trajectory veers with height (Fig. 2.8b) and goes eventually northwest. At 19:10 UTC the balloon descends slightly and due to baroclinic and frictional constraints the wind backs. The balloon goes up and the wind veers again. At 19:34 the balloon prepares for landing and remains during 10 minutes below 200 [m]. The balloon goes again in southerly directions and the wind turns further to northwesterly directions. The wind is more steady with speeds of 4 [ $ms^{-1}$ ] which is in contrast with the variable winds at the beginning of the flight.

In Figure 2.9 we compare the balloon wind data during the last 20 minutes of the flight with HARMONIE data and with the observations at Cabauw. The HARMONIE data consist of the +01 and +02 forecasts starting from the analysis at 18:00 UTC. The wind-profiler is located at Cabauw and the data is available as a 30 [min] average. Due to the radar reflections from the nearby obstacles ( i.e. tower) the wind-profiler data are unreliable under 400 [m]. Also the averaged wind data from anemometers from the mast are shown. There is some wind shear in the model but it is under estimated. The wind-profiler and tower observations as well as the balloon derived winds reveal more gradient. Perhaps the turbulence scheme is not able to represent this gradient due its parameterisation and due to an insufficient vertical resolution. Another reason might be the representativity of the roughness length in the grid-box of the model. Further it should be noted that there are slight timing and location mismatches between the moving balloon and the observations at Cabauw.

All in all the balloon derived winds are closer to the other observations than to

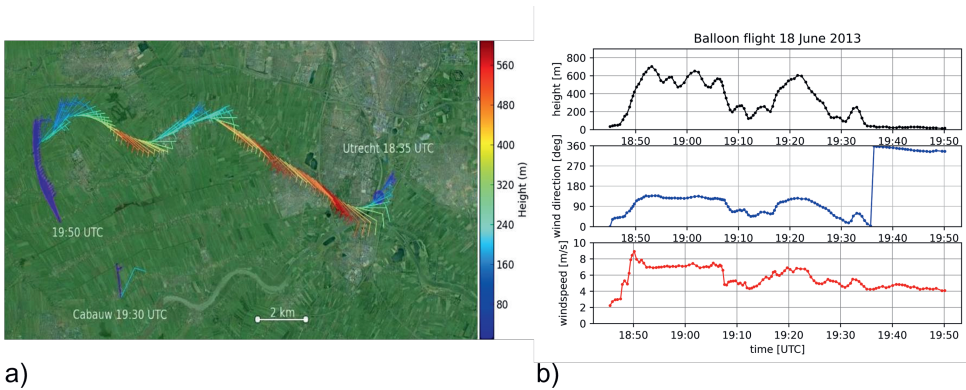


**Figure 2.8:** a) Wind data derived from a hot-air balloon flight from Utrecht to Cabauw during 18 June 2013 18:40-19:50 UTC, also the tower observations at Cabauw at 60 [m] and 200 [m] are depicted at 19:30 UTC. b) Height, wind direction and -speed during 18 June 2013 along the trajectory of the hot-air balloon.

the HARMONIE model. It is obvious that this trajectory reveals an interesting Lagrangian representation of an atmospheric flow in baroclinic conditions with veering and backing winds.

#### 2.4.4 Low level jet, 28 September 2013

Now we present the final case with a typical ABL and a baroclinic effect in an area where no other observations are present. This flight which is depicted in Figure 2.10a, takes place early in the morning in a stable atmosphere with clear sky conditions. The Low Level Jet (LLJ) usually occurs on top of the stable boundary layer when the turbulent mixing ceases when the ABL becomes stable due long wave radiation cooling (see Baas et al., 2009). The frictional effects are reduced in a shallow layer above the top of the surface inversion and within the residual layer from the previous convective mixed layer. The ageostrophic wind in the residual layer was in balance with the frictional forces in the late afternoon and goes through an inertial oscillation and the period is around 15 hours. This flight takes place at the end of this oscillation during the morning transition.

As soon as the balloon takes off, the wind speed increases from 0 to 12 [ $ms^{-1}$ ] and it is clear that the balloon has entered the LLJ. This jet is located in a small vertical zone not higher than 500 [m] (see (Baas et al., 2009)) and also occurs in HARMONIE (see Fig. 2.11). The sharp gradient in the wind speed is recognized in the model and in wind data from the hot-air balloon track. Note that the first 10

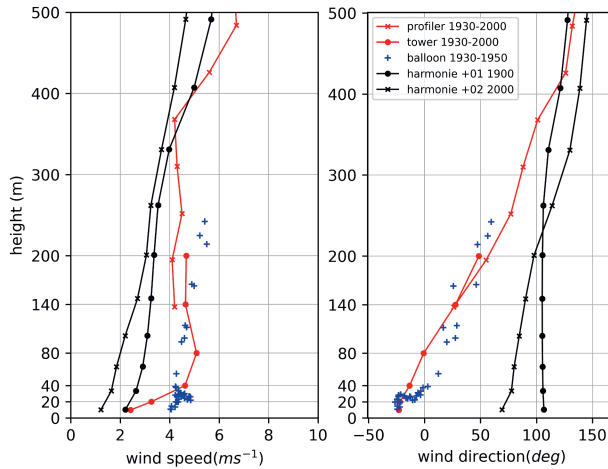


**Figure 2.9:** Inter comparison of wind observations at Cabauw (tower, profiler, balloon) and HARMONIE data during 18 June 2013 19:30-20:00 UTC.

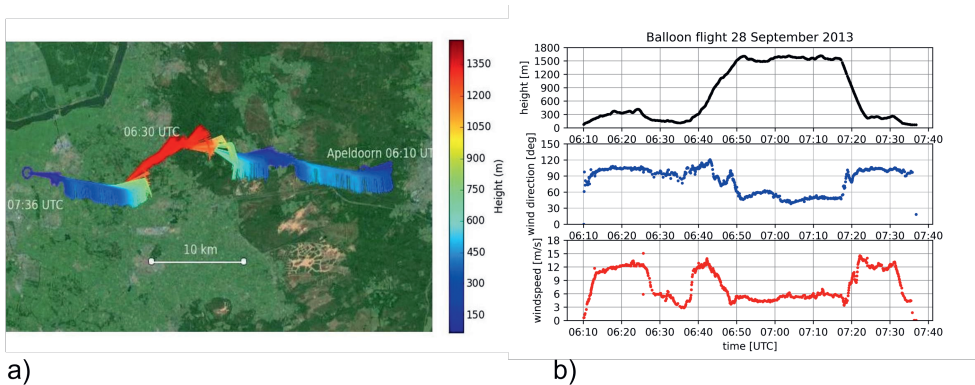


**Figure 2.10:** a) Balloon wind data from a morning flight during 28 September 2013 06:10-07:36 UTC b) Height, Wind speed and -direction during 28 September 2013 06:10-07:36 UTC.

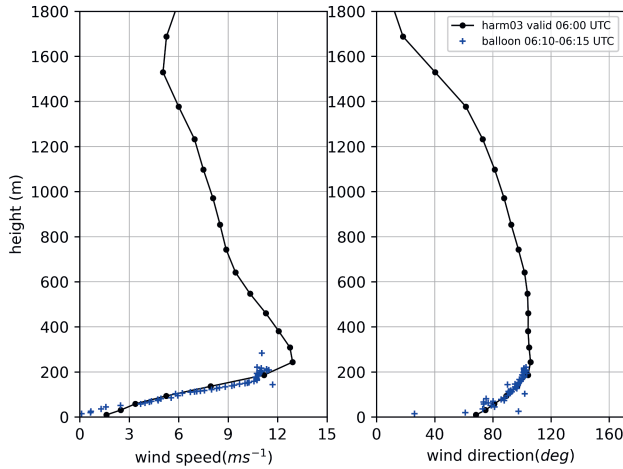


**Figure 2.11:** HARMONIE profile 2013092803 +03 valid at 06:00 UTC and balloon derived wind data, just after taking off near Apeldoorn.

minutes are shown and model and observations are in good accordance. However the observation show some noise, possibly caused due to the unsettled conditions during the take-off.

At 06:25 UTC (see Fig.2.10b) the balloon descends about 100 [m] and leaves the jet immediately. Subsequently the balloon rises gradually and crosses the LLJ again and arrives at a height of 1500 [m] which is also the ceiling of the flight. The change in the wind speed and direction is clearly present in the recorded data. At 1500 [m] the wind speed decreases to values of 4 [ $ms^{-1}$ ], but it is remarkable that the wind direction changes from east to northeasterly direction. It is seen that during the ascend the wind direction changes counter-clock wise. This change in wind direction is caused by the advection of cold air, which is confirmed by HARMONIE (see Fig. 2.11 right panel). While descending to lower levels the balloon encounters again the wind direction change and the LLJ and it is clear that the flow has been quite stationary.

## 2.5 Discussion

In this paper we have shown that balloon-derived winds are an interesting new type of upper air observations, however there are some remarks which have to be

made. At low altitudes the movement of the balloon is also influenced by other forces like surface friction when the balloon is dragged over the ground. For this reason, the observations under 10 [m] are excluded in the data-set. An automatic quality control algorithm as developed by Houchi et al. (2015) would have been useful. Such an algorithm does the pre-processing and creates a reliable data-set with reduced errors. Since the data-set consists of 4 case-studies only, we have inspected the data visually and removed outliers by hand.

The short term fluctuations in the wind vector are also not properly measured, as a result of the inertia as discussed in section 2.2.2. Moreover we have neglected the acceleration term in the derivation for the wind speed. For the application in data assimilation it is essential that the observations are in agreement with the dimensions of grid box. Due to the response time of the balloon, the small scales are inherently filtered out. A spectral analysis of the hot-air balloon data would reveal which scales are present and this a subject for future research.

Finally we address the inaccurate vertical coordinate which is caused by instrument noise and by the coordinate system. The local geoid can deviate from the WGS'84 ellipsoid as applied in the GNSS system, but this error is not substantial.

## 2.6 Conclusions and outlook

Hot-air balloon tracks revealed interesting meteorological features ranging from the meso- to the micro scale and can be useful for process studies and for validating a NWP model. Process studies presented in this paper, comprise the scope of turbulence, shallow convection and air-surface interaction.

Hot-air balloon data are obtained without large investments or without the presence of an operator. However, the data are available in a limited period of the day and only during fair weather conditions. The data were collected with simple instrumentation by frequently sampled positions and time stamps from a GNSS-receiver. The wind speed and direction were derived by simple time differencing. We showed that a hot-air balloon responds quickly on a step-wise changing wind in the beginning and the velocity difference decays slowly asymptotically. This can be expressed in terms of a response length. We presented four interesting trajectories which reveal valuable wind information of the lower atmosphere.

This study is based on off-line GNSS navigation data which are received from collaborating balloonists. This new observation type can also be used in the operational weather service as an ABL wind observation and might be useful for guidance of other balloonists .

For that an infrastructure to collect the data in timely fashion is necessary. There are two ways to proceed: Firstly, data can be collected via Air Traffic Control (ATC), in that case the hot-air balloons should be equipped with a transponder. There are technical constraints because a transponder requires a power-supply and also navigational data should be provided.

Secondly, citizen technology can be applied. This means that the data are collected by balloonists and passengers who carry a smart phone with a dedicated app. At KNMI work is in progress to realize this possibility and the first results are encouraging.

## 2.7 acknowledgments

The balloonists Peter Barlo, Dick Klein Lugtenbelt and Willem Hijink are gratefully thanked for providing their GNSS navigation data of the balloon flights in this paper. Henk Klein Baltink is thanked for providing the wind profiler data at Cabauw and Wouter Lablans (†) is acknowledged for supplying critical comments which have improved the manuscript. Finally, we thank the reviewers for their positive criticism and comments which have improved this paper.



## Chapter 3

# Measuring Low Altitude Winds with a Hot-air Balloon and Their validation with Cabauw Tower observations

This chapter is based on:

Evert I.F. de Bruijn, Fred C. Bosveld, Siebren de Haan, Bert G. Heusinkveld, Measuring Low Altitude Winds with a Hot-Air Balloon and Their Validation with Cabauw Tower observations, *J. Atmos. Oceanic Technol.*, **2020**, 43, 263–277, doi:10.1175/JTECH-D-19-0043.1

## Abstract

A field experiment with a hot-air balloon was conducted in the vicinity of the meteorological observatory of Cabauw in the Netherlands. Recreational hot-air balloon flights contain useful wind information in the Atmospheric Boundary Layer (ABL). On a yearly basis between 8000 and 9000 flights are taking place in The Netherlands, mainly during the morning- and evening transition. An application (app) for smartphones has been developed to collect location data. We report about a feasibility study of a hot-air balloon experiment where we investigated the accuracy of the smartphone's Global Navigation Satellite System (GNSS)-receiver using an accurate geodetic GNSS-receiver as a reference. Further, we study the dynamic response of the hot-air balloon on variations in the wind by measuring the relative wind with a sonic anemometer which is mounted below the gondola. The GNSS comparison reveals that smartphones equipped with a GNSS-chip, have in the horizontal plane an absolute position error standard deviation of 5 [m], but their relative position error standard deviation is smaller. Therefore the horizontal speeds, which are based on relative positions and a time step of 1 [s], have standard deviations of  $\sigma_u = 0.8[ms^{-1}]$ ,  $\sigma_v = 0.6[ms^{-1}]$ . The standard deviation in altitude is 12 [m]. We have validated the hot-air balloon derived wind data with observations from the Cabauw tower and the results are encouraging. We have studied the dynamics of a hot-air balloon. An empirical value of the response length has been found which accounts for the balloon's inertia after a changing wind, and which compared favorable with the theoretical derived value. We have found a small, but systematic movement of the hot-air balloon relative to the surrounding air. The model for the balloon dynamics has been refined to account for this so-called inertial drift.

## 3.1 Introduction

There is a growing need for wind observations in the Atmospheric Boundary Layer (ABL), for numerical weather forecasts, air pollution, and for site investigations of wind farms. Hot-air balloon tracks can provide interesting wind information of the lower atmosphere. Hot-air balloon flights usually take place during atmospheric conditions without strong convection and turbulence. These conditions can be found just after dawn and just before dusk and they are called the transition periods. The evening transition has been extensively investigated, for instance by Lothon et al. (2014), but the decaying turbulence in a stabilizing ABL is still not fully understood and more experimental data are necessary. There is a long tradition in launching upper-air balloon soundings, but these observations are infrequent and sample a vertical profile of the atmosphere and while ascending the balloon remains relatively short in the ABL. There are several other methods to measure ABL winds, such as wind profilers, sodars and wind-lidars. These observations are collected at fixed locations. Wind observations in the ABL can be also obtained from moving platforms. Laakso et al. (2007) and Petäjä et al. (2012) used a hot-air balloon to study aerosols in the ABL. Also, Doerenbecher et al. (2016) showed that balloons are useful for sampling the atmosphere and that horizontal winds can be derived from the data of drifting low-atmosphere balloons. They used constant level super-pressure balloons, which could remain in the troposphere for several days.

In this paper, the focus is on a typical recreational hot-air balloon which can remain a couple of hours airborne. The principle of flying is buoyancy. Ambient air is burned with propane and the hot exhaust gas has a lower density than the surrounding air which gives buoyancy. Hot-air balloons are also called Montgolfière's after the French Montgolfière brothers who flew the world's first hot-air balloon at the end of the 18th century. Hot-air balloon flights are a leisure activity, but will be possibly applied to explore other planets. Fathpour et al. (2014) studied the feasibility of the reconnaissance of Titan, Mars, and Venus with hot-air balloons. A Montgolfière does not have to be inflated with a light gas such as helium and is not vulnerable to leaks, because leaking air can be quickly replaced and re-heated. However, the balloon flight time is restricted to an external heat source.

The Royal Netherlands Meteorological Institute (KNMI) provides special forecasts for hot-air balloon operators which are useful for guidance and trajectory planning. The start location is usually selected in a way that the balloon is not going to land in undesirable areas like cities, motorways or lakes and the balloonist tries to avoid damage to crops and livestock, if a landing in a rural area is foreseen. Of course

also the weather conditions should be favorable with regard to cloud base, visibility and wind(gusts).

De Bruijn et al. (2016) revealed that trajectories from recreational hot-air balloon flights provide interesting wind information in the ABL. They showed interesting meteorological phenomena like wind jumps near fronts and low-level jets which were not captured by the standard observation network of KNMI.

This paper describes a scientific field experiment in the surroundings of the Cabauw meteorological tower (213 [m]) and we investigate if smartphones can be applied to track hot-air balloons and if we can derive wind data from it. The idea is that many balloon pilots or passengers will start using a special smartphone app that exchanges location data. This will result in wind measurements of the lower part of the atmosphere. The attractiveness of a smartphone app is that it can sample the position and transfer the data using the telecommunication network. A dedicated app is developed which controls this functionality. It is clear that this observation method does not require big investments but will rely on the collaboration of people on board of a hot-air balloon.

The main goal of the hot-air balloon flight experiment is to assess the accuracy of the smartphone app and the validation of the obtained wind data. To achieve this, measurements have been collected from an accurate geodetic GNSS-receiver and two smartphones. A second goal is to study the airflow relative to the balloon by measuring data from a sensitive sonic anemometer which is mounted in a rigid frame underneath the gondola. Canut et al. (2016) conducted an experiment with a 3D sonic anemometer underneath a tethered balloon and their goal was to study the turbulence in the ABL. In our experiment, the sonic anemometer was mounted on a moving platform and the aim was to study the relative wind and the response of the balloon on the changing wind. Our hot-air balloon flight took place in the vicinity of the village of Cabauw and closely passed along the KNMI observatory which comprises also a meteorological instrumented tower.

At first, we describe in section 2 the instrumentation and the focus is on the smartphones and the sonic anemometer. In section 3, we present results from the hot-air balloon test flight which took place in the surroundings of Cabauw. In section 4, we study the noise characteristics and temporal drift of the GNSS sensors of the smartphones. Subsequently, we determine how the error in position (lon,lat) propagates into the derived wind components ( $u, v$ ). In section 5, we validate the balloon derived wind with tower observations at Cabauw. In the following section 6, we will discuss in more detail the measurements from the sonic anemometer and the geodetic GNSS-receiver. We will derive a mathematical explanation for the

fact that the observed relative flow is not equal to zero. Finally in section 7, we will make an attempt to find an empirical value for the length scale in the response function as proposed by De Bruijn et al. (2016). This paper ends with a discussion (section 8), followed by conclusions and recommendations (section 9).

## 3.2 Instrumentation

Here we describe the instruments that we have used during the experiments and we limit ourselves to describe the instrumentation on board of the moving platform. For a description of the meteorological tower measurements, we refer to Van Ulden & Wieringa (1996). Further, we have used off-the-shelve smartphones with proprietary technology and took their performance capabilities and limitations as a constraint for our experiment. Our focus was to calculate wind information from hot-air balloon tracks. Consecutive GNSS positions of the moving hot-air balloon and the corresponding time difference were ingested to our algorithm which delivered wind information. Our aim was not to conduct a profound investigation of the geodetic aspects of the GNSS devices.

### 3.2.1 Smartphones and portable GNSS-devices

The low-cost smartphones Nexus 5 and 5x, equipped with ordinary GNSS-receivers, are used to track the hot-air balloon. GNSS chip sets are omnipresent in smartphones these days. Yet the underlying position accuracy of these GNSS-receivers is rather poor, compared to geodetic GNSS receivers. Under good conditions, 2-to-3-meter-accurate positioning is typical; under adverse conditions, the accuracy degrades to 10 meters or worse.

The smartphones were equipped with a smartphone application (app), which was developed by KNMI. This app performed the collection of the sensor data and transmission of the data to a server at KNMI. The apps were developed for Android and IOS operating systems.

The apps could not directly access the physical sensors embedded in the smartphones. Raw sensor signals from physical sensors were processed by the smartphone's operating system (OS) and made available to applications in a standardized format as a smartphone sensor (Kos et al., 2016). Also the raw data, received from the orbiting satellites were not accessible for the end user. We applied the already processed data provided from the OS of the smartphones, which were the coordinates (longitude, latitude, altitude). During the field experiment, smartphone Nexus 5 was held by a person and was also used to take photographs during

the flight. The smartphone Nexus 5x was firmly mounted on the rim of the gondola of the balloon. This smartphone recorded information of location, magnetic field, acceleration, orientation, roll, pitch, angular velocity as well as sound level and light intensity.

The smartphone apps were written in Java and dedicated API's were applied to retrieve the data of the sensors. Information of the different sensors was combined and stored with a sampling rate of 0.1 and 1 [s] for respectively the Nexus 5x and the Nexus 5 smartphone. The Nexus smartphones were equipped with Assisted GNSS (A-GNSS) which was a technique where Almanac and Ephemeris data were obtained from the telecommunication network when staying in poor satellite signal conditions.

We also used navigational data from the balloonist (Garmin 60Csx). The navigation data were stored in irregular intervals varying from 4 to 20 [s]. The sampling rate was dependent on the curvature of the track to reduce the storage of data. In previous studies, these data have been used to render ABL winds (De Bruijn et al., 2016) and we investigate how this navigation device compares with other GNSS sensors in this experiment.

Finally, it should be noted that only the smartphones were able to transfer their data to a server at KNMI. This offers the possibility to apply the wind data in the data-assimilation module of a NWP model, when a timely availability is crucial. A limitation is that the transfer can only take place when the smartphones are in range of the telecommunication network. The other devices stored their data on local media and were not linked to an external network.

### 3.2.2 Geodetic GNSS device

During the experiment flight the hot-air balloon's position was measured with a Trimble R7 GNSS-receiver, an accurate device with a standard deviation in longitude, latitude and, altitude coordinates in the order of centimeters. This geodetic receiver uses data from GPS and GLONASS satellites. A special light weight pole-antenna was firmly tightened to the gondola. Unfortunately, the position data were not real-time available. During the flight the raw GNSS-receiver observations were collected and stored. The accurate location data were obtained after post-processing. The applied method is called D-GPS (Differential Global Positioning System). Using a reference network of fixed GNSS-receivers on exact locations in the Netherlands (NETPOS), the biases of (e.g. satellite position, ionospheric and troposphere delay) were characterized and applied on the collected data of the moving platform. In this paper, the Trimble R7 GNSS-receiver data will be

regarded as the reference.

### 3.2.3 Sonic anemometer

In the experiment, we have measured the relative wind using the IRGASON 3D Sonic anemometer (Campbell, USA), hereafter labeled as SONIC. This device is designed specifically for eddy-covariance flux measurements. The SONIC measures simultaneously carbon dioxide, water vapor density, barometric pressure, three-dimensional wind speed, and sonic air temperature and its sampling rate is 50 [Hz]. Acoustic pulses are sent and received between transducers. Wind speed is obtained by measuring the changes in travel time of the pulses. The offset error of the measurement is  $\pm 0.008$  [ $m s^{-1}$ ] for the u,v components, and  $\pm 0.002$  [ $m s^{-1}$ ] for the w-component.

A special frame was constructed which could be easily attached to the gondola. The SONIC was mounted in this frame (Figure 3.1) after the balloon was airborne. Subsequently, the SONIC was deployed under the gondola by lowering a pivotal aluminum beam (Figure 3.2). The SONIC was leveled and pointed parallel to the long side of the gondola, where the Nexus 5x smartphone was fitted. The vertical distance between the Nexus 5x smartphone and the SONIC below is 2.48 [m]. The vertical distance between the SONIC and the envelope of the hot-air balloon is 5.80 [m]. The horizontal distances between the Nexus 5x smartphone and the Trimble R7 Patch antenna and the SONIC are less than 2.0 [m] and given the horizontal accuracy of the smartphones, they can be neglected.

The SONIC delivers wind data in a local coordinate frame and these data have to be transformed to the coordinate system of the GNSS-receiver, which is the WGS-84 Geoid surface plane. In order to transform data we have used data from the Nexus 5x smartphone which was properly fitted on the rim of the gondola. The smartphone Nexus 5x had sensors which measured the position and attitude like accelerators, gyros and magnetic field components. From these sensors azimuth, roll, and pitch were obtained and these data were applied to rotate the SONIC data to the appropriate coordinate system. The Nexus 5x smartphone was equipped with the Bosch BMI160 Inertial Unit which delivered gyroscope and accelerometer readings with an accuracy of respectively 0.0011 [rad/s] and 0.0025 [m/s/s] and the Bosch BMM150 magnetometer which delivered 3D magnetic fields readings with an accuracy of [0.0] deg. The small sensors were designed for mobile applications like indoor navigation, which required high accurate real time sensor data, and were considered as sufficiently accurate for our application. It should be noted that the Android operating system itself calculated the orientation, pitch, and roll. We used those variables to assess the attitude of the gondola and to transform the SONIC

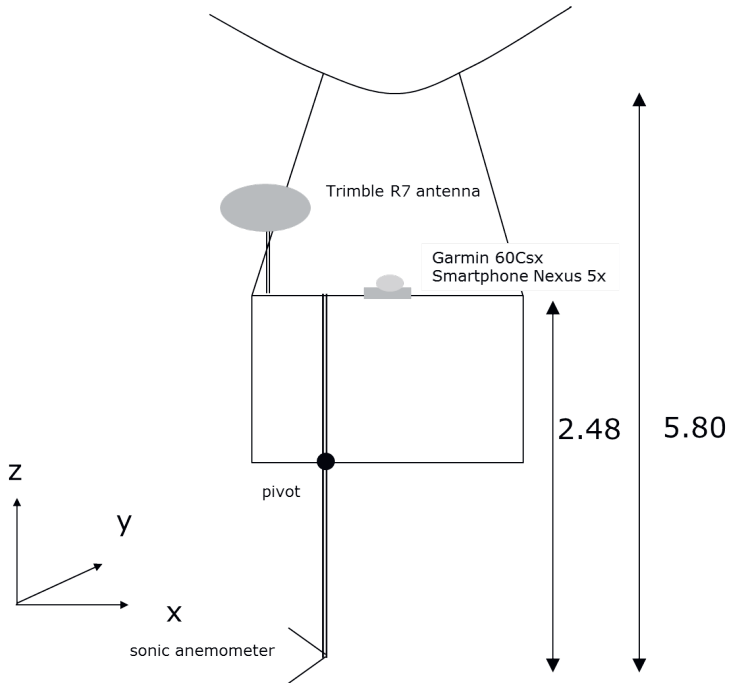


**Figure 3.1:** Rigid frame for mounting the sonic anemometer underneath the gondola



**Figure 3.2:** Sonic anemometer in operation below the hot-air balloon during the flight, one of the authors Bert G. Heusinkveld is checking the alignment of the sonic anemometer. This picture was taken from the gondola with a camera, which was mounted on a long telescopic golf ball retriever stick.

data measurements in the WGS'84 coordinate system.

The balloon is floating in a moving medium and when there is a difference in the balloon speed and the surrounding air, it will interact with it. The airflow will be deflected around the balloon which leads to a change of the relative wind speed. Batchelor (1956) describes the flow around a rigged sphere by the velocity potential:

$$\phi = U \left( r \cos\theta + \frac{R^3}{2r^2} \cos\theta \right) \quad (3.1)$$

where  $R$  is the radius of the sphere,  $r$  is the distance from the middle point and  $\theta$  is the angle with the horizontal velocity vector. The distances are given in [m]. The flow  $u(r, \theta)$  can be derived from  $\nabla\phi$  in cylinder coordinates:

$$u(r, \theta) = \left( U \cos\theta \left(1 - \frac{R^3}{r^3}\right), -\left(1 + \frac{R^3}{2r^3}\right) U \sin\theta, 0 \right) \quad (3.2)$$

The hot-air balloon has a volume of 6000 [m<sup>3</sup>] which leads to  $R=11.27$  [m]. If we take  $\theta = \pi/2$  and  $r = 1.51R$  which corresponds with the position of the SONIC in the cylinder coordinate frame, we arrive at the following expression:

$$u(r, \theta) = (0, 1.22U, 0) \quad (3.3)$$

The horizontal flow will increase with a factor of 1.22 at the relative location of the SONIC. There are uncertainties in this derivation and two remarks should be made. Firstly, we have assumed that the balloon's shape is a sphere, but a pear shape would be more realistic. Secondly, we have also neglected the presence of the suspended gondola.

### 3.3 Hot-air balloon flight during 17 May 2016

Here we describe the field experiment with a hot-air balloon equipped with instruments in the vicinity of the Cabauw meteorological tower, which is situated in the western part of the Netherlands. The area is characterized by fields, meadows and scattered villages. Southwesterly winds are predominant in this area and during the flight the meteorological conditions are typical for the time of the year. The test flight took place in the evening of 17 May 2016 from 18:45-19:30 UTC (Local Time = UTC + 2) and there were moderate westerly winds of 6 [ms<sup>-1</sup>] at 200 [m] height. The flight was during the evening transition and no significant wind gusts occurred, which was essential for a safe take-off.

In Figure 3.3 the flight of the hot-air balloon (call-sign PH-GSP) is depicted, which lasted 45 [min] and the traveled distance was 15 [km]. The average altitude was 200

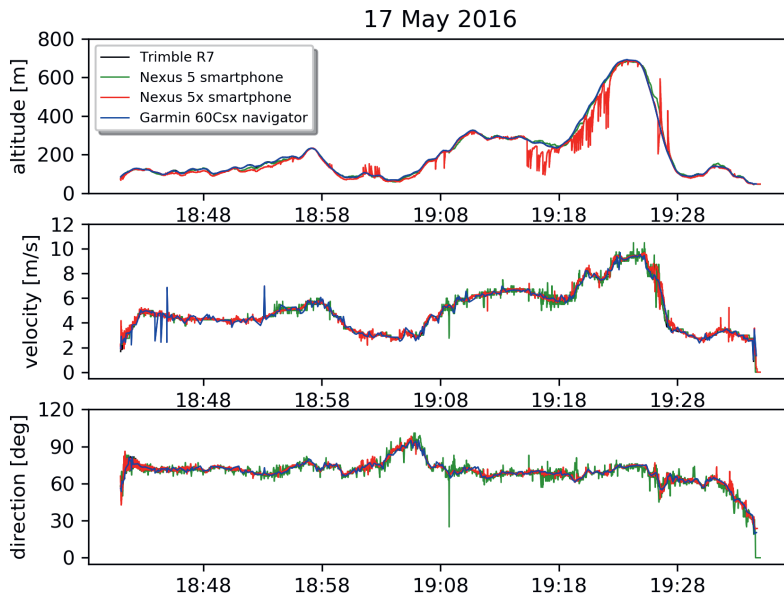
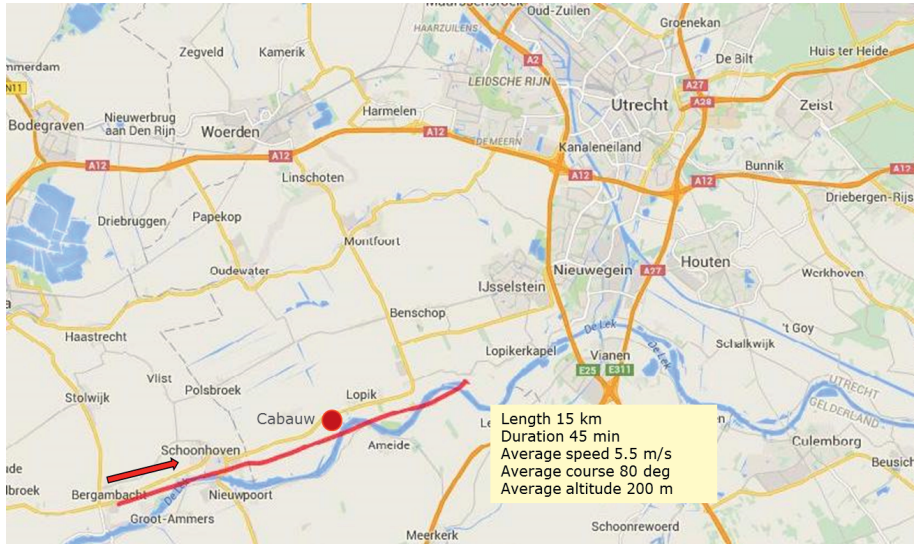


**Figure 3.3:** Hot-air balloon flight from Bergambacht to Uitweg (ground track (up) and trans-sect (below)) during 17 May 2016. In the trans-sect the altitude and velocity components of the hot-air balloon as measured from four GNSS devices are shown as a function of time.

[ $m$ ] above surface level and the ceiling altitude was 700 [ $m$ ]. The crew consisted of 7 persons, inclusive the pilot and the total weight of the gondola was approximately 700 [ $kg$ ]. The volume of the balloon's envelope was approximately 6000 [ $m^3$ ].

We took off upwind of the Cabauw site and the aim was to pass over the observatory as closely as possible. The start location was chosen using the pilot's expertise and the guidance of the KNMI duty forecasters. At 19:00 UTC the pilot changed altitude to adjust the course of the balloon more towards the Cabauw observatory. In the ABL there is a so-called Ekman layer. Due the variation of the stress, the wind vector changes with height (see Holton (1967)). Based on this principle, the wind usually turns clockwise with height (wind veers with height). This mechanism offers the pilot of a hot-air balloon the possibility to steer the aircraft to some extent. During our test flight, the meteorological conditions were not neutral. It became clear that the wind even backed with height. The balloonist was aware of this and descended slightly to find a more favorable wind which would bring the aircraft closer to the tower. An explanation for this non neutral wind profile is that a small sea-breeze front has just passed the area, which caused some baroclinicity. Also the influence of the Lek river might have had impact on the wind regime in the ABL. During the flight we followed the meandering river Lek in upstream direction and we crossed the river five times (see Figure 3.3).

During the launch the gondola was out of equilibrium relative to the balloon, underwent a shock which resulted in an oscillation. This is clearly recognized in the data of the Trimble R7 geodetic GNSS-receiver where in the beginning wiggles are observed. These wiggles are also recognized later during the flight. A Fourier decomposition of the derived speeds from the Trimble R7 data is made (Fig. 3.4). There is a peak at 0.1 [ $Hz$ ] and we have found a similar spectrum from the acceleration sensor of the Nexus 5x smartphone (not shown) and it is clear that the system balloon with gondola experienced a small pendulum motion during the flight. We have processed all the measurements to eliminate this oscillation. We realize that this oscillation might have caused turbulence which would have had impact on the measurements. We have therefore checked the amplitude of the oscillation, which appeared to be small (0.4[ $m$ ]) and could be further neglected.

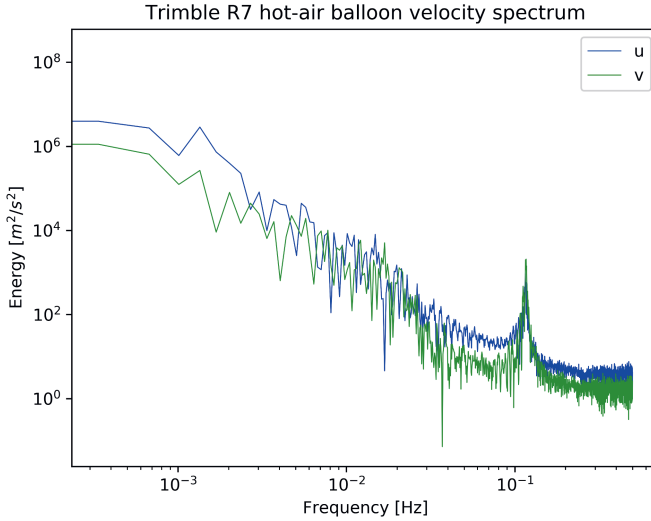


**Figure 3.4:** Velocity spectrum derived from data of the Trimble R7 geodetic GNSS receiver with a peak at 0.1 [Hz]

### 3.4 Assessment of the noise in location and speed

As stated previously in section 2b, we consider the measurements from a Trimble R7 geodetic GNSS-receiver as the reference. This instrument has also position errors, but they are an order of magnitude smaller than the other GNSS devices. In our set-up the Trimble GNSS Receiver does not deliver speed components, so the speed is calculated, based on position data only. The Nexus 5 and 5x smartphones have different sampling rates, namely 1 and 0.1 [s], respectively. The Trimble R7 GNSS-receiver data are available every 1 [s] and for a fair comparison all the data are re-sampled to 1 [s]

#### 3.4.1 Quantification of the position errors in the xyz-plane

In Figure 3.5 the time series of the position errors are shown.  $Dx$ ,  $Dy$ , and  $Dz$  are the deviations in [m] from the Trimble R7 geodetic GNSS-receiver which is the reference. The errors in the horizontal plane are smaller than the altitude errors. The position errors are not evenly distributed around the time-axis which is an

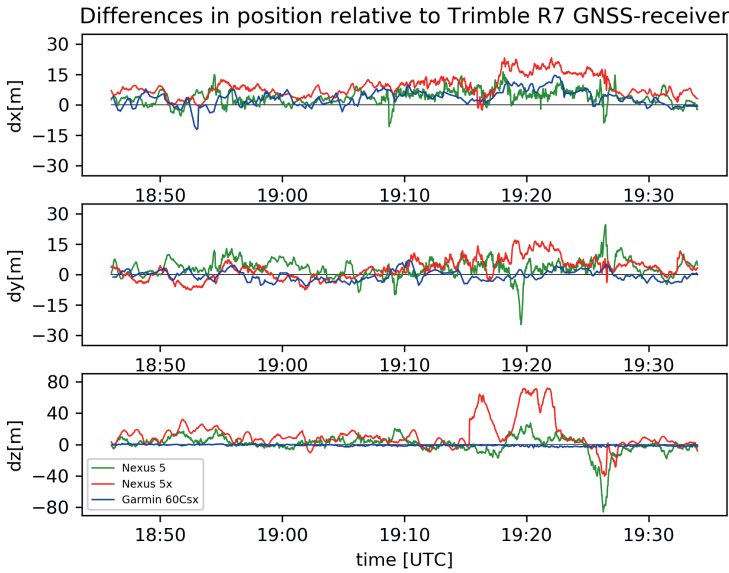


**Figure 3.5:** Time series of the 3D position errors of the smartphones Nexus 5, Nexus 5x, and the Garmin 60Csx relative to the Trimble R7 GNSS-receiver. Note that the sampling rate is 1[s]

indication of correlated noise. This becomes also manifest when we study the errors in a x-y diagram as depicted in Figure 3.6. The biases are not centered around the origin. The statistics in terms of bias and standard deviation are summarized in Table 3.1.

Now we study in more detail the vertical position noise in Figure 3.5. In the lower panel, we clearly see that the Garmin 60Csx outperforms the other devices, which is also obvious from the scores in Table 3.1. The Garmin 60Csx is a portable navigation system of the pilot, which is on board for the aircraft's safety. The Garmin 60Csx is equipped with a pressure sensor and the algorithm applies this data for the calculation of the 3D-position. It should be noted that the altitude information does not play a role in the calculation of the horizontal speed.

The largest deviations for the Nexus smartphones occur in the interval 19:13-19:28 UTC, the period of ascent to 700 [m] and the subsequent descent. The lack of a pressure sensor data could have caused these spurious data.

**Table 3.1:** Statistics of the position noise, Trimble R7 GNSS-receiver versus the smartphones Nexus 5, Nexus 5x, and the Garmin 60Csx

	dx		dy		dz	
	bias [m]	$\sigma$ [m]	bias [m]	$\sigma$ [m]	bias [m]	$\sigma$ [m]
Nexus 5	3.73	3.51	3.26	4.37	0.31	11.79
Nexus 5x	8.86	4.99	2.83	5.08	11.86	17.95
Garmin 60Csx	3.79	4.14	-0.46	2.58	-1.27	1.10

### 3.4.2 Characterization of the horizontal position and velocity noise

Now we investigate the horizontal position noise in more detail and we study how this error propagates in the derived wind components. Now we elaborate on how an error in position  $(x, y)$  is propagated in an error of the wind  $(u, v)$ . The balloon speed components are derived from the displacement of the balloon and are discretized as follows:

$$u_i = \frac{x_{i+1} - x_{i-1}}{2\Delta t} \tag{3.4}$$

$$v_i = \frac{y_{i+1} - y_{i-1}}{2\Delta t} \tag{3.5}$$

where  $x_i, y_i$  are respectively the longitudes and latitudes [deg],  $\Delta t$  is the time step[s] and  $u_i, v_i$  are the speed components [ $ms^{-1}$ ]. In Figure 3.7 the velocity error scatter plots are given, note that  $\Delta t = 1[s]$ . Now  $du$  and  $dv$  are the velocity deviations in [ $ms^{-1}$ ] relative to the velocities from the Trimble R7 GNSS-receiver data. The velocity differences have a standard deviation ranging from 0.14 to 1.01 [ $ms^{-1}$ ]. Apparently the relative positions have a smaller error than the absolute positions. To study the characteristics of the noise of the GNSS receivers more profoundly, we average the data over an increasing interval  $n\Delta t$  within the time series and for each sub-interval we calculate the variance. We know from the theory that if the variance decays according to the  $\frac{1}{n}$  curve, the noise can be regarded as uncorrelated. From Figure 3.8 it is evident that the noise is correlated over small intervals. For intervals beyond 100 [s] the decay of the noise is more according to the  $\frac{1}{n}$  curve. We repeat the above-mentioned procedure for the velocity components and from Figure 3.9 it is clear that the error is significantly smaller. The noise in the speed components is correlated for small averaging periods and beyond 10[s] the decay approaches the  $\frac{1}{n}$  curve.

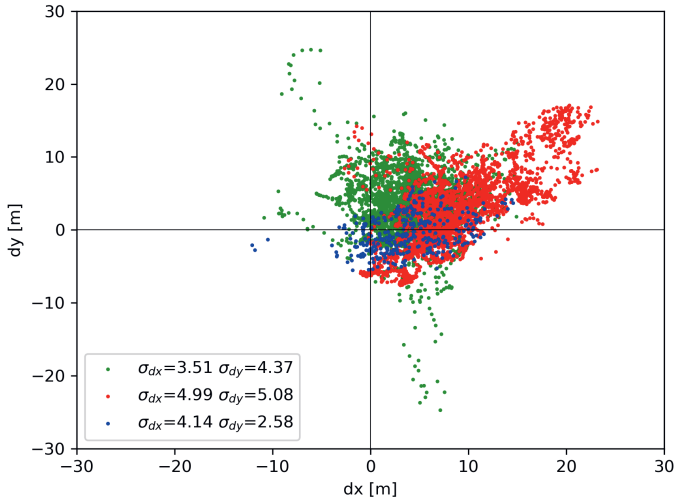


**Figure 3.6:** Horizontal position errors of the smartphones Nexus 5(green), Nexus 5x(red) and Garmin 60Csx(blue) relative to the Trimble R7 GNSS-receiver, for the same period as shown in Figure 3.5.

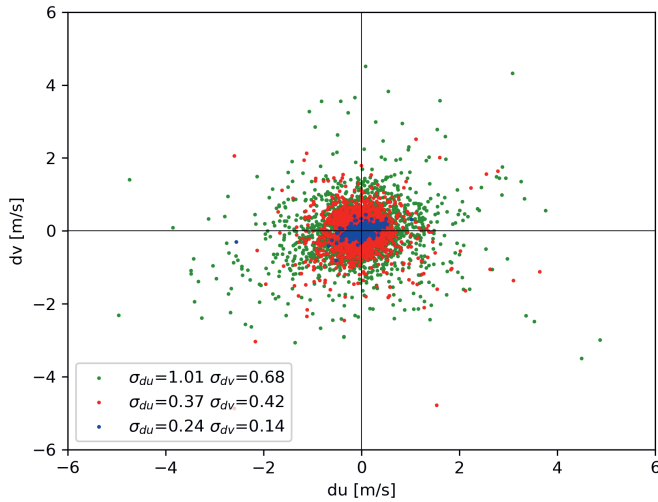


**Figure 3.7:** Velocity error scatter in the smartphones Nexus 5(green), Nexus 5x(red) and Garmin 60Csx(blue).

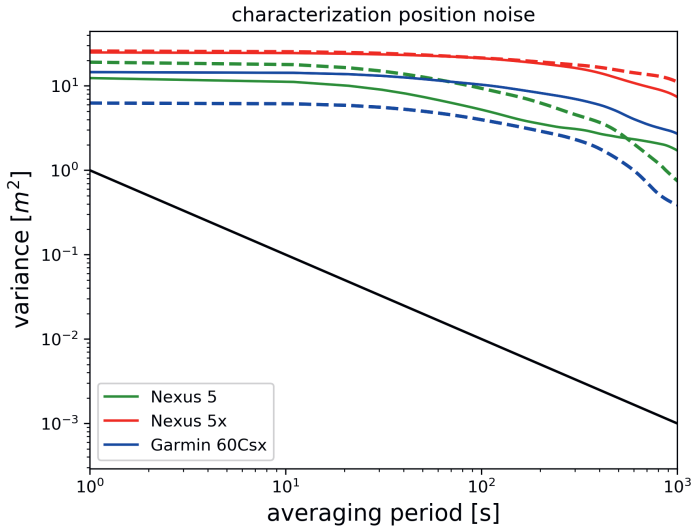


**Figure 3.8:** Variance of position errors as function of averaging time  $n$ , the solid and dashed lines correspond respectively with the position errors in x and y. The solid black line represents the  $\frac{1}{n}$  curve, which is the reference for the white noise decay.

### 3.5 Validation of hot-air balloon winds with data from the meteorological tower of Cabauw

For the comparison of the hot-air balloon wind data we selected an episode during the flight where the balloon was between the levels of the anemometers of the Cabauw tower at respectively 10, 20, 40, 80, 140, and 200 [m]. These requirements were met during 18:50 and 19:10 UTC and for this period we compare the balloon wind data with the Cabauw tower wind data (see Fig. 3.10). Because the hot-air balloon is traveling towards the Cabauw mast, we also present the distance balloon-tower in Figure 3.10. In Figure 3.10, we compare the balloon wind data with tower data, which are averaged to 600 [s]. The anemometers are calibrated and the data are corrected for flow obstruction of the mast. The hot-air balloon wind data are averaged in time to meet the same time coordinate as the mast data (600 [s]). Subsequently, the mast wind data are interpolated to the level of the

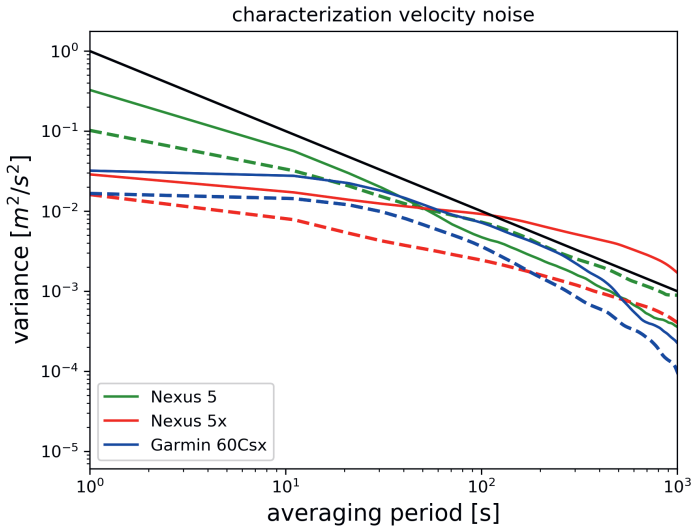


**Figure 3.9:** Variance of velocity errors as function of averaging time  $n$ , the solid and dashed lines correspond respectively with velocity errors in  $u$  and  $v$ . The solid black line represents the  $\frac{1}{n}$  curve, which is the reference for the white noise decay.

balloon using the wind shear as observed at the mast. We compare data from the Trimble R7 geodetic GNSS-receiver, the two Nexus smartphones and the Garmin 60Csx navigator. Although the horizontal distance from the hot-air balloon to the meteorological tower varies from 10 [km] in the beginning to 4 [km] at the end of the validation interval, the hot-air balloon wind data corresponds reasonably well. Deviations observed at 19:00 UTC may be related to the fact that the hot-air balloon is still 10 [km] away from the tower, but despite this horizontal mismatch the hot-air balloon wind data is in accordance to some extent with the observations. It should be noted that the hot-air balloon approached the observatory, but did not fly over the tower and the closest distance was approximately 1500 [m]. By varying the height the pilot has tried to approach the tower as near as possible. Note that the tower observations hardly vary during the depicted interval. At 19:00 UTC when the hot-air balloon has passed the small city of Schoonhoven, the wind speed decreases which is realistic; the hot-air balloon feels the wind of the increased roughness of the built up area. Further, the hot-air balloon follows the river in the upstream direction, the temperature of the water which differs from surface temperature at Cabauw might have had impact on the stability and therefore also on the wind profile.

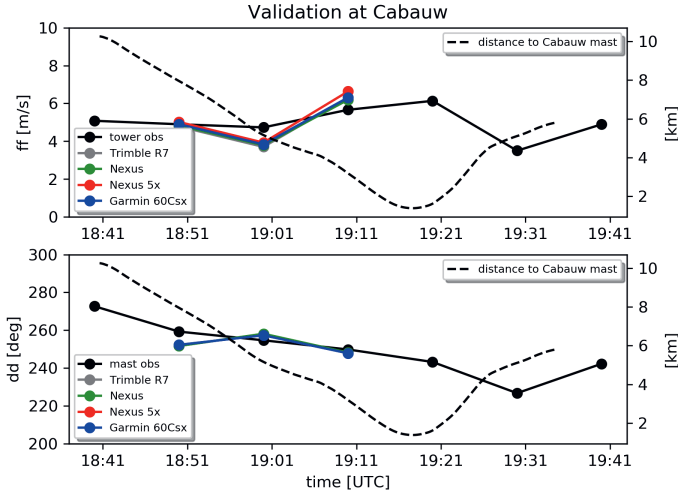


**Figure 3.10:** A comparison of hot-air balloon wind data with tower measurements at Cabauw during 17 May 2016. Note that also the distance from the hot-air balloon to the Cabauw mast is shown by the dashed line.

### 3.6 Interpretation of the SONIC data

Here we study the SONIC data which represent the relative speed of the hot-air balloon to the surrounding air. We will study the small scale variations in the relative speed in relation to the acceleration of the hot-air balloon and we will address some typical features. From the GNSS data accelerations of the balloon can be derived, which are representative for the forces on the balloon. The sonic data represent the relative speed between the hot-air balloon and the surrounding air and are a metric for the thrust on the hot-air balloon. In Figure 3.11, the measurements of the SONIC and the GNSS derived accelerations are depicted. Recall that the SONIC data have been processed as described in section 3.2.3. Note that the time series start 15 [min] after the take-off, because some time was needed to deploy the SONIC. Between 19:00 UTC and 19:18 UTC the averaged SONIC data show a negative bias in both u and v-components of respectively -0.39 and -0.27 [ $m.s^{-1}$ ]. Here we try to understand this bias.

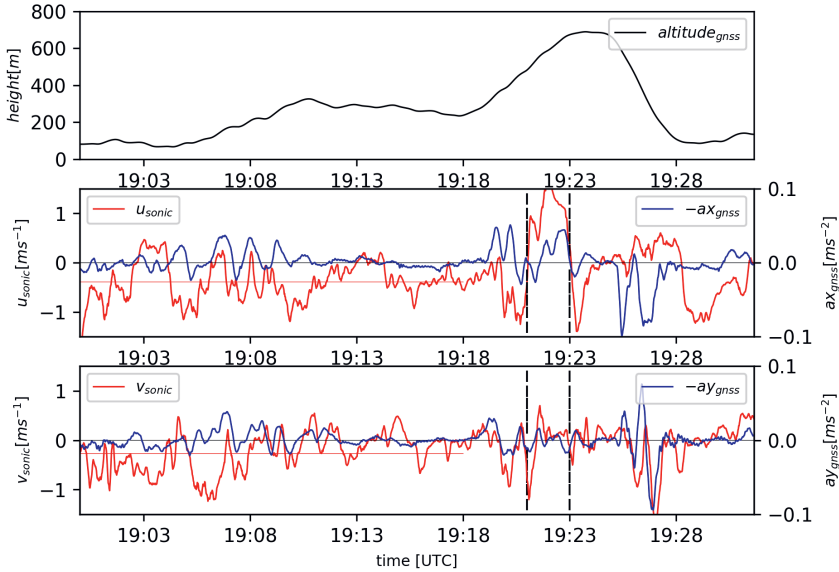


**Figure 3.11:** Processed relative winds from the SONIC (Y-axis left) and accelerations of the balloon (GNSS-receiver) (Y-axis right). Note that the average sonic speed components are  $\bar{u}_{sonic} = -0.39[m s^{-1}]$  and  $\bar{v}_{sonic} = -0.27[m s^{-1}]$  during an interval when the balloon's displacement is almost horizontal. The interval for the estimate of the a-coefficient is marked with the dashed vertical lines.

### 3.6.1 Influence of wind shear

The distance between the virtual point where the wind forces impact on the balloon and the position of the SONIC is  $18 [m]$ . Thus when a wind shear is present, the SONIC will measure a bias. To quantify the wind shear, we have applied the Cabauw mast data. The hot-air balloon flies between  $100$  and  $300 [m]$  altitudes during this period and we use the  $140$  and  $200 [m]$  levels of the mast to calculate a representative wind shear. For the u- and v-shear components we have found values of respectively  $-0.015$  and  $-0.008 [s^{-1}]$ . Applying this information we find relative speed components of  $-0.27$  and  $-0.14 [m s^{-1}]$  for the u- and v-components, respectively. For clarity we summarize the bias components in table 3.2. If we confront these values with the averaged SONIC components we notice a certain mismatch. In an attempt to explain the residual, we take a closer look at the equations of motion of the ABL and the hot-air balloon in the ABL.

### 3.6.2 Dynamic equations of a hot-air balloon in the ABL.

At first sight a hot-air balloon moves with the surrounding air. If any velocity difference occurs between the air and the balloon, the resulting thrust on the balloon will level out such a difference. The scale at which this balloon response operates can be expressed in terms of a length ( $L$ ) of the air-mass that has to pass the balloon for an  $e^{-1}$  response of the velocity decrease.  $L$  is typically 100 [m] (De Bruijn et al., 2016). Inspection of the observations taken during the hot-air balloon flight revealed however that the accelerations of the balloon, as observed with a geodetic GNSS often did not correspond to wind speed differences measured with the SONIC (see Figure 3.11). At times wind differences are observed which do not induce accelerations. This urged us to re-think the force balance of a hot-air balloon in flight. The air in which the balloon is sub-merged follows a force balance equation in which three forces play a role: pressure gradient; Coriolis acceleration; and stress divergence. For an air parcel we find in a formula:

$$\frac{dU_a}{dt} = +f_c(V_a - V_g) - \frac{1}{\rho} \frac{d\tau_x(z)}{dz} \quad (3.6)$$

$$\frac{dV_a}{dt} = -f_c(U_a - U_g) - \frac{1}{\rho} \frac{d\tau_y(z)}{dz} \quad (3.7)$$

$U_a, V_a$  are the  $u, v$  components of atmospheric flow.  $U_g, V_g$  are the  $u, v$  components of the geostrophic flow, and  $\rho$  is the density of the air parcel. Here the pressure term has been cast in terms of the geostrophic wind. The stress term  $\tau_x, \tau_y$  results from the process of vertical turbulent exchange of momentum between the air parcel and the layers above and below. In the atmospheric boundary layer in general this exchange is stronger at the lower side of the air parcel than at the upper side. This results in apparent friction and deceleration of the air parcel. A balance of forces results in which the actual wind is somewhat smaller than the geostrophic wind and backed (turned towards the low pressure). From the resulting cross isobaric flow the air gains momentum which compensates for the loss due to friction. The balloon is also subject to the pressure force and the Coriolis force, but turbulent exchange is prohibited by the canvas of the balloon. Instead there is the drag at the sides of the balloon due to velocity differences. This leads to the following dynamic equation:

$$m_b \frac{d\vec{u}_b}{dt} = \frac{1}{2} c_d \rho \pi R^2 |\vec{u}_b| \cdot \vec{u}_b \quad (3.8)$$

where the right hand side term is the drag force, further  $|\vec{u}_b| = \sqrt{(U_b - U_a)^2 + (V_b - V_a)^2}$ , where  $(U_b, V_b), (U_a, V_a)$  are respectively the speed components of the hot-air balloon and the surrounding air,  $c_d$  is the dimensionless drag

coefficient,  $\rho$  is the air density [ $kgm^{-3}$ ],  $\pi R^2$  is the cross sectional area [ $m^2$ ] of the hot-air balloon and  $m_b$  is the mass [kg] of the balloon including the payload. In equation (3.8) we recognize the a-coefficient  $a = \frac{c_d \rho \pi R^2}{2m_b}$ , which is the inverse response length ( $L$ ). Note that the a-coefficient comprises all the relevant physical properties of the hot-air balloon. For further details we refer to (De Bruijn et al., 2016). All together the momentum equation for a hot-air balloon becomes:

$$\frac{dU_b}{dt} = +f_c(V_b - V_g) - a|\vec{u}_b|\vec{u}_b \quad (3.9)$$

$$\frac{dV_b}{dt} = -f_c(U_b - U_g) - a|\vec{v}_b|\vec{v}_b \quad (3.10)$$

Note that the drag experienced by the balloon has its counterpart as a drag acting on the surrounding air. This effect is neglected in equations (3.6) and (3.7). These equations describe the air flow which is not disturbed by the balloon.

### 3.6.3 Stationary solution for a constant level balloon

Under stationary conditions the acceleration terms on the left hand side of equations (3.6),(3.7) and (3.9),(3.10) will be zero. We will show that the balloon movement will deviate from the actual wind due to the absence of the turbulent stress divergence and we will call this deviation the inertial drift. Similar to the inertial oscillation in the stable boundary layer, which may lead to the formation of the low-level jet, the vector  $\Delta\vec{U}_b = \vec{u}_b + \Delta\vec{U}_a$  (a-geostrophic balloon vector) start to turn around the geostrophic wind (Van de Wiel et al., 2010). This turning stops as soon as the thrust is in balance with the pressure - and Coriolis force. We will now solve this system of equations for the stationary condition. The force balance of the balloon reads:

$$0 = f_c|\Delta\vec{U}_b| - a|\vec{u}_b|^2 \quad (3.11)$$

and thus  $|\vec{u}_b|$  can be solved:

$$|\vec{u}_b| = \sqrt{\frac{f_c}{a}|\Delta\vec{U}_b|} \quad (3.12)$$

To calculate the a-geostrophic wind vector  $|\Delta\vec{U}_b| = |\vec{U}_b - \vec{U}_g|$  the geostrophic wind is required. The geostrophic wind is derived from pressure sensors in a 75 [km] range from Cabauw (Bosveld et al., 2014). The geostrophic wind at Cabauw is depicted in Figure 3.12 with the black line. We estimate  $|\vec{U}_b|$  by taking the balloon wind averaged between 19:00 UTC and 19:18 UTC. This is allowed, because we expect

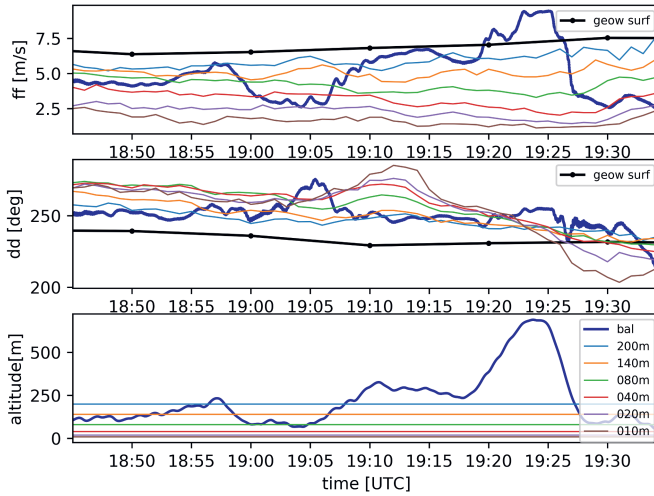


**Figure 3.12:** Tower wind measurements at fixed levels at Cabauw and the balloon wind speed based on GNSS data. Also the geostrophic wind at surface level (black line) is depicted

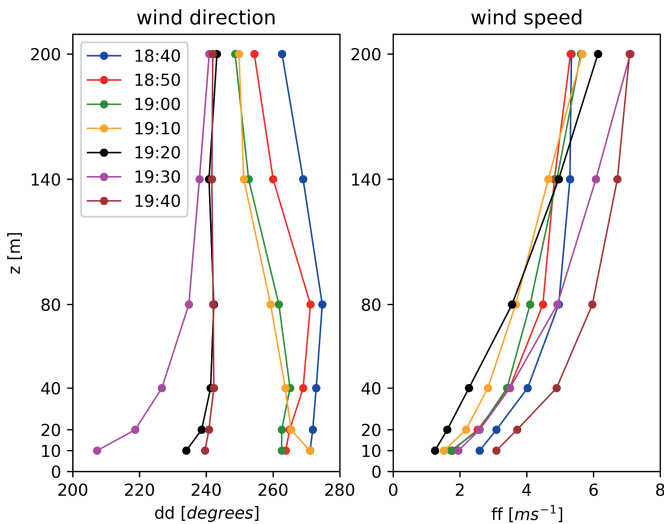


**Figure 3.13:** Tower measurements of the wind at Cabauw during 17 May 2016 18:40-19:40 UTC in a 10 [min] interval. Note the non-stationary conditions.

**Table 3.2:** Overview of the bias components in the SONIC data during 19:00-19:18 [UTC]

	u [ $ms^{-1}$ ]	v [ $ms^{-1}$ ]	$ \vec{u} $ [ $ms^{-1}$ ]
Total (SONIC measurements)	-0.39	-0.27	0.47
Shear (Tower 140-200 [m])	-0.27	-0.14	0.30
Residual	-0.12	-0.13	0.18
Inertial drift	-0.18	0.06	0.19
Residual	0.06	-0.19	0.20

that the inertial drift will be small. If we calculate the averaged a-geostrophic wind between 19:00 UTC and 19:18 UTC, we arrive at a value of  $|\Delta\vec{U}_b|=2.24$  [ $ms^{-1}$ ] and substituting this in equation (3.12), we find  $|\vec{u}_b|=0.186$  [ $ms^{-1}$ ]. This is defined in the wind vector system and if we convert this to the GNSS coordinate system we obtain  $\tilde{u}_b=-0.175$  and  $\tilde{v}_b=0.064$  [ $ms^{-1}$ ]. We have obtained a similar result by solving the differential equations (3.9) and (3.10) numerically with stationarity as a constraint. The obtained values together with the shear correction do not explain fully the systematic wind bias as observed with the SONIC (see Table 3.2). The norm of the inertial drift corresponds satisfactorily with the residual, but there is a some mismatch in the direction. One reason may be that the geostrophic wind is derived for the surface level, but we need to have it at the balloon level. Thus, the presence of a thermal wind will have an influence on our estimation of the inertial drift. A second reason is that the meteorological situation is rather complex, because the atmosphere is baroclinic and the flow is non-stationary. In general, under barotropic conditions the geostrophic wind is larger and veered to the ABL wind. Apparently this is not case here (see Figure 3.12) and if we study the mast observations in more detail we notice that from 18:45 UTC until 19:17 UTC the wind backs with height, after 19:17 UTC the levels below 80m veer with height and the upper levels slightly back with height. Due to a horizontal gradient in temperature, causing a baroclinic effect, the wind profile is obviously affected. What becomes clear is that the flow is non-stationary in contrast with the assumption under which we derived the inertial drift. This is also manifest if we study the wind profiles in Figure 3.13. In the time span of the balloon flight the wind changes considerably, which is related to the passage of a front.

Another relevant issue is the response time toward the inertial drift. The time scale  $\tau$  associated with the adjustment of the balloon can be found by observing that initially the acceleration is given by the Coriolis term of equation (3.11). The time  $\tau$  required to reach the equilibrium speed of equation (3.12) with this acceleration

is then given by

$$\tau = \frac{1}{\sqrt{af_c|\Delta\vec{U}_b|}} \quad (3.13)$$

From the solution we can deduce that it takes about 600 [s] before an equilibrium is established. This means that the balloon is adapting during the major part of the analyzed period and therefore added to the effects of non-stationary synoptic conditions, we have a further uncertainty in the validation of the inertial drift.

### 3.7 Empirical assessment of the inverse length scale (*a*-coefficient)

In the second part of the time series (Figure 3.11), the balloon raised sharply and was not in equilibrium with its driving force. In De Bruijn et al. (2016) an estimate of the inverse response length was made ( $a=0.013 [m^{-1}]$ ). Here we make an attempt to derive an empirical *a*-coefficient and we select a small period between 19:21 UTC and 19:23 UTC, because we recognize some signal in the terms of the differential equation (3.14) and (3.15). Since the timescale of the drag force is relatively short, we neglect the Coriolis terms in the differential equation (3.9) and (3.10) and arrive at:

$$\frac{dU_b}{dt} = -a|\vec{u}_b|\tilde{u}_b \quad (3.14)$$

$$\frac{dV_b}{dt} = -a|\vec{u}_b|\tilde{v}_b \quad (3.15)$$

Now we recall that  $\tilde{u}_b$ ,  $\tilde{v}_b$  are directly measured by the SONIC. The left term in the equations (3.14) and (3.15) represents the acceleration and is derived from the GNSS data. Now we discretize the differential equation as follows:

$$\frac{dU_b}{dt} = U_b^{i'} = \frac{x_{i+2} - 2x_i + x_{i-2}}{4\Delta t^2} \quad (3.16)$$

$$\frac{dV_b}{dt} = V_b^{i'} = \frac{y_{i+2} - 2y_i + y_{i-2}}{4\Delta t^2} \quad (3.17)$$

$$|\vec{u}_b^i| = \sqrt{(\tilde{u}_b^i)^2 + (\tilde{v}_b^i)^2} \quad (3.18)$$

From the right hand term the product of the wind speed difference can be estimated from the SONIC data. The index *i* corresponds with the index of the time series of

the data sets. The time series of the vectors  $|\vec{u}_b^i|, |\vec{v}_b^i|$  should obey the differential equation, for a certain  $a$ . This value can be found by minimizing the Cost function derived from the differential equation, that reads as follows:

$$F(a) = \sum_{i=0}^N \left( U_b^{i'} + a |\vec{u}_b^i| \tilde{u}_b^i \right)^2 + \sum_{i=0}^N \left( V_b^{i'} + a |\vec{v}_b^i| \tilde{v}_b^i \right)^2 \quad (3.19)$$

We used the Nelder-Mead simplex algorithm (Nelder & Mead, 1965) to find the minimum of the Cost function and this gives the optimal choice for the response coefficient ( $a$ ). By minimizing the Cost function we obtain an estimate of the response coefficient and we arrive at a value of  $a=0.012 [m^{-1}]$ . It is remarkable that the  $a$ -coefficient is so close to the theoretical value. The authors realize that this result is achieved by coincidence, because the visual match in the physical terms is not very convincing.

### 3.8 Discussion

In this paper, we have found that wind observations can be obtained from hot-air balloon flights by tracking them with smartphones. Using the telecom network, position data can be transferred to a server, and from this wind information can be obtained. The GNSS-chip in the smartphone is less accurate than the geodetic GNSS used in this study. The accuracy of the position and other features in smartphones will always be a moving target, so our findings depend very much on the used smartphones. Improvement of smartphones is expected in the combined processing of GNSS and cellular signals. Currently the API software delivers the 3D-coordinates of the position. If pseudo ranges become available, a more sophisticated mathematical model with Kalman filters can be applied in which more sensor data can be integrated. The presence of the pseudo ranges is foreseen in a coming version of the Android operating system (Banville & van Diggelen, 2016). Vertical positions are less accurate than horizontal positions. The errors in altitude do not have immediate impact on the calculated wind, because only the horizontal displacement is needed. Of course, spurious data can be removed by a time filter and a beneficial effect is expected when more sensors like pressure and temperature, are used to calculate the vertical displacement.

The second objective of this paper is the interpretation of the SONIC data in combination with the accurate geodetic GNSS-receiver measurements. Unexpected behavior of the balloon's acceleration and the relative speed between the balloon and the air turned up, which could not be described by the simple dynamic model introduced by (De Bruijn et al., 2016). In this paper we have made an effort to

improve the dynamic equation of the hot-air balloon. We realize that the reality might be even more complicated. In our newly developed model we neglected for instance baroclinic effects. Further, the pressure term, which was cast in terms of the geostrophic wind (Eqs 3.6, 3.7) is usually attributed to the large scale component related to the synoptic pressure distribution. It is likely that this term will also contain smaller scale components which may vary in space and time. This mesoscale variation will exert the same influence on both the balloon and the surrounding air. They will therefore be characterized by variations in the balloon speed but without a change in the wind speed difference between the balloon and the surrounding air.

In the ideal case the SONIC should be placed on the level, where the balloon feels the maximum drag, preferably in an undisturbed flow, but for practical reasons this was impossible. In our evening transition case the balloon is immersed in a stabilizing atmosphere and turbulent eddies are becoming smaller. Large eddies will have a similar wind effect along the total balloon-gondola system, on the contrary the smaller eddies will introduce more vertical variability in the wind. This causes uncertainty in the interpretation of the measurements of the SONIC in terms of the difference between balloon - and air speed. In summary, the effective wind speed that drags the balloon-gondola system will be different from the wind underneath the gondola at the level of the SONIC. Further the ABL is stabilizing and it is well known that the drag coefficients for laminar and turbulent flows have different values. In the transition zone the drag coefficient can suddenly drop to very small values (Munson et al. (1990)) and this process causes another uncertainty in our experiment. For the calculation of the response coefficient ( $a$ ) we have assumed that the balloon is a sphere. However, in reality the balloon is not a sphere and is moreover slightly deformed during the flight. Also the volume is not constant. The pilot can rotate the balloon or change altitude by letting escape air via (lateral) vents and warm air is released to reduce buoyancy. Therefore the shape might change during the flight and this may have impact on the response coefficient.

### 3.9 Conclusions and recommendations

Smartphones are not very accurate in absolute positions, compared to geodetic GNSS receivers. The standard deviations are ( $\sigma_x = 5m, \sigma_y = 5m, \sigma_z = 12m$ ), but the relative positions have a better accuracy. Therefore horizontal speeds which are based on relative positions and a time step of 1 [s] have standard deviations of  $\sigma_u = 0.8[ms^{-1}], \sigma_v = 0.6[ms^{-1}]$ . We have found that the instrumental noise is

correlated and averaging in time reduces the standard deviation in the speed error less quicker than that would have been the case for uncorrelated noise. However, averaging wind speeds over longer time periods will inherently lead to smaller errors. For time scales beyond 600 [s] which is a typical time step of a NWP model, the  $\sigma_u$  and  $\sigma_v$  become smaller than  $0.03 [ms^{-1}]$ .

The vertical position of the current smartphones is inaccurate, compared to the horizontal position. In future the vertical coordinate might be improved if sensors like pressure and accelerations are integrated in the algorithm that delivers the position. In this way the bias and standard deviation can be reduced.

We have conducted a field experiment with a hot-air balloon equipped with sensors on special instruments and smartphones. We have collected an unique data-set of a SONIC to measure the relative speed of the balloon to the air and a geodetic GNSS-receiver from which the accelerations of the balloon could be derived. This allowed us to study the dynamics of a hot-air balloon. By performing the flight in the proximity of the Cabauw meteorological tower we were able to give further interpretation of the atmospheric conditions during the flight. During most part of the flight a relative flow of less than  $1 [ms^{-1}]$  was recorded with the SONIC and it was peculiar that the crew hardly experienced this flow. Only during the ascending/descending excursion at the end of the flight when a relative wind speed of about  $1 [ms^{-1}]$  was observed, a slight wind sensation was felt. We may conclude that the SONIC is a more sensitive device than the receptors on the human face. The response coefficient  $a$  as estimated from theoretical considerations in (De Bruijn et al., 2016), was found to be in reasonable agreement with the empirical derived value from the current experiment.

On the basis of accurate measurements, we have seen that a hot-air balloon does not precisely follow the wind in the ABL, but reveals a slight deviation, the so-called inertial drift. For a quantitative test of the inertial drift it is important to have a balloon flight under conditions with a stationary geostrophic wind. The authors would like to underline that the meteorological conditions were more complex than foreseen. Especially the passing of a baroclinic disturbance made it difficult to validate the theory of the drifting balloon. A possible next experiment should be planned preferably under more synoptic stationary conditions.

Not every phenomenon in the data of the geodetic GNSS-receiver and SONIC is completely understood. Using accurate GNSS - and SONIC devices on hot-air balloons might be a way to detect the footprint of mesoscale variations in pressure.

It is recommended to make the developed apps available in the repositories Play

Store and App Store, so that the crowd sourcing can be initiated. In this way ABL-wind information during a leisure activity can be collected in an economic manner.

### **3.10 Acknowledgments**

Bob van de Berg from the instrumental department of KNMI is kindly acknowledged for constructing the frame of the SONIC. Wageningen University is thanked for providing staff (Martin Sikma) equipment and expertise which have been crucial for the field experiment. For the app development the help of the software engineers Jonatan Leloux and Werner Dierssen is very much appreciated. Hans van der Marel (TUD-CITG) is gratefully acknowledged for providing the Trimble R7 GNSS-receiver and the processing of the geodetic data. Bert Holtslag (Wageningen University) and four anonymous reviewers are thanked for their constructive comments on the draft of this paper.

## Chapter 4

# Opportunistic Sensing with Recreational Hot-air Balloon Flights

This chapter is based on:

Evert I.F. de Bruijn, Fred C. Bosveld, Siebren de Haan, Albert A.M. Holtslag, Opportunistic Sensing with Recreational Hot-Air Balloon Flights, *Bulletin of the American Meteorological Society*, 2021, **102**, 2, doi :10.1175/BAMS-D-19-0285.1

## Abstract

We report about a new third party observation, namely wind measurements derived from Hot-Air Balloon (HAB) tracks. At first we compare the HAB winds with wind measurements from a meteorological tower and a radio acoustic wind profiler, both situated at the topographically flat Cabauw observatory in the Netherlands. To explore the potential of this new type of wind observation in other topographies, we present an intriguing HAB flight in Austria with a spectacular mountain-valley circulation. Subsequently, we compare the HAB data with a Numerical Weather Prediction (NWP) model during 2011-2013 and the standard deviation of the wind speed is  $2.3 \text{ ms}^{-1}$ . Finally, we show results from a data-assimilation feasibility experiment that reveals that HAB wind information can have a positive impact on a hind-casted NWP trajectory.

## 4.1 Introduction

Can you imagine that a balloon trip can improve your weather forecast or even improve the safety of your balloon trip? We envision that in the near future you might be able to transfer the location data from your smartphone to a meteorological center, where it is immediately assimilated to improve your short term forecast. In this paper we discuss some components of such a system. We commence with data from HAB pilots and reveal the added value of just ordinary Global Navigation Satellite System (GNSS) location data. On board a HAB wind information can be derived and it is opportunistic, because the location data were originally not intended to measure the wind components (De Vos et al., 2020). Based on this concept we have developed an app for a smartphone that can collect data and transfer them in a timely manor to a meteorological datacentre. Subsequently the data have to be ingested in a data assimilation module of a NWP model and the updated forecast with a balloon trajectory should be disseminated via a dedicated app or the normal communication channels to the front end user.

NWP models with a horizontal resolution of 2 km or finer need detailed information for estimating the initial state of the atmosphere. Ground-based remote-sensing instruments like Sodars, Doppler lidars and Radar Wind Profilers provide already meteorological information of the Atmospheric Boundary Layer (ABL). The observational network has been extended over the years, but there are still gaps and it is not cost-efficient to extend the network infinitely.

Therefore we have commenced research to investigate data from third parties. We focus on wind-information of the ABL from recreational HAB flights. On yearly basis 6000 flights take place in The Netherlands and during an instance there might be more than 30 HAB's airborne. HAB flights take usually place during the transition period (Lothon et al., 2014) when the atmosphere becomes stable. In the basic equipment of a HAB-pilot there is a professional navigator, which is compulsory for safety reasons. Similarly to routinely launched weather balloons, the Global Navigation Satellite System (GNSS) data from consecutive positions and the elapsed time are the basis of the calculation of the horizontal wind vector. The HAB responds to changing wind with a response length of approximately 100 m. This response length which comprises the physical properties of the HAB, is derived theoretically in De Bruijn et al. (2016) and validated empirically in De Bruijn et al. (2020).

Collecting data can be achieved by using the off-line navigational data of a HAB-flight. Data are available in the archives of balloonists, but these data are not suitable for real-time application. Another method might be the application of

smartphones which has been investigated in De Bruijn et al. (2020). This method relies on the collaboration of balloonists and passengers who should carry a smartphone and apply a dedicated app during a HAB flight. This requires some effort, but the collaboration is also for their own benefit, because they might receive better weather forecasts. Alternatively the collection of data could be organized via Air Traffic Control (ATC) using a transponder. However a transponder is not a compulsory device, and installing transponders on every HAB requires a lot of effort. HAB wind data have a limited availability, but HAB flights can give complementary and detailed wind information of the ABL. Of course the HAB winds are only present in a small time-slot, but if they are applied in a more flexible 4DVAR data assimilation module, its added value can be incorporated more effectively in a NWP model. Every third party wind instrument has its pro's and con's. The HAB wind is a simple straightforward measurement technique. Data from gliders and sailplanes are more complicated, because it requires also the measurement of the relative airspeed. Wind turbines deliver wind data continuously at one location at a fixed height and their number is growing rapidly.

## 4.2 Comparison with other observations

We start with comparing HAB wind data from a flight of 18 June 2013 with observational wind data from the observatory at Cabauw (Bosveld et al. (2020)). We have used wind data from the instrumental tower and from a Radio Acoustic Sounding System (RASS) wind profiler for the comparison. The meteorological site is located in a flat rural area with scattered villages. The HAB flight started in the outskirts of the city of Utrecht at 18:23 UTC and the touch down was 1.25 hours later at 4.8 km distance from the observatory. Details of this flight can be found in De Bruijn et al. (2016).

In Figure 4.1 we show the last twenty minutes of the flight when the HAB was descending and approaching the observational site from the north. The HAB wind data are based on 30 s averages of the positions. Up to 200 m mast observations are shown, more aloft, data from the RASS wind-profiler are also presented. All the site data are available as 30 min averages. For the mast observations also the standard deviations are presented. The standard deviations are rather small, indicating that turbulence is dying out. The lower part of the HAB data is clearly affected by the local conditions like farmhouses and bushes. At the higher levels of the approach the match with observations improves, because the wind is less disturbed and representative for a larger footprint.

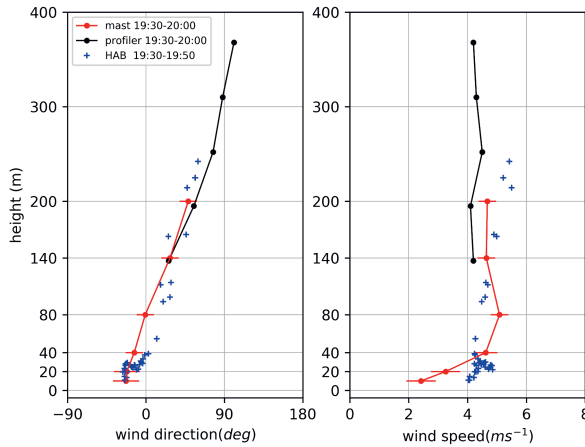


**Figure 4.1:** 18 June 2013 19:30-20:00 UTC, Comparison of HAB-wind with tower - and RASS wind profiler observations at Cabauw, The Netherlands. The solid lines correspond with wind data with a fixed horizontal position, while the moving HAB is depicted in plusses. For the mast data the standard deviation of the wind is also presented.

### 4.3 Complex terrain

This example of a HAB-wind observation was taken from a topographically flat region in the Netherlands, but would this method also work in more complex terrain? We show an intriguing example of ballooning in mountainous terrain during winter conditions. The flight took place in Austria and is shown in Figure 4.2. The take-off was at Sankt Johann (Tyrol) and the flight lasted 96 min. The surface was covered with snow (see the photograph in Figure 4.2), which prevented the development of thermals and therefore this flight could start during the course of the morning, namely at 10:18 UTC. In the beginning the HAB went in northerly direction, and as soon as the balloon had gained height, it entered a different wind regime. The HAB turned around and returned to its starting position and went further South. Descending after 1 hour, at the valley bottom southerly winds prevailed and the HAB passed through a layer with considerable wind shear. Close to the surface the HAB was again advected in northerly direction. There was a weak synoptic influence allowing local wind effects to dominate (Zardi & C.D. Whiteman, 2013). The synoptic situation showed a high pressure system centered over eastern Europe with a secondary center over northern Italy. This pressure distribu-

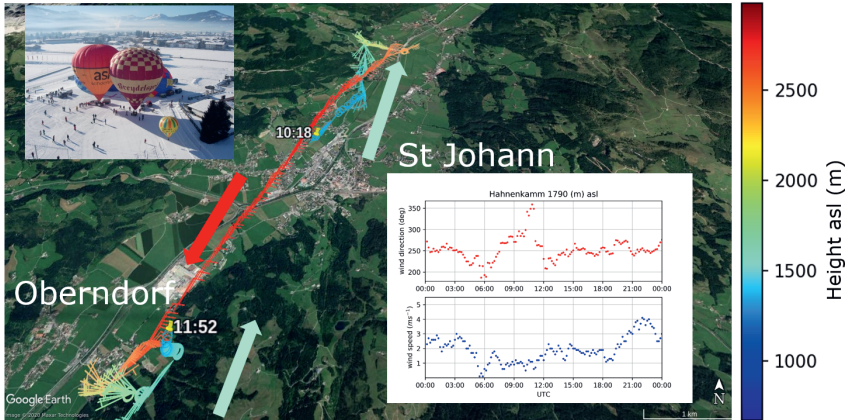


**Figure 4.2:** 16 January 2005 10:18-11:52 UTC, Mountain HAB flight near Sankt Johann (Tyrol, Austria), in the valley the winds are opposite to the winds above the inversion. The left and right subplots show respectively the take-off and the nearby Hahnenkamm AWS wind observations.

tion favored an inversion in the valleys and the valley flow direction was obviously South to North. In the upper levels the region was under a ridge with a northerly flow. The collected balloon data was in some agreement with the local AWS station Hahnenkamm (see the right subplot in Figure 4.2), which was located 10 km south south-west of landing point. For NWP models it is a truly challenge to make a weather forecast of such a complex situation, see Goger et al. (2018).

## 4.4 Validation with a NWP model

In Figure 4.3 we compare HAB-winds with analyses of the High Resolution Limited Area Model (HIRLAM) (Undén et al., 2011) during 2011-2013. These data are based on 71 flights from Dutch balloonists who have shared their flight tracks with KNMI. We have run an experimental version of HIRLAM and its characteristics are summarized in table 4.1. We have applied a bi-linear interpolation method to obtain the model data at the HAB's location. The balloon data is interpolated to 30 s averages. The data set contains HAB flights mainly from The Netherlands, but also some flights from Belgium, France and Austria. The majority of the flights took place in the summer season, but occasionally flights took also place during the winter in snow conditions. Most HAB launches were made during the cooler hours of the day, at dawn or two to three hours before sunset. At these times of the day, the winds were typically light and less turbulent, making it easier for the launch

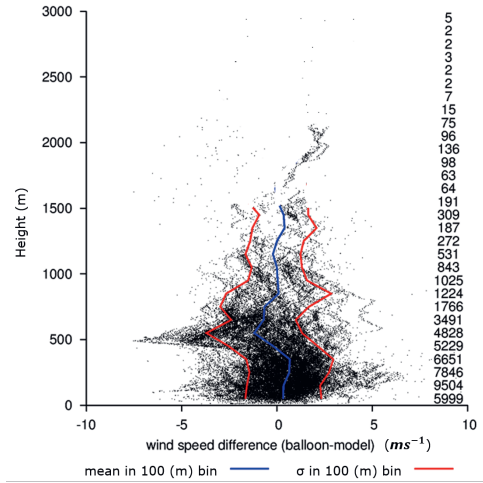


**Figure 4.3:** Validation of HAB-wind speed versus HIRLAM analyses (time window 1 hour) during 2011-2013. The data are binned in vertical bins of 100 m and per bin the bias and standard deviation are given. The sample size is depicted on the right. Only the significant statistics are plotted.

and landing of the balloon. The large biases are attributed to extreme cases like for example a thermal updraft (De Bruijn et al., 2016), which were not captured by HIRLAM. The total vertical averaged values for bias and standard deviation are respectively  $0.4 \text{ m s}^{-1}$  and  $2.3 \text{ m s}^{-1}$ .

## 4.5 Data assimilation

Based upon the above results, we take the next innovative step namely the application of HAB data in the HIRLAM model. We conducted a data assimilation feasibility study with data from another HAB flight from The Netherlands (Figure 4.4), which started in De Bilt at 15 September 2012 16:02 UTC and ended in Amersfoort at 17:03 UTC with a traveled distance of 19.5 km. At 16:30 UTC the HAB reached the ceiling of the flight which was 1428 m. At that point we see a remarkable change in direction. Apparently, the balloon has entered a layer with a different wind regime. We now study a trajectory which is based on hindcasted NWP wind fields and which is depicted by the red line in Figure 4.4. The output field frequency is 15 min and we have used the Petterson (1956) scheme to compute the trajectory. For a fair comparison, the vertical displacement is completely prescribed by the HAB. Clearly, the NWP trajectory is different and the position

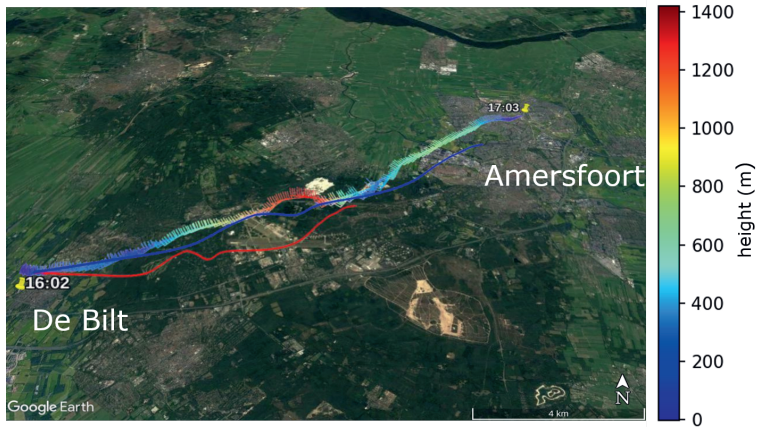


**Figure 4.4:** 15 September 2012 16:02-17:03 UTC, Trajectories from a HAB flight depicted in wind flags, calculated trajectories from NWP depicted in a red solid line, calculated trajectories from NWP with assimilated HAB data, depicted as a blue solid line.

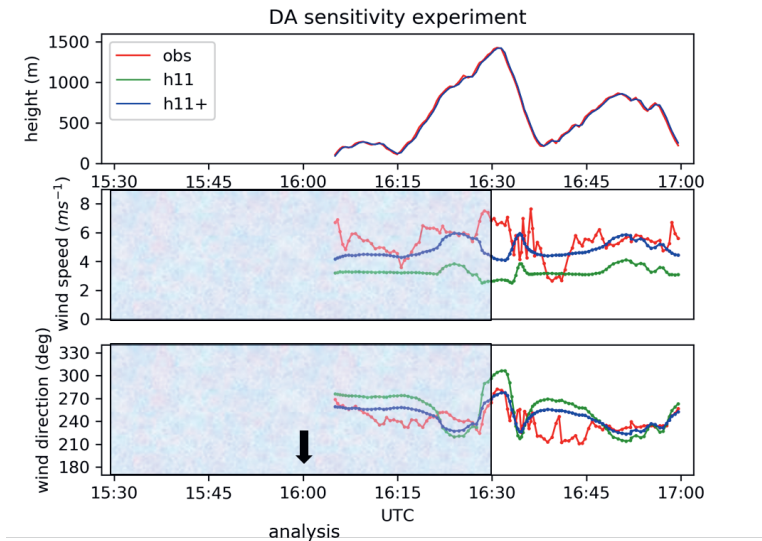


**Figure 4.5:** 15 September 2012 16:02-17:03 UTC, Transect of a HAB flight (red), NWP model (green), NWP model with assimilated HAB data (blue), the light blue box is the assimilation time window, the analysis time is at 16:00 UTC.

**Table 4.1:** Model characteristics of HIRLAM

Domain:	Europe and North Atlantic
Hor. res.:	11×11 km <sup>2</sup>
Vert. res.:	60 layers; surface – 10 hPa
Data assimilation:	every 1 h, 3DVAR
Lateral boundaries:	every 3 h, from ECMWF model
Physical parameterisation:	TKE-l, ISBA surface scheme

error at the endpoint is 8.8 km. We have assimilated the observed HAB winds during 28 min of the flight and interpolated the observations to the analysis time at 16:00 UTC. In the pre-processing we have rejected the HAB data just after take-off, because the HAB cannot move freely at that stage. With the updated run, we calculate the trajectory which is depicted in blue in Figure 4.4. The deviation at the endpoint reduces to 2.9 km. When we study the transect in Figure 4.5, again we recognize a clear improvement. Note that the adjustment is alternating between negative and positive values. Note that also outside the assimilation time window which ends at 16:30, the improvement is still present, which is encouraging. Despite this positive result, we have to make some remarks. The predictive value in this experiment is rather short, the model improvement is very local and ideally the validation should be performed over a larger area with independent observations. Nonetheless, we may conclude that HAB winds are realistic and potentially useful for data assimilation.

## 4.6 Conclusions

Thus, HAB flights provide interesting wind information in the ABL and are in agreement with other upper air observations. Comparison with HIRLAM reveals that the error characteristics are acceptable. Mountain flights could provide data from local decoupled flows embedded in a larger scale circulation which are interesting phenomena especially when such phenomena are not captured by a NWP model or by the regular observational network. HAB derived winds make sense and can be applied in data assimilation and have a positive impact on the forecast. However, the NWP model should be implemented in a rapid update cycling method and the timely availability of the new observation type is crucial for a successful application. Given the current state of the technique, it is a challenge to meet these requirements. Nonetheless, these third party observations are a welcome supplement to the existing observation network and can be used for process

studies, model validation and forecasting through data assimilation. And to answer the initial question, the answer is Yes, if you use your smartphone on board a HAB you may in future be able to improve the weather forecast.

## Chapter 5

# Wind observations from Hot-air Balloons and their application in NWP models

This chapter is based on:

Evert I.F. de Bruijn, Fred C. Bosveld, Siebren de Haan, Gert-Jan Marseille, Albert A.M. Holtslag, Wind observations from Hot-air Balloons and their application in NWP models, submitted to *Meteo. Appl.*, 2022.

## Abstract

In this paper, we report about a wind observation method based on the movement of Hot-Air Balloons (HABs). A quality assessment is carried out by comparing against wind observations at the meteorological tower of Cabauw in the Netherlands during May-September 2018 and the obtained error standard deviations are  $\sigma_u = 0.65ms^{-1}$  and  $\sigma_v = 0.69ms^{-1}$  for the measured zonal and meridional wind components respectively. Subsequent comparison against short-term model forecasts of the HARMONIE-AROME model reveals a standard deviation of  $2.5 ms^{-1}$  for the wind vector difference. From the HAB observation set a case is selected with a rapid changing wind field belonging to a small intensifying depression. The HAB wind observation is applied in data assimilation using a single observation experiment and it is shown that in a complex baroclinic situation the model state is slightly improved.

## 5.1 Introduction

Mesoscale NWP models need high spatial and temporal observational data for the analysis (initial state) and for verification. As a result, there is a great demand for high resolution observations. The Atmospheric Boundary Layer (ABL) is not frequently sampled and more data is desirable. The winds derived from Hot-Air Balloon (HAB) tracks provide useful information, as revealed by De Bruijn et al. (2016).

Planetary scales as well as small scale phenomena have to be captured adequately in a NWP model to obtain successful forecasts (Gustafsson et al., 2018). The planetary scales enter a limited area model via the lateral boundaries, which are obtained from a global model in which the limited area model is embedded. In the small domain, the initial state of the atmosphere has to be analyzed and therefore high resolution observations (in space and time) are a welcome source of information. Beare et al. (2006) discovered using a LES model that ABL observations are important for the initial state and that they improve the predicted wind profile. The morning and evening transitions are flow regimes which are not fully understood and more measurements are needed (Lothon et al., 2014).

Wind lidars (Knoop et al., 2021) can provide wind profiles at one location, unmanned aircraft (Lappin et al., 2022), (Rautenberg et al., 2018) deliver ABL data on a larger spatial scale. Air traffic provides a huge amount of wind data (Petersen, 2016), (De Haan, 2011). The data have a good time resolution, but they are concentrated in flight corridors and the ABL is hardly sampled. Only in the vicinity of airports profiles can be obtained. Satellites, like for instance Aeolus (Rennie et al., 2021) provide wind information on a global scale, i.e. transects of wind information along a swath but they lack resolution in the ABL.

More observations are needed for a better understanding of ABL turbulence. During the evening transition the convective ABL transforms in a neutral - and subsequently in a stably stratified ABL, during the morning transition this process is reversed. Scaling variables like for example the buoyancy flux are key in ABL parameterizations. The scaling variables change and the turbulence scheme can not adequately handle the different flow regimes. For instance too much mixing will not represent sharp gradients of low level jets (Bosveld et al., 2014).

Sun et al. (2022) and Nielsen-Gammon et al. (2007) have shown that local ABL wind observations have a positive impact on the analysis of mesoscale models. So far wind measurements from HAB tracks have never been assimilated in NWP models and a feasibility study is recommended.

In this paper, we want to assess the quality of HAB observations. We also want to know if they can help to detect and solve model deficiencies. Finally, we commence with a study on the feasibility of data assimilation of the HAB data. We investigate if this is technically possible and if HAB wind can push the NWP model in the right direction.

Obviously weather balloons can be applied to obtain more observations, but they are expensive and infrequently launched at sparse locations and remain relatively short in the ABL. On the contrary a HAB is a low cost observation and remains in the ABL all the time. HAB derived wind is a typical crowd sourced observation, because HABs are not primarily launched for gathering wind information. In fact, it is a leisure activity that also can provide useful wind data.

In section 5.2 we describe the high quality Cabauw mast wind measurements and the HAB wind observations and we compare them with each other. We study the HAB wind error and investigate how this error behaves as function of distance to the Cabauw tower. Subsequently we give an overview of the HARMONIE-AROME model in section 5.3 and we explain the pre-processing of the HAB data which is necessary for comparison with a NWP model. In section 5.4 we firstly validate the HARMONIE-AROME model with Cabauw wind mast data, which provides the reference. Then secondly, we repeat the procedure with HAB wind data. In section 5.5 we elaborate on a case-study which took place during the pre-conditions of approaching severe weather. The impact of a single HAB wind observation is studied in section 5.6 by applying a special data assimilation set-up. Subsequently in section 5.7 we discuss all the obtained results of this paper and finally conclusions are drawn in section 5.8.

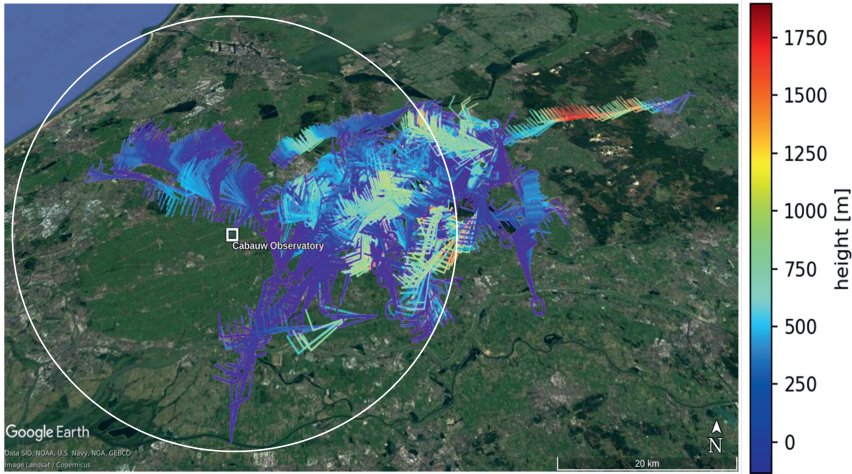


**Figure 5.1:** Map of the observation set of HAB flights during May-September 2018, maximum height is 2000 *m*. The circle is centered at Cabauw and has a radius of 30 *km*. The wind data are depicted as flags and one shaft corresponds with 5  $ms^{-1}$ .

## 5.2 Observations

### 5.2.1 Cabauw wind observations

The Cabauw meteorological tower is located in the western part of the Netherlands (51.971 N, 4.927 E) in a predominantly rural area (Bosveld et al., 2020). In the north there are scattered farmhouses, in the east there is the village of Lopik and the other sectors comprise open fields and the river Lek. The average roughness length is 0.15 *m*. Cup anemometers and wind vanes are mounted at respective heights of 10, 20, 40, 80, 140, 200 *m*. The accuracy of the cup anemometer is 1% for wind speeds (or 0.1  $ms^{-1}$  for low wind speeds) and is less than 3 degrees for wind directions of the wind vane. Precautions are taken to avoid large flow obstruction from the 213 *m* tall mast and the main building. The response length of the cup anemometer is 3 *m*, which means that air has traveled 3 *m* before 63% of a step-wise wind change has been adapted. In the Cabauw data-set we have selected time-slots which corresponded with the begin and end time of the HAB trajectories. The wind tower data are available as 5 minutes averages, which corresponds with the processed time resolution of the HAB wind data (De Bruijn et al., 2020).

### 5.2.2 HAB wind observations

Our data-set consists of 90 HAB flights during the months May-September 2018. We have sent an email to balloonists with a request of HAB flight data from the surroundings of the Cabauw mast. Their responses are the basis of our data set and basically the HAB data are Global Navigation Satellite System (GNSS) data from the pilot's navigator (Figure 5.1). Two successive positions in combination with the time interval deliver the balloon ambient air velocity (De Bruijn et al., 2016). The accuracy of the measured position depends mainly on the constellation of the GNSS satellites. If we average in time (5 *min*) the typical values for the standard deviation in the horizontal and vertical plane become 2.5 *m* and 30 *m*, respectively (De Bruijn et al., 2020). Note that we neglect the altitude difference between the GNSS-receiver in the gondola and the center of mass of the aircraft. A HAB is a large body with substantial inertia and does not respond immediately to a changing wind. In De Bruijn et al. (2016) a response length for a HAB has been derived and for an averaged sized HAB the response length is approximately 100 *m*, meaning air has to travel 100 *m* along the HAB before 63% of a step wise wind change has been adapted. With an initial difference of 2  $ms^{-1}$  this takes about 5 *min*, see (De Bruijn et al., 2016).

For the present study, a subset is defined by a circular area with a 30 km radius centered at the location of the Cabauw mast. The start location can be inside or outside this zone and is determined by the balloonist. A part of the flight should be in the circular area. A good start location has no tall obstacles with an undisturbed wind. The pilot makes an estimate of where he could possibly land using predicted winds, the payload and the amount of fuel. A favorable landing place is an uninhabited area far away from power lines, (rail)roads and inland waters. The flights commence in the evening around 18:00 UTC and the duration of the flight is on average between 60 and 90 *min*.

In Figure 5.2 we see that HAB flights are not occurring every day and gaps are recognized. HAB flights can only take place when the weather conditions are favorable e.g. a stabilizing ABL with light winds, no wind gusts, clouds, and rain. Note that most of the flights take place in July and August, typical months characterized by calm weather and a long daylight period. Ideally, the HAB flights should have surpassed the Cabauw site.

### 5.2.3 Assessment of the HAB error

Now we compare HAB and the Cabauw winds and investigate how the deviation between the HAB and the Cabauw mast wind behaves as a function of distance

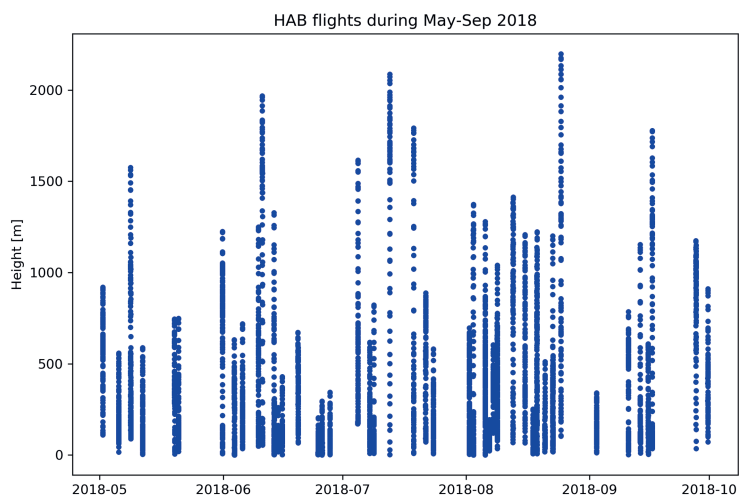


**Figure 5.2:** Observation set of HAB flights showing the vertical range during May-September 2018 in an area with a 30 km radius around Cabauw. Note that the gaps in time are related to not suitable flying conditions.

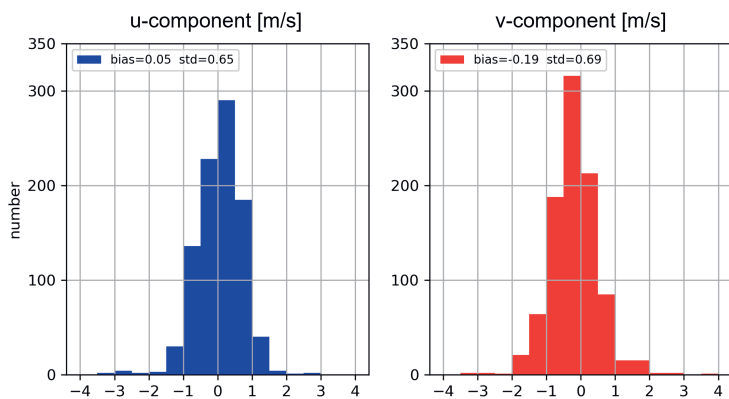


**Figure 5.3:** May-September 2018, distribution of the wind error (HAB - Cabauw mast) in an area with a 30 km radius around Cabauw.

**Table 5.1:** HAB errors as function of distance to the Cabauw mast

distance ( <i>km</i> )	$\sigma_u(m s^{-1})$	$\sigma_v(m s^{-1})$	N
00-15	0.40	0.45	440
16-30	0.60	0.80	487
31-45	1.20	1.50	221

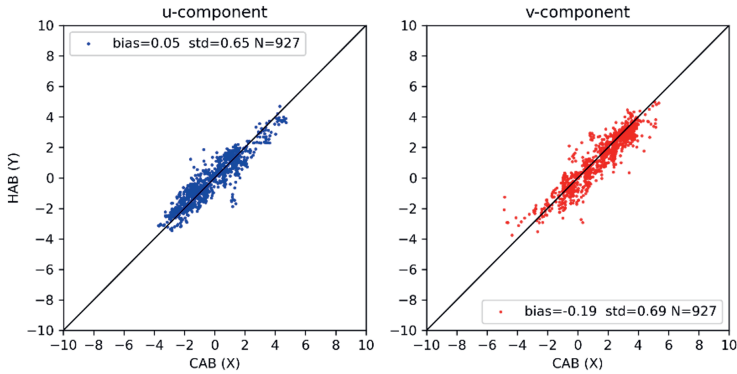
to the Cabauw mast. As a first step, the mast wind observations are vertically interpolated to the HAB elevation. We have selected those HAB observations which are in the range of the 213 *m* tall mast. In an area with a radius of 15 *km* the standard deviations of the difference between the zonal (u) and meridional (v) wind components measured by the Cabauw mast and HAB are rather small:  $\sigma_u = 0.40 \text{ m s}^{-1}$  and  $\sigma_v = 0.45 \text{ m s}^{-1}$ , but the sample size N is also small, namely N=440. In order to increase the sample size, we decide eventually to enlarge the radius to 30 *km*. The standard deviations increase slightly  $\sigma_u = 0.65 \text{ m s}^{-1}$  and  $\sigma_v = 0.69 \text{ m s}^{-1}$ , but the number of observations becomes twice as much (N=912). In Figure 5.3 the frequency diagram depicts the distribution of the HAB-Cabauw wind component differences. These differences are small in general and the largest difference is just beyond  $-3 \text{ m s}^{-1}$ . In Figure 5.4 the HAB and Cabauw wind observations are presented in a scatter diagram. The cloud of points is close to the 1-to-1 line, which means that the uncertainty in both observational systems is small. Both systems are sampling a neutral-stable ABL with a rather homogeneous wind field. Further the maximum u,v components are not beyond  $6 \text{ m s}^{-1}$ , which confirms the light wind regime.

Table 5.1 shows that part of the wind error can be attributed to the distance between HAB to the Cabauw mast; the error increases with increasing distance. As the uncertainty in the Cabauw cup anemometer wind is substantially smaller, the estimated errors in the first bin (0-15 *km* distance) provide a best estimate of the HAB error, for larger distances the total error is the summation of the HAB error and wind variations.

## 5.3 NWP model

### 5.3.1 HARMONIE-AROME

The main characteristics of the HARMONIE-AROME model (Bengtsson et al., 2017), are summarized in Table 5.2. A 3D-Var Data Assimilation (DA) scheme is used to assimilate conventional observations from synops, buoys, ships, radioson-



**Figure 5.4:** HAB flights as depicted in Figure 5.1, but now cross validated with mast observations at Cabauw (the Netherlands) during May-September 2018.

des and observations from aircraft and satellites which are available in the model domain. In a 3D-Var DA scheme, it is assumed that all observations have been measured at the analysis time. This is generally true for conventional observations. However, aircraft and satellite observations are asynoptic, introducing a time shift between observation and model background state (Marseille & Stoffelen, 2017). This timing error can be mitigated by choosing a narrow time window or can be resolved by using a 4D-Var DA scheme which is currently only available in research mode. Note that HAB observations are also asynoptic.

HARMONIE-AROME is embedded in the global ECMWF model and it receives large scale information via the lateral boundaries. As such the model benefits indirectly from the world wide satellite observations used by the ECMWF model (Bauer et al., 2015). HARMONIE-AROME has a boundary layer scheme that is based on the evolution of the Turbulent Kinetic Energy (TKE) equation (Lenderink & Holt-slag, 2004). In 2.5 km models, like the non-hydrostatic HARMONIE-AROME model, the spatial scales smaller than approximately 7 times the model grid size i.e. 20 km are not resolved (Skamarock (2004), Mile et al. (2021)) and to account for them, they have to be parameterized and ideally the model departure should not contain scales smaller than 20 km.

In this paper we use only the model background state which is the forecast of the previous assimilation cycle with a lead time equal to the cycling time or assimilation

**Table 5.2:** Model characteristics of the non-hydro-static HARMONIE-AROME

Domain:	Europe and North Atlantic
Horizontal grid:	2.5×2.5 km <sup>2</sup>
Vertical discretization.:	65 layers; surface – 10 hPa
Data assimilation:	every 3 h, 3D-Var
Lateral boundaries:	every 3 h, from ECMWF model
Turbulence:	TKE-1 (Lenderink & Holtslag, 2004)

window length. Statistics of observations minus background, shortly denoted as (O-B) is an important diagnostic for NWP models to check for model and/or observations errors. Biased observations are detrimental for data assimilation and should be removed. We have chosen a model set-up with a cycling time of 3 hours, which means that every 3 hours the analysis takes place where observations and the +03 hours forecast are merged to a model analysis, which is the initial state for the next cycle. Note that we have used a hind-cast experiment, which means that all observations are available for data assimilation and forecasting. We have used background information (+03h forecast) to validate the observations and to trace back biases. Note that the HAB and Cabauw observations in our study are not assimilated in the HARMONIE-AROME model, which prevents an incestuous comparison between model and observations.

### 5.3.2 Pre-processing of the HAB data

The HAB data have to be processed before they can be used for NWP model validation and data assimilation. Now we describe which steps have to be taken. HAB observations can be considered as a sequence of point observations. and consist of three dimensional coordinates and a timestamp. The coordinates are referenced to a spheroid of a geographical coordinate system. A spheroidal height is a geometric quantity and does not have a physical base and may fall above or below the actual earth surface. Therefore the spheroidal heights have to be converted to gravity-related elevations. This is usually done in the balloonist’s navigator. Subsequently, the elevations have to be merged into the hybrid coordinate system of HARMONIE-AROME (Bengtsson et al., 2017). The model levels are defined by the a- and b-coefficients, and the surface pressure. The vertical plane in the hybrid coordinate system is defined as follows

$$P_i = a_i + b_i \cdot P_s \tag{5.1}$$

$P_i$  is the pressure at model level  $i$ ,  $a_i, b_i$  are the coefficients which determine the closeness of the system to  $\sigma$ -coordinates ( $a_i=0$ ) or p-coordinates ( $b_i=0$ ) and  $P_s$  is

the surface pressure. The coordinate system is non-orthogonal and terrain following and the vertical spacing is defined with 15 levels below an elevation of 2000 m. The model levels which are expressed in pressure coordinates using equation 5.1 have to be transformed to  $z$ -coordinates. To achieve this we assume a temperature and humidity profile of the standard atmosphere as proposed by (Holton, 1967) and we integrate the thickness equation

$$\Delta Z = -\frac{RT(1 + 0.61q)}{g_0} \ln\left(\frac{P}{P_s}\right) \quad (5.2)$$

to obtain the required elevation.  $R$  is the gas constant,  $T$  the average layer temperature,  $q$  the specific humidity,  $g_0$  the gravity acceleration at surface level,  $P$  the pressure,  $P_s$  the surface pressure. The advantage of using the standard atmosphere is that observations and NWP output are not mixed, which avoids correlated errors. Alternatively profiles of temperature and humidity from the NWP model could have been used, which would give a better estimate of elevation, accepting the possibility of correlated errors. The HAB data have a high temporal resolution. In our data-set there are flights with a sampling rate of 4 s and to reduce the noise of GNSS positions the data are averaged to 5 min see (De Bruijn et al., 2016). Subsequently, the HAB observations are interpolated to the model levels. The pre-processing is completed with the elimination of the measurements below 10 m. Lower observations are erroneous, because a HAB usually stops by being dragged over the ground.

## 5.4 Validation of HARMONIE-AROME applying Cabauw mast - and HAB wind data

At first, the Cabauw tower observations are compared with HARMONIE-AROME and subsequently, the exercise is repeated with the HAB winds instead. We recall that the verification period is May-September 2018 and the timestamps are identical to the HAB observation data-set. The Cabauw validation can be regarded as a reference validation. In Figure 5.5 we compare the first guess model state (+03h forecast) with the mast observations. At the lowest levels (10, 20 m) the bias of the u-component is negative, more aloft it becomes almost zero. The v-component shows a positive bias which increases with height. This can be explained by the fact that the mast observations especially the ones at the lowest levels are not representative for a 2.5 km grid.

Next we focus on the HAB data. The HAB winds have varying coordinates and are only present during a flexible time-slot of about 90 minutes. HAB flights usually

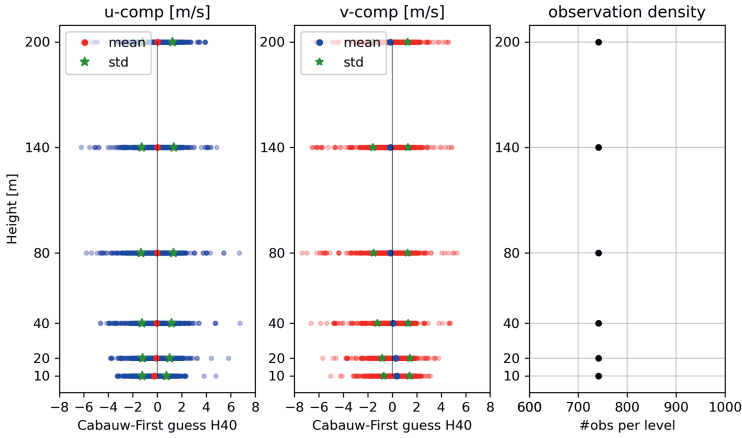


**Figure 5.5:** (O-B) statistics of Cabauw tower wind observations (O). The background (B) is the HARMONIE-AROME +03 forecast of the previous run. The standard deviations are depicted in green stars and the biases are depicted in red and blue dots for the zonal and meridional wind components respectively.

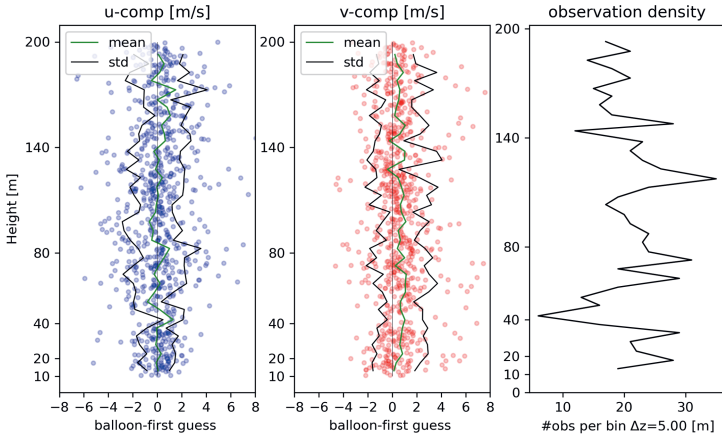


**Figure 5.6:** (O-B) statistics of HAB wind observations for altitudes lower than 200 *m* in a 30 *km* radius around Cabauw. The standard deviations are shown in the black solid lines, the biases are shown in green solid lines.

occur when the atmosphere is changing from unstable to stable and vice versa. In Figure 5.6 the +03h forecast (background) is compared with the HAB winds in the same vertical range as the Cabauw observational tower. The data are binned in vertical intervals of 5 *m* and per bin the bias and standard deviation are calculated. The number of observations per bin are presented in the right panel. Because the HAB observations are from a moving platform, the land surface characteristics vary along the trajectory, for instance land use, albedo and roughness length. These heterogeneity's are also defined in the NWP model context, but due to the limited grid box size not every detail is described. This has impact on the wind and this deviation is the so-called representation error.

Also in Figure 5.6 we find a slight positive bias in the v-component and an negligible bias in the u-component. The mean bias of the wind vector is  $0.5 \text{ ms}^{-1}$  and the mean standard deviation ( $\sigma$ ) is  $2.5 \text{ ms}^{-1}$  and it is encouraging to see that other wind observing systems show similar errors. For example De Haan (2011), De Haan (2016) showed that the accuracy of wind observations derived from an air traffic control surveillance radar (Mode-S EHS) were around  $2.5 \text{ ms}^{-1}$ , when compared to radiosonde and NWP data. Houchi et al. (2015) compared radiosondes with the ECMWF model and found similar values in the ABL. Ingleby & Edwards (2018) compared radiosondes observations in Germany during the summer of 2018 and found a Root Mean Square Error (RMSE) values of  $2.5 \text{ ms}^{-1}$  for heights from 0-2000 *m*.

In Figure 5.7 we present the complete HAB data-set, including the observations at heights above the Cabauw tower, and including those at larger distance than 30 *km* from the Cabauw tower. The maximum data density per bin is at 120 *m*, because this is the cruising height where the balloon is safe from obstacles like trees and power-lines and where the passengers in the gondola still can enjoy the scenery below.

The height averaged bias is  $0.5 \text{ ms}^{-1}$  and the height averaged standard deviation ( $\sigma$ ) is  $2.5 \text{ ms}^{-1}$ . We also recognize a varying bias with height, which was also present in the profile of the restricted area (see Figure 5.6). This variation of bias in height was also noted by De Rooy & de Vries (2017). They discovered that the TKE scheme was under performing in weakly stable conditions. The wind speeds were overestimated and this could be resolved by allowing more mixing.

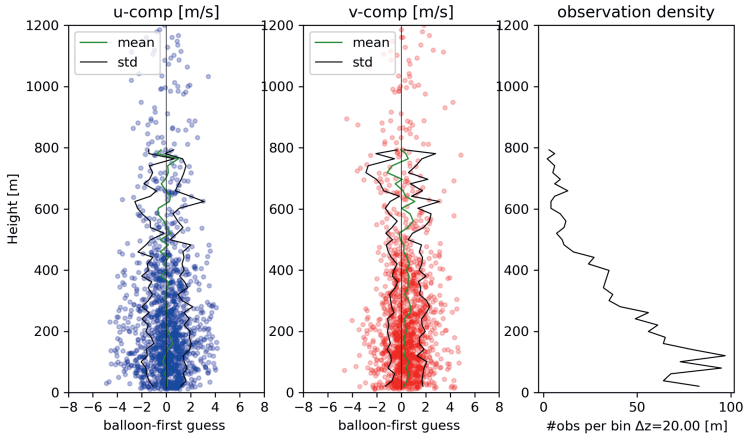


**Figure 5.7:** (O-B) statistics of all available HAB data in the Netherlands during May-September 2018. Bias and standard deviations of the wind components are shown as long as they are significant.

## 5.5 Case study: Small low pressure area with rapid changing wind fields

Overall statistics as presented in the previous section may hide the characteristics of extreme events. In this section we focus on such a case which are the pre-conditions of adverse weather. During 07 August 2018 in the late afternoon, there was a small low pressure system in the southern part of the North sea, which deepened and moved in northeasterly direction over the Netherlands. The wind changed gradually in strength, but the wind direction remained constant during the HAB flight. The HAB took off in Buren (36 km from Cabauw) in quiet conditions, see Figure 5.8. After taking off there was immediately considerable wind shear in terms of wind direction. This was probably caused by local conditions and by the fact that wind usually veers with height (De Bruijn et al., 2016). Note that initially the HAB speed was lower than the predicted wind speed, see Figure 5.9. More aloft the HAB moved in westerly direction with a velocity of  $2 \text{ ms}^{-1}$ . Later during the flight, the wind started to increase, which was not predicted by the model.

In Figure 5.9 we show the HARMONIE-AROME wind data interpolated to the HAB trajectory. For the model data, between 18:38 UTC and 18:52 UTC, there is a small increase in  $u$  and a large decrease in  $v$  which implies the wind direction has backed. A similar pattern (increase in  $u$ , decrease in  $v$ ) is visible in the HAB



**Figure 5.8:** 07 August 2018 17:51-19:02 UTC, HAB flight (11 km) Buren-Culemborg (left hand side of the picture). Note that the raw HAB data are depicted.

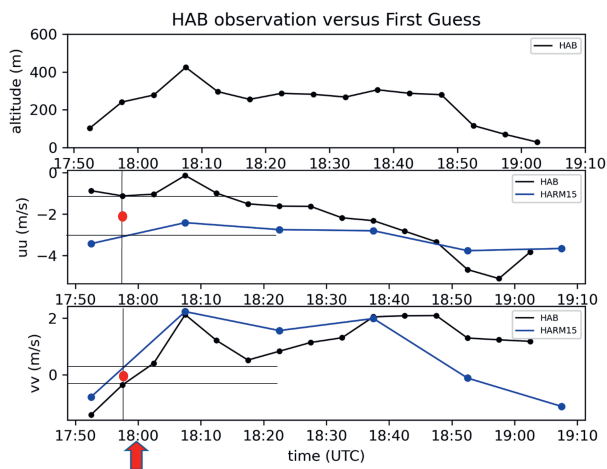


**Figure 5.9:** 07 August 2018, Buren-Culemborg, HAB wind observations versus the First Guess (2018080715 +03h), only the wind observation at 17:57 UTC (red arrow) is assimilated. At that time  $(O-B)=2$  and  $(O-B)=-0.8$  for respectively the  $u$ - and  $v$ -component. The impact of assimilating the HAB observation is represented by the red dots.

data from 18:48 UTC to 18:52 UTC. So it is obvious that both sets of data do show a change in direction. Of course, the HAB is descending at this time, so this is exactly what we would expect due to surface roughness/drag (even without any change in the geostrophic wind direction). The change in direction is also visible in Figure 5.8 at the point where the balloon drops below 200 *m*. Eventually, the balloonist was forced to land on the outskirts of Culemborg (25 *km* from Cabauw), fearing a further increase of wind speed. At the Cabauw mast at 200 *m* height at 21:00 UTC a wind speed of more than 10 *ms*<sup>-1</sup> was measured, which confirmed that the pilot has made the right decision. It is clear that HARMONIE-AROME was not able to pick-up the right position of this depression, resulting in erroneous wind fields, which was already foreseen in the large O-B values of this case.

## 5.6 Study of analysis impact

A question that arises is whether assimilation of observations from HABs can draw the model to the actual atmospheric conditions. From data assimilation theory, the 3D-Var analysis equation reads as

$$J = (\vec{X} - \vec{X}_b)^T B^{-1} (\vec{X} - \vec{X}_b) + (\vec{Y} - H(\vec{X}))^T R^{-1} (\vec{Y} - H(\vec{X})) \quad (5.3)$$

$\vec{X}$  is the model state in terms of the state variables (u,v,t,q),  $\vec{Y}$  are observations,  $B$  is background matrix,  $R$  is the observation matrix and  $H(\vec{X})$  is the observation operator. The “apriori” information is the previous model run, valid on the analysis time, the model background ( $B$ ). The challenge in data assimilation is to find the optimal analysis  $\vec{X}_a$  field that minimizes a (scalar) cost function, where the cost function is defined as the distance between  $\vec{X}$  and the background  $\vec{X}_b$ , weighted by the inverse of the background error covariance  $B$ , plus the distance to the observations  $\vec{Y}$ , weighted by the inverse of the observation error covariance  $R$ . The minimum variance solution is

$$\vec{X}_a = \vec{X}_b + K(\vec{Y} - H(\vec{X}_b)) \quad (5.4)$$

where  $K$  is defined as

$$K = BH^T [HBH^T + R]^{-1} \quad (5.5)$$

$K$  is called the Kalman gain matrix which determines the spatial structure of the increment and the relative weight given to the observation and background in the analysis. A complete data assimilation experiment requires a 4D-Var DA system and a large sample to demonstrate the statistical significance of the results. This is outside the scope of this paper. Instead, we will focus on the impact of a single

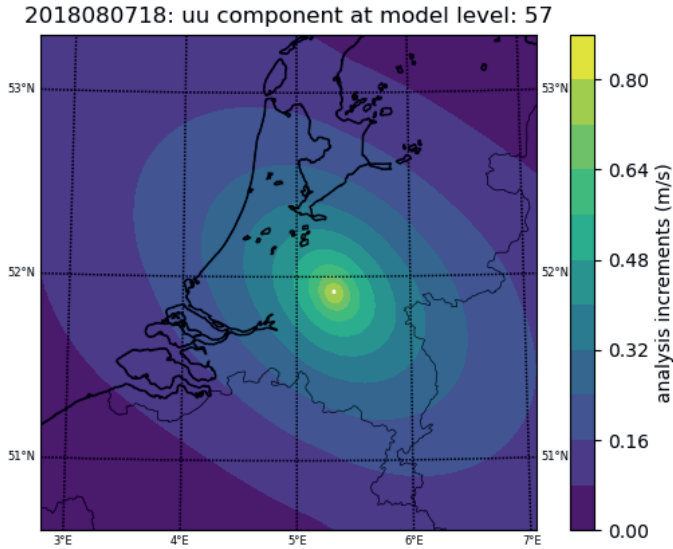


**Figure 5.10:** 07 August 2018 18:00 UTC, u-component increment (A-B). The dot corresponds with the location of the observation at 17:57 UTC, the pressure altitude is 247 m and the closest model level is 57.

wind vector observation from a HAB on the model state and discuss the need for a more extensive impact study.

For the single wind vector experiment, we used the three-dimensional variational (3D-Var) assimilation system, operational at KNMI. We focus on the case-study as presented in section 5.5. In 3D-Var all observations are assumed to be measured at analysis time, i.e., 18:00 UTC in our case. From Figure 5.8, many wind vector observations are available from HAB near analysis time and we select the one at the exact analysis time. At KNMI we run 3D-Var 8 times per day, i.e., in 3-hourly cycles. In 3D-Var we start the 18:00 UTC analysis from the 3-hr forecast from the previous analysis at 15:00 UTC, the so-called background or first-guess ( $\vec{X}_b$ ). The observation operator ( $H$ ) interpolates the model state to the observation ( $\vec{Y}$ ) location to yield the so-called innovation ( $\vec{Y} - H(\vec{X}_b)$ ), in short (O-B). The model analysis state ( $\vec{X}_a$ ) is then obtained from Eq 5.4, with  $K$  the Kalman gain matrix which determines the spatial structure of the increment ( $\vec{X}_a - \vec{X}_b$ ). Figure 5.10 shows the 2-dimensional increments of the zonal and meridional wind components

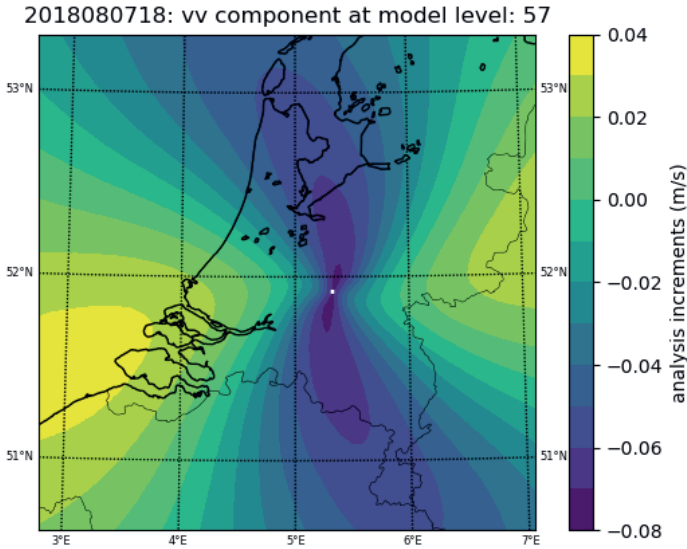


**Figure 5.11:** as the previous Figure, but now (A-B) for the v-component increment.

for the selected case, and the HAB wind vector observation at 18:00 UTC. It is good to note that the structure of the increment is mainly determined by the background error covariance matrix, which is part of the Kalman gain matrix. For single observation experiments, the increment structure is isotropic (concentric) by construction with the maximum amplitude at the location of the observation. Assimilation of the complete wind vector is not a single observation experiment, which explains the non-isotropic structures of the increments in Figure 5.10 and 5.11. From Figure 5.9, the background innovation ( $\vec{Y} - H(\vec{X}_b)$ ), for a single observation shortly denoted as (O-B), equals  $2 \text{ ms}^{-1}$  and  $-0.8 \text{ ms}^{-1}$  for the u and v wind component respectively. From Figure 5.10, and 5.11, the increment (A-B) at the observation location equals  $0.8 \text{ ms}^{-1}$  and  $-0.08 \text{ ms}^{-1}$  for the u and v wind component respectively. As a result, we can write for the analysis innovation, for a single observation shortly denoted as (O-A):  $\text{O-A} = (\text{O-B}) - (\text{A-B})$ . This equals  $1.2 \text{ ms}^{-1}$  and  $-0.72 \text{ ms}^{-1}$  for the u and v wind components, respectively, see also the red dots in Figure 5.9. In other words, assimilation of the HAB observation has drawn the model state toward the real atmospheric state, represented by the atmospheric observation.

The static nature of the used background error covariance matrix does not guarantee a similar positive effect on the model state away from the observation, in particular for complex atmospheric conditions as for this typical case. The use of additional observations along the balloon track can further improve the simulated atmospheric state. This requires the correct use of the observation time of the additional observations, in other words a four-dimensional variational (4D-Var) assimilation system. 4D-Var is currently in an experimental set-up, but not yet operational at KNMI.

## 5.7 Discussion

In this paper, we have seen that Hot-air Balloon (HAB) observations are an unique data source for sampling the ABL, in particular for the beginning of a nocturnal boundary-layer and to diagnose the initial conditions. However there are still some issues which have to be addressed. First of all the data set of HAB data is rather limited, but there are potentially more data available. Real time collection can be used if an appropriate infrastructure is available. Off line collection of data gives access to an abundance of data, because balloonists tend to store their flights. In the future also the meta data of the HAB should be collected, because this might be useful for the processing of the data. Knowledge of the call-sign of the HAB would give access to typical balloon parameters, like the volume, shape (balloon type) and mass.

HAB data can be collected using smartphones (De Bruijn et al., 2016), but alternatively transponders can also be applied. Currently more and more HABs are equipped with transponders, so that they are under surveillance of Air Traffic Control. These data are also used by [www.luchtballonradar.nl](http://www.luchtballonradar.nl), a website where HABs can be tracked real-time. Interestingly this website offers an archive for completed flights as well.

Another issue is on what scale is it still meaningful to assimilate information. What scales are observable and what scales are described by the model? The next step would be to assimilate all available HAB observations to improve the initial stages of typical ABL phenomena in the model. Depending on the atmospheric scales to adapt in the analysis one could choose to assimilate all HAB observations along a trajectory, but with reduced weight to avoid overfitting and the introduction of observed spatial scales in the analysis, which the model cannot resolve (Skamarock, 2004).

The high resolution HARMONIE-AROME is a promising model and offers numer-

ous opportunities for improvement. The asynchronous HAB observations will have probably more impact as soon as the 4D-Var assimilation will be available. The impact should also be considered relative to other observations.

In this study, the focus was on the validation of the +03h forecasts (First Guess). Clearly, HAB wind observations can also be applied for longer forecast periods and this is a subject for future research. It should be realized that verification in terms of RMSE is not sufficient to validate the high resolution model outcome. More advanced verification like neighborhood methods are necessary to reveal the benefit of the high resolution models and to mitigate the double penalty problem (Van der Plas et al., 2017).

## 5.8 Conclusions

This study shows that HAB flights provide valuable wind information in the ABL and are in agreement with other observations. In an area with a 30 km radius the HAB winds deviate only slightly from the high quality Cabauw wind mast observations during neutral-stable conditions. The standard deviations for HAB measured u and v wind components relative to those from the Cabauw mast are  $\sigma_u = 0.65 \text{ ms}^{-1}$  and  $\sigma_v = 0.69 \text{ ms}^{-1}$  respectively.

Comparison with the background state of the HARMONIE-AROME model revealed a standard deviation of  $2.5 \text{ ms}^{-1}$  for the wind vector error, which is in the same range as aircraft measurements and radiosondes. HAB flights could provide data from local flows which are interesting phenomena, especially when such phenomena are not captured by a NWP model or by the regular observational network.

We have shown that HAB observations can be ingested by the data assimilation module of HARMONIE-AROME and that they have the potential to push the NWP model in the right direction even in complex baroclinic conditions.

All in all, these crowd sourced observations are a welcome addition to the existing observation network and can be used for a better understanding and forecasting of the ABL and can be applied in NWP models.

## 5.9 acknowledgments

We would like to thank the balloonists Fred Kool and Martijn de Vries for sharing their data. The following KNMI colleagues Steven Knoop, Ad Stoffelen and Jan Barkmeijer are acknowledged for their contributions during the course of this research, which has been beneficial for this paper.



## Chapter 6

# Synthesis

## 6.1 This work

The Atmospheric Boundary Layer (ABL) is undersampled and this thesis reveals how this shortage of data can be mitigated. By means of Hot-air Balloon (HAB) flights, wind can be measured in the ABL and interesting flows can be observed. The wind observations can be used for the guidance of small aviation, air pollution, and wind turbine park applications. HAB observations can be applied at several stages of the NWP chain, for instance in data assimilation and verification, and it has the potential to evaluate the turbulence parameterizations in NWP models.

In Chapter 1 we have commenced with a historic overview of wind measurements, followed by the history of the HAB itself. Before taking off with the real science, we have presented some anecdotes and movies where HABs played a role. Subsequently, the buoyancy principle has been introduced, because this helps the understanding of why a HAB floats. Ballooning takes place in the ABL and some typical features which make the wind turn in height have been introduced. Finally, the research questions have been formulated.

In Chapter 2 we have studied the dynamics of a HAB and derived theoretically the response length of the HAB. We have studied the collected data based upon the navigational data of balloonists and discovered that HAB wind data reveal interesting meteorological features ranging from the meso- to the micro scale. Because the altitude is controlled by the pilot, only the horizontal wind components are considered in this study.

In Chapter 3 we have investigated whether smartphones and navigational instruments of pilots can be used to collect data. We have compared these data to a geodetic GNSS receiver and found that these devices are not very accurate in absolute positions. The standard deviations are  $\sigma_x = 5m$ ,  $\sigma_y = 5m$ ,  $\sigma_z = 12m$ , but the relative positions have a better accuracy. The horizontal speeds which are based on relative positions and a time step of  $1s$  have standard deviations of  $\sigma_u = 0.8ms^{-1}$ ,  $\sigma_v = 0.6ms^{-1}$ . We have found that the instrumental noise of smartphones is correlated and averaging in time reduces the standard deviation in the speed error less quickly than that would have been the case for uncorrelated noise. However, averaging wind speeds over longer time periods will inherently lead to smaller errors. For time scales beyond  $600s$  which is a typical time step of an NWP model, the  $\sigma_u$  and  $\sigma_v$  become smaller than  $0.03ms^{-1}$ . We have investigated the dynamics of the HAB pertaining to a step-wise change of the wind and found an empirical  $\alpha$ -coefficient that was in good agreement with the theoretical value. We have used a sonic anemometer and studied the behavior of the relative flow around

a HAB. We have also discovered a systematic relative movement that is explained by noting that the momentum exchange over the balloon's vertical dimension differs from the exchange in the surrounding air and we called this effect the inertial drift.

In Chapter 4 we have used another upper air observation instrument for validation, namely using the RASS wind profiler, which was located at Cabauw. So far, all collected flights were situated over flat terrain in the Netherlands. Driven by curiosity, we studied also flights that took place in Austria. We discovered very interesting patterns and we reported about a mountain valley circulation where the valley wind was completely decoupled from the synoptic scale forcing aloft. Subsequently, we validated HAB data with HIRLAM for two years and the errors were small enough for application in the data assimilation module of the HIRLAM model. We went a step further by performing data assimilation and a small local positive impact on the forecast was found. A key element in the set-up was that the hydrostatic HIRLAM was implemented in a rapid update cycling method. We have used hindcasts, but in an operational application, the timely availability of the new observation type is crucial for a successful application.

In Chapter 5 we have validated the HAB data directly with the wind observations at Cabauw during the summer season of 2018. It was found that in an area with a 30 km radius centered at Cabauw, the HAB winds deviated slightly from the high-quality Cabauw wind mast observations. The standard deviations for HAB measured u and v wind components relative to those from the Cabauw mast were  $\sigma_u = 0.65ms^{-1}$  and  $\sigma_v = 0.69ms^{-1}$  respectively. These positive results encouraged us to take the next step by applying HAB observations in the non-hydrostatic HARMONIE-AROME. We have created first-guess statistics and found a standard deviation of  $2.5 ms^{-1}$  for the wind vector error, which is in the same range as aircraft measurements and radiosondes. Data assimilation in a mesoscale model is a difficult task and we have made a start by studying the impact of the analysis increments of a single observation. We have chosen a case study with baroclinic conditions and a small impact was found.

## 6.2 Answers to research questions

In Chapter 1 research questions were posed and finalizing this thesis, it is now time to answer them:

1. Are HAB-winds a pie-in-the-sky conjecture or a novel method for ABL wind retrieval? *It is a novel method for wind retrieval and can be carried out by third parties, including citizen science.*
2. What makes the HAB wind measurements so unique? *They are opportunistic observations, based on a recreational activity and they are virtually for free. The measurement principle is straightforward and similar to the radiosonde. For this research, very little data has been used which resulted eventually in at least three peer-reviewed papers.*
3. What correction is necessary to account for the balloon's inertia? *The GNSS data have noise and averaging is necessary. The averaging time is 300 s which coincides with the response time of the HAB as proposed in Chapter 2.*
4. Can smartphones be used to collect the data? *Smartphones are not very precise in positions, but the relative positions are good enough for wind measurements (Chapter 3). However, a software application (app) should be developed and become available in a general repository.*
5. What is a typical error in the wind of a HAB? *Compared to Cabauw mast observation the standard deviation is  $0.6 \text{ m}^{-1}$ . If we apply first guess statistics, it is  $2.3 \text{ ms}^{-1}$  for the hydrostatic HIRLAM and  $2.5 \text{ ms}^{-1}$  for the non-hydrostatic HARMONIE-AROME.*
6. What kind of devices do you need to obtain the measurements? *Off-the-shelf smartphones can be used as well as transponders which allows tracking from ATC. Also, position data from commercial navigators for balloonists contains a lot of data. (Chapter 3).*
7. Can HAB observations be applied in NWP models? *They can be applied in data assimilation, in the development of parameterizations, and in calculating first guess statistics. (Chapters 4 and 5).*
8. What are typical circulations that are described by HABs? *Typical circulations are wind profiles with variations due to baroclinic effects, low-level jets, and mountain-valley circulations (Chapters 1 and 4).*
9. What is the recommended application of HAB winds? *The recommended*

*applications of HAB winds are ABL wind forecasts and guidance for small aviation, such as for pilots of HABs in particular.*

## 6.3 Outlook

In this study, the data predominately originate from the Netherlands, but in principle data can be collected from any place in the world. Hot-air ballooning is a leisure activity that takes place in the countryside and in the vicinity of urban areas. HAB flights happen when there are no strong up-and-down drafts. Moreover daylight is also a prerequisite, because with night vision, it is difficult to find a safe landing area. In practice, this means that flights take place just before dusk and just after dawn and also when the surface is covered with snow. It is evident that oceans and very remote places are not suitable for hot-air ballooning. The presence of road infrastructure is a relevant constraint because the recovery of the HAB, gondola, and passengers usually takes place by a pickup truck and a trailer.

For operational application, the HAB wind observations should be collected in a timely manner. There are two possibilities to achieve this. One option is the collection of data by smartphones from balloon pilots and/or from passengers on board a HAB. With a dedicated app, data can be collected and sent to a central data server (see Chapter 3). To encourage the people to take part, something should be given in return. One could think of trajectories on the basis of NWP output and tailor-made guidance for balloonists. In this way, a so-called win-win situation is created.

The other possibility is the collection of data via Air Traffic Control (ATC). This method can be implemented fully automatically and does not depend on human interaction. Transponders can be installed in the gondola and some adjustments in the data registers must be made. The infrastructure is already present, but some modifications are necessary to achieve a successful data upload. Being under the surveillance of an ATC means extra safety for the balloon pilot. Collecting data also necessitates a need for automatic Quality Control (QC), which should be further developed. Automatic QC produces a set of high quality observations and ideally an observation is labeled with a quality flag and an adjustment is made to remove biases. The collected data should become available on a portal with easy access for everybody. In Chapter 5, we have reported about a website where HAB data can be found. It should be noted that in dealing with third party data there is a need for addressing the ownership of the data.

The major meteorological data centers are using 4D-VAR in a Rapid Update Cy-

cle (RUC) and then a-synchronous observations can be processed adequately. In this way, the First Guess (FG) does not deviate too much from the observation which makes the analysis increments more accurate. For a successful application in data assimilation, the observation error statistics should be derived. Observational errors are important for the weighing of observations in the data assimilation process. The assessment of observational error statistics requires a lot of data. It is recommended to collect more HAB data and this data can be either historic data from flights in the past or real-time collected data.

People sometimes argue that HAB flights only take place in favorable weather conditions. In this thesis, two examples are given in chapter 2 and 5 with adverse weather. In chapter 2, a passing front caused an accident and the HAB ended up in a ditch and in chapter 5 the HAB was able to land before the thunderstorm arrived. Due to commercial profit, pilots tend to take risks and sometimes fly on the edge. In their decision-making, they rely upon accurate weather information in combination with the guidance of duty forecasters. Especially, wind gusts can be troublesome when taking off and also the landing conditions should be favorable. Extreme wind gusts are typically very small scale and so the measurements performed at official weather stations alone are not sufficient. Additional weather observations from third parties including HAB wind data can complement the observations of the regular network to improve spatial-temporal resolution.

# References

- Baas, P., Bosveld, F. C., & Burgers, G. (2015). The impact of atmospheric stability on the near-surface wind over sea in storm conditions. *Journal of Wind Energy*, (pp. 1099–1824). doi:10.1002/we.1825.
- Baas, P., Bosveld, F. C., Klein Baltink, H., & Holtslag, A. A. M. (2009). A climatology of nocturnal low-level jets at Cabauw. *J. Appl. Meteor. Climatol.*, *48*, 1627–1642. doi:10.1175/2009JAMC1965.1.
- Banville, S., & van Diggelen, F. (2016). Precise position from a phone. *GPS world*, (pp. 43–48). doi:www.gpsworld.com.
- Batchelor, G. (1956). Introduction to Fluid Mechanics. *J. Fluid Mechanics*, *177*.
- Bauer, P., Thorpe, A., & Brunet, G. (2015). The quiet revolution of numerical weather prediction. *Nature*, *525*, 1476–4687. doi:10.1038/nature14956.
- Beare, R. J. (2008). The Role of Shear in the Morning Transition Boundary Layer. *Boundary-Layer Meteorology*, *129*, 395–410. doi:10.1007/s10546-008-9324-8.
- Beare, R. J., Edwards, J. M., & Lapworth, A. J. (2006). Simulation of the observed evening transition and nocturnal boundary layers: Large-eddy simulation. *Q.J.R. Meteorol. Soc.*, *132*, 81–99. doi:10.1256/qj.05.64.
- Bengtsson, L., Andrae, U., Aspelien, T., Batrak, Y., Calvo, J., & de Rooy et al, W. (2017). The HARMONIE–AROME Model Configuration in the ALADIN–HIRLAM NWP System. *Mon Wea Rev*, *145*, 1919–1935. doi:10.1175/MWR-D-16-0417.1.
- Bosveld, F. C. et al. (2014). The GABLS Third Intercomparison Case for Boundary Layer Model Evaluation Part B: Results and Process Understanding. *Boundary-Layer Meteorology*, *152*, 157–187. doi:10.1007/s10546-014-9919-1.
- Bosveld, F. C., Peter Baas, Anton C.M. Beljaars, and Jordi Vilà-Guerau de Arellano, A., & Bas J.H. van de Wiel (2020). Fifty Years of Atmospheric Boundary-

- Layer Research at Cabauw Serving Weather, Air Quality and Climate. *Boundary-Layer Meteorology*, . doi:10.1007/s10546-020-00541-w.
- Bowman, D., Norman, P. E., Pauken, M. T., Albert, S. A., Dexheimer, D., Yang, X., Krishnamoorthy, S., Komjathy, A., & Cutts, J. A. (2020). Multihour stratospheric flights with the heliotrope solar hot-air balloon. *J. Atmos. Oceanic Technol.*, *37*, 1051–1066. doi:10.1175/JTECH-D-19-0175.1.
- Businger, S., Johnson, R., & Talbot, R. (2006). Scientific insights from four generations of Lagrangian smart balloons in atmospheric research. *Bull. Amer. Meteor. Soc.*, *87*, 1539–1554. doi:10.1175/BAMS-87-11-1539.
- Buys-Ballot, C. (1857). Note sur le rapport de l'intensité et de la direction du vent avec les écarts simultanés du baromètre. *Comptes rendus hebdomadaires, TOME XLV*, 765–768.
- Canut, G., Couvreur, F., Lothon, M., Legain, D., Pignatelli, B., Lampert, A., Maurel, W., & Moulin, E. (2016). Turbulence fluxes and variances measured with a sonic anemometer mounted on a tethered balloon. *Atmos. Meas. Tech.*, *9*, 4375–4386. doi:10.5194/amt-9-4375-2016.
- De Bruijn, E. I. F., Bosveld, F. C., de Haan, S., & Heusinkveld, B. G. (2020). Measuring Low Altitude Wind with a Hot-Air Balloon and Their Validation with Cabauw Tower Observations. *J. Atmos. Oceanic Technol.*, *43*, 263–277. doi:10.1175/JTECH-D-19-0043.1.
- De Bruijn, E. I. F., Bosveld, F. C., de Haan, S., Wichers Schreur, B., & Holtslag, A. A. M. (2016). Observing Boundary Layer Wind from Hot-air Balloon Flights. *Wea. Forecasting*, *31*, 1451–1463. doi:10.1175/WAF-D-16-0028.1.
- De Haan, S. (2011). High-resolution wind and temperature observations from aircraft tracked by Mode-S air traffic control radar. *J. Geophys. Res.*, *116*, 2156–2202. doi:10.1029/2010JD015264.
- De Haan, S. (2016). Estimates of Mode-S EHS aircraft-derived wind observation errors using triple collocation. *Atmos. Meas. Tech.*, *9*, 4141–4150. doi:10.5194/amt-9-4141-2016.
- De Rooy, W., & de Vries, H. (2017). Harmonie verification and evaluation. *HIRLAM Technical report*, 70.
- De Vos, L. W., Droste, A. M., Zander, M. J., Overeem, A., Leijnse, H., Heusinkveld, B. G., Steeneveld, G. J., & Uijlenhoet, R. (2020). Hydrometeorological monitoring using opportunistic sensing networks in the Amsterdam metropolitan area. *Bulletin of the American Meteorological Society*, *101*, E167–E185. doi:10.1175/BAMS-D-19-0091.1.

- Doerenbecher, A., Basdevant, C., Drobinski, P., Durand, P., Fesquet, C., Bernard, F., Cocquerez, P., Verdier, N., & Vargas, A. (2016). Low-Atmosphere Drifting Balloons: Platforms for Environment Monitoring and Forecast Improvement. *B. Am. Meteorol.*, *97*, 1583–1599. doi:10.1175/BAMS-D-14-00182.1.
- FAA (2008). Balloon flying handbook. *U.S. Department of Transportation Federal Aviation Administration*, (pp. 1–252).
- Fathpour, N., Blackmore, L., Kurwata, Y., Assad, C., Wolf, M. T., Newman, C., Elfes, A., & Reh, K. (2014). Feasibility Studies on Guidance and Global Path Planning for Wind-Assisted Montgolfière in Titan. *IEEE Systems Journal*, *8*, 1112–1125. doi:10.1109/JSYST.2013.2282700.
- Galvin, J. (1999). Forecasting for hot-air balloons and airships in the Midlands of England. *Meteorological Applications*, *6*, 351–362. doi:10.1017/S1350482799001292.
- Garcia-Marti, I., Overeem, A., Noteboom, J. W., de Vos, L., de Haij, M., & Whan, K. (2022). From proof-of-concept to proof-of-value: Approaching third-party data to operational workflows of national meteorological services. *International Journal of Climatology*, (pp. 1–18). doi:10.1002/joc.7757.
- Goger, B., Rotach, M. W., Gohm, A., Fuhrer, O., Stiperski, I., & Albert A. M. Holt-slag (2018). The impact of Three-Dimensional Effects on the Simulation of Turbulence Kinetic Energy in a Major Alpine Valley. *Boundary-Layer Meteorol.*, *168*, 1–27. doi:10.1007/s10546-018-0341-y.
- Gustafsson, N. et al. (2018). Survey of data assimilation methods for convective-scale numerical weather prediction at operational centres. *Quarterly Journal of the Royal Meteorological Society*, *144*, 1218–1256. doi:10.1002/qj.3179.
- Holton, J. (1967). An introduction to dynamic meteorology. *Academic Press Inc.*, *23*, 1–391. doi:0-12-354360-6.
- Houchi, K., Stoffelen, A., Marseille, G., & de Kloe, J. (2015). Statistically Quality Control of High-Resolution Winds of Different Radiosonde Types for Climatology Analysis. *Journ. Atmos. Qcean. Tech.*, *32*, 1796–1811. doi:10.1175/JTECH-D-00160.1.
- Ingleby, B., & Edwards, D. (2018). Radiosonde descent reports look promising. *ECMWF newsletter*, *157*.
- Intrieri, J., de Boer, G., Shupe, M., Spackman, J., Wang, J., Neiman, P., Wick, G., Hock, T., & Hood, R. (2014). Global Hawk dropsonde observations of the Arctic atmosphere obtained during Winter Storms and Pacific Atmospheric Rivers (WISPAR) field campaign. *Atmos. Meas. Tech.*, *7*, 3917–3926. doi:10.5194/amt-

- 7-3917-2014.
- Johnson, J. C. (1954). *Physical Meteorology*. Wiley and Sons, inc. and the Technology Press of M.I.T., (p. 393).
- Jonassen, M. O., Tisler, P., Altstädter, B., Scholtz, A., Vihma, T., Lampert, A., König-Langlo, G., & C.Lüpkes (2015). Application of remotely piloted aircraft systems in observing the atmospheric boundary layer over Antarctic sea ice. *Polar Res.*, *34*, 25651. doi:10.3402/polar.v34.25651.
- Knoop, S., Bosveld, F. C., de Haij, M. J., & Apituley, A. (2021). A 2-year intercomparison of continuous-wave focusing wind lidar and tall mast wind measurements at cabauw. *Atmospheric Measurement Techniques*, *14*, 2219–2235. doi:10.5194/amt-14-2219-2021.
- Kos, A., Tomažič, S., & Umek, A. (2016). Evaluation of Smartphone Inertial Sensor Performance for Cross-Platform Mobile Applications. *Sensors*, *16*. doi:10.3390/s16040477.
- Kristensen, L. (1998). Cup Anemometer Behavior in Turbulent Environments. *J. Atmos. Oceanic Technol.*, *15*, 05–17.
- Laakso, L., Grönholm, T., Kulmala, L., Haapanala, S., and E. R. Lovejoy, A. H., Kazil, J., Kurtén, T., Boy, M., Nilsson, E. D., and I. Riipinen, A. S., Stratmann, F., & Kulmala, M. (2007). Hot-air balloon as a platform for boundary layer profile measurements during particle formation. *Boreal Env. Res.*, *12*, 279–294.
- Lappin, F. M., Bell, T. M., Pillar-Little, E. A., & Chilson, P. B. (2022). Low-level buoyancy as a tool to understand boundary layer transitions. *Atmospheric Measurement Techniques*, *15*, 1185–1200. doi:10.5194/amt-15-1185-2022.
- Lean, P., Migliorini, S., & Kelly, G. (2015). Understanding atmospheric motion vector vertical representativity using a simulation study and first-guess departure statistics. *Journal of Applied Meteorology and Climatology*, *54*, 2479 – 2500. doi:10.1175/JAMC-D-15-0030.1.
- Lenderink, G., & Holtslag, A. A. M. (2004). An updated length-scale formulation for turbulent mixing in clear and cloudy boundary layers. *Quarterly Journal of the Royal Meteorological Society*, *130*, 3405–3427. doi:10.1256/qj.03.117.
- Lothon, M. et al. (2014). The BLLAST field experiment: Boundary-Layer Late Afternoon and Sunset Turbulence. *Atmos. Chem. Phys.*, *14*, 10931–10960. doi:10.5194/acp-14-10931-2014.
- Marseille, G., & Stoffelen, A. (2017). Toward Scatterometer Winds Assimilation in the Mesoscale HARMONIE Model. *IEEE*, *11*, 1796–1811. doi:10.1175/JTECH-D-00160.1.

- Mile, M., Randriamampianina, R., Marseille, G.-J., & Stoffelen, A. (2021). Supermodding – a special footprint operator for mesoscale data assimilation using scatterometer winds. *Quarterly Journal of the Royal Meteorological Society*, *147*, 1382–1402. doi:10.1002/qj.3979.
- Monin, A., & Obukhov, A. (1954). Basic laws of turbulent mixing in the atmosphere near the ground. *Trudy Geofiz Inst AN SSSR*, *24*, 163–187.
- Munson, B. R., Young, D. F., & Okiishi, T. (1990). Fundamentals of Fluid Mechanics. *Wiley*, .
- Nelder, J. A., & Mead, R. (1965). A Simplex Method for Function Minimization. *The Computer Journal*, *7*, 308–313. doi:10.1093/comjnl/7.4.308.
- Nielsen-Gammon, J. W., McNider, R. T., Angevine, W. M., White, A. B., & Knupp, K. (2007). Mesoscale model performance with assimilation of wind profiler data: Sensitivity to assimilation parameters and network configuration. *Journal of Geophysical Research: Atmospheres*, *112*. doi:10.1029/2006JD007633.
- Petäjä, T. et al. (2012). In-situ observations of Eyjafjallajökull ash particles by hot-air balloon. *Atmospheric Environment*, *48*, 1359–2310. doi:10.1016/j.atmosenv.2011.08.046.
- Petersen, R. A. (2016). On the impact and benefits of amdar observations in operational forecasting—part i: A review of the impact of automated aircraft wind and temperature reports. *Bulletin of the American Meteorological Society*, *97*, 585 – 602. doi:10.1175/BAMS-D-14-00055.1.
- Petterson, S. (1956). Weather Analysis and Forecasting, Motion and Motion Systems. *McGraw-Hill*, *1*, 428.
- Rautenberg, A., Graf, M. S., Wildmann, N., Platis, A., & Bange, J. (2018). Reviewing wind measurement approaches for fixed-wing unmanned aircraft. *Atmosphere*, *9*. doi:10.3390/atmos9110422.
- Rennie, M., Isaksen, L., Weiler, F., de Kloe, J., Kanits, T., & Reitenbuch, O. (2021). The impact of aeolus wind retrievals on ecmwf global weather forecasts. *132*, (pp. 1–32). doi:10.1002/qj.4142.
- Schuler, T. K., Bowman, D. C., Izraelevitz, J. S., Sofge, D., & Thangavelautham, J. (2022). Long duration flights in venus’ atmosphere using passive solar hot air balloons. *Acta Astronautica*, *191*, 160–168. doi:10.1016/j.actaastro.2021.10.030.
- Seity, Y., Brousseau, P., Malardel, S., Hello, G., Bénard, P., Bouttier, F., Lac, C., & Masson, V. (2011). The AROME-France Convective-Scale Operational model. *Mon. Wea. Rev.*, *139*, 976–991. doi:10.1175/2010MWR3425.1.

- Siebesma, A. P., Soares, P. M. M., & Teixeira, J. (2007). A combined eddy-diffusivity mass-flux approach for the convective boundary layer. *Journal of the Atmospheric Sciences*, *64*, 1230 – 1248. doi:10.1175/JAS3888.1.
- Skamarock, W. (2004). Evaluating mesoscale nwp models using kinetic energy spectra. *Monthly Weather Review*, *132*, 3019–3032. doi:10.1175/MWR2830.1.
- Strajnar, B., Žagar, N., & Berre, L. (2015). Impact of new aircraft observations mode-s mmar in a mesoscale nwp model. *Journal of Geophysical Research: Atmospheres*, *120*, 3920–3938. doi:10.1002/2014JD022654.
- Stull, R. (1988). An introduction to boundary layer meteorology. *Kluwer Acad. Publ.*, (p. 666).
- Sun, W., Liu, Z., Song, G., Zhao, Y., Guo, S., Shen, F., & Sun, X. (2022). Improving wind speed forecasts at wind turbine locations over Northern China through assimilating nacelle winds with WRFDA. *Wea. Forecasting*, . doi:10.1175/WAFD-21-0041.1.
- Sziroczak, D., Rohacs, D., & Rohacs, J. (2022). Review of using small uav based meteorological measurements for road weather management. *Progress in Aerospace Sciences*, *134*, 100859. doi:10.1016/j.paerosci.2022.100859.
- Undén, P., Rontu, L., Järvinen, H., Lynch, P., & Calvo-Sanchez, J. (2011). Coauthors, 2002: Hirlam-5 scientific documentation. *Swedish Meteorological and Hydrological Institute, Norrköping, Sweden*, .
- Van de Wiel, B. J. H., Moene, A. F., Steeneveld, G. J., Baas, P., Bosveld, F. C., & Holtslag, A. A. M. (2010). A conceptual view on inertial oscillations and nocturnal low-level jets. *67, 8*, 2679–2689. doi:10.1175/2010JAS3289.1.
- Van der Plas, E., M. Schmeits, E. Hooijman, & K. Kok (2017). A Comparative Verification of High-Resolution Precipitation Forecasts Using Model Output Statistics. *Monthly Weather Review*, *145*, 4037–4052. doi:10.1175/MWR-D-16-0256.1.
- Van Ulden, A. P., & Wieringa, J. (1996). Atmospheric Boundary Layer Research at Cabauw. *Boundary Layer Meteorology*, *78*.
- Voss, P. B., Hole, L. R., Helbling, E. F., & Roberts, T. G. (2013). Continuous in-situ soundings in the Arctic boundary layer: A new atmospheric measurement technique using controlled meteorological balloons. *J. Intell. Robotic Syst.*, *70*, 609–617. doi:10.1007/s10846-012-9758-6.
- World Meteorological Organization (2003). Aircraft Meteorological Data Relay (AMDAR) reference manual. *WMO-958*, (pp. 1–84). Available online at url: <http://www.wmo.int/pages/prog/www/GOS/ABO/AMDAR/publications/>

AMDAR-Reference-Manual-2003.pdf.

Zardi, D., & C.D. Whiteman (2013). Diurnal Mountain Wind Systems In: Chow F., De Wekker S., Snyder B. (eds) Mountain Weather Research and Forecasting. *Springer Atmospheric Sciences*, (pp. 35–119). doi:10.1007/978-94-007-4098-3.



# About the author

Evert Izaak Franciscus de Bruijn (Cisco) was born in Bennekom, the Netherlands on 30 september 1962. As a boy he was already interested in science, he was reading popular scientific magazines and started experimenting with kites and boomerangs. Later he got interested in sportive hobbies like ice skating and sailing. He was intrigued by how the weather could be predicted. In 1981 he finished Atheneum B at the Heldring College in Zetten. He studied hydrography at the Senior Nautical College in Amsterdam where he graduated in 1985 with a BSc degree. He started working at a private company as a hydrographic surveyor and also developed software. He was outsourced to dredging companies and worked offshore at the North Sea.

The author joined KNMI in 1987 and his first project was the development of the air mass transformation model. It consisted of an Atmospheric Boundary Layer (ABL) module, which was advected along predicted trajectories. It was implemented operationally and the model was documented in a scientific paper (Holtslag et al., 1990). Then, his topic became the development of NWP models. The author conducted research with high-resolution modeling, nesting strategy, horizontal diffusion and the validation of the model results. This research was conducted in the framework of his masters' thesis at the University of Utrecht where he graduated in 1997 with a MSc degree. More specifically a sea breeze circulation in the Netherlands and orographically forced rainfall in the Wicklow Mountains (Ireland) were studied. The latter subject was studied at Met Éireann (Dublin) where he had been seconded in 1998 to work on Quantitative Precipitation Forecasts with HIRLAM in the framework of the TELFLOOD project.

Subsequently, the author returned to Single Column Models (SCM). Instead of the advection along a predicted trajectory, the Eulerian approach was chosen, where a column was evaluated at a fixed position. This research was embedded in the GEWEX/GABLS project with the focus on the performance of ABL parameteri-

zations. Special attention was given to the dynamic tendencies and the validation with observations. With the SCM, process studies were conducted and in a later stage the SCM was evaluated with observations in the KNMI Parameterization Testbed. The author conducted research with a SCM version of the lake parameterization (FLake) within the HARMONIE model. He implemented a stand-alone one-dimensional (1D) version and ice thickness predictions were evaluated. The 1D FLake model was forced with observations and HARMONIE data and evaluated at Cabauw and at lake Sloten in the Netherlands.

After this, the author changed topic and his working field moved toward observations. Aircraft observations were assimilated in NWP models (HIRLAM, HARMONIE) and the impact was investigated. At that time, during a coffee break with Siebren de Haan, the idea of HAB wind measurements was born and this research was commenced, which resulted eventually in this PhD thesis.

---

## First author peer-reviewed journal publications

De Bruijn, E.I.F., Fred C. Bosveld, Siebren de Haan, Gert-Jan Marseille, Albert A.M. Holtslag (2022). Wind observations from Hot-air Balloons and their application in NWP models, submitted to *Meteo. Appl.*

De Bruijn, E.I.F. Fred C. Bosveld, Siebren de Haan, Albert A.M. Holtslag (2021). Opportunistic Sensing with Recreational Hot-Air Balloon Flights, *Bulletin of the American Meteorological Society*, 102(2), E273–E278, doi:10.1175/BAMS-D-19-0285.1

De Bruijn, E.I.F., Fred C. Bosveld, Siebren de Haan, Bert G. Heusinkveld (2020). Measuring Low Altitude Winds with a Hot-Air Balloon and Their Validation with Cabauw Tower observations, *J. Atmos. Oceanic Technol.*, (37(2)), 263–277, doi:10.1175/JTECH-D-19-0043.1

De Bruijn, E.I.F., Fred C. Bosveld, Siebren de Haan, Ben Wichers Schreur, Albert A.M. Holtslag (2016) Observing Boundary Layer Wind from Hot-air Balloon Flights, *Wea. Forecasting*, 31(5), 1451-1463, doi:10.1175/WAF-D-16-0028.1

De Bruijn, E.I.F., Bosveld, F.C., Van der Plas, E.V. (2014). An intercomparison study of ice thickness models in the Netherlands, *Tellus A, Series A: Dynamic Meteorology and Oceanography*, 66, 1, 21-44, doi:10.3402/tellusa.v66.21244

De Bruijn, E.I.F., De Rooy, W.C. (2012). Evaluation of HARMONIE in the KNMI Parameterisation Testbed, *Advances in Science and Research*, 8, 1, 167-170, doi:10.5194/asr-8-167-2012.

De Bruijn, E.I.F., Tijm, A.B.C., Steeneveld, G.J.(2006) Single-column modeling versus mesoscale modeling for an episode with three diurnal cycles in CASES99, *17th Symp. BLT, 27th AMS conference.*

De Bruijn, E.I.F., Brandsma, T. (2000). Rainfall prediction for a flooding event in Ireland caused by the remnants of Hurricane Charley, *Journal of Hydrology*, 239, 1-4, 148-161.

Cisco de Bruijn, Siebren de Haan, Peter Barlo, (2013,2). Windwaarnemingen uit ballonvaarten, *Meteorologica*, 24-29.

Cisco de Bruijn en Fred Bosveld, (2016,2), Een vergelijkende studie van ijs-groeimodellen in Nederland , *Meteorologica*, 18-20.

## Other peer-reviewed journal publications

Neggers, R.A.J., Ackerman, A.S., Angevine, W.M., Bazile, E., Beau, I., Blossey, P.N., Boutle, I.A., de Bruijn, C., Cheng, A., van der Dussen, J., Fletcher, J., Dal Gesso, S., Jam, A. Kawai, H., Cheedela, S.K., Larson, V.E. Lefebvre, M.-P., Lock, A.P., Meyer, N.R., de Roode, S.R., de Rooy, W., Sandu, I., Xiao, Xu, K.-M. (2017) Single-Column Model Simulations of Subtropical Marine Boundary-Layer Cloud Transitions Under Weakening Inversions, *Journal of Advances in Modeling Earth Systems*, 9,6, 2385-2412, doi:10.1002/2017MS001064

Bosveld, F.C., Baas, P., Steeneveld, G.-J., Holtslag, A.A.M., Angevine, W.M., Bazile, E., de Bruijn, E.I.F., Deacu, D., Edwards, J.M., Ek, M., Larson, V.E., Pleim, J.E., Raschendorfer, M., Svensson, G. (2014). The Third GABLS Intercomparison Case for Evaluation Studies of Boundary-Layer Models. Part B: Results and Process Understanding, *Boundary-Layer Meteorology*, 152,2,157-187, doi:10.1007/s10546-014-9919-1

Bosveld, F.C., Baas, P., van Meijgaard, E., de Bruijn, E.I.F., Steeneveld, G.-J., Holtslag, A.A.M. (2014), The Third GABLS Intercomparison Case for Evaluation Studies of Boundary-Layer Models. Part A: Case Selection and Set-Up, *Boundary-Layer Meteorology*, 152, 2, 133-156, doi:10.1007/s10546-014-9917-3

Svensson, G., Holtslag, A.A.M., Kumar, V., Mauritsen, T., Steeneveld, G.J., Angevine, W.M., Bazile, E., Beljaars, A., De Bruijn, E.I.F., Cheng, A., Conangla, L., Cuxart, J., Ek, M., Falk, M.J., Freedman, F., Kitagawa, H., Larson, V.E., Lock, A., Mailhot, J., Masson, V., Park, S., Pleim, J., Söderberg, S., Weng, W., Zampieri, M. (2011). Evaluation of the diurnal cycle in the Atmospheric Boundary Layer over land as Represented by a Variety of Single-Column models: The second GABLS Experiment, *Boundary-Layer Meteorology*, 140,2, 177,206,1573-1472, doi:

Steenefeld, G.-J., Mauritsen, T., De Bruijn, E.I.F., Vilà-Guerau de Arellano, J. (2008). Evaluation of limited-area models for the representation of the diurnal cycle and contrasting nights in CASES-99, *Journal of Applied Meteorology and Climatology*, 47(3), 869-887, doi:https://doi.org/10.1175/2007JAMC1702.1

Steenefeld, G.J., Mauritsen, T., De Bruijn, E.I.F., Svensson, G., Holtslag, A.A.M. (2006) Mesoscale model intercomparison and observational evaluation for three contrasting diurnal cycles in CASES99: Focus on the stable boundary layer, *17th Symp. BLT, 27th AMS Conference*. 1007/s10546-011-9611-7

Holtslag, A.A.M., De Bruijn, E.I.F., Pan, H.-L.(1990). A high-resolution air mass transformation model for short-range weather forecasting, *Mon. Wea. Rev.*, 118, 8, 1561-1575.

## Presentations at conferences

- EMS2022 *Sensing the Wind with Hot-air Balloons and their Application in NWP Models*, Bonn [poster]
- EMS2019 *Opportunistic sensing with recreational hot-air balloon flights*, Copenhagen [poster]
- EMS2018 *New insights from an experimental hot-air balloon flight for measuring low level winds in the surroundings of Cabauw*, Budapest [oral, presented by Fred C. Bosveld]
- EMS2017 *Results from an experimental hot-air balloon flight for measuring low level winds in the surroundings of Cabauw*, Dublin [oral]
- AMS2016 22BLT *Wind measurements from hot-air balloon flights*, Salt Lake City [poster]
- EMS2015 *Assimilation of MODE-S EHS observations in HARMONIE*, Sofia [oral]
- EMS2015 *Wind measurements with smart-phones in the Atmospheric Boundary Layer*, Sofia [oral]
- EMS2014 *Sampling the atmospheric boundary layer on a moving platform; wind observations derived from hot air balloon flights*, Prague [oral]
- EMS2013 *Wind information derived from hot air balloon flights for use in short term wind forecasts: quality and first impact results*, Reading [oral]
- EMS2011 *Evaluation of HARMONIE using a Single Column Model in the KNMI Parameterisation Testbed*, Berlin [oral]

## Reviews

- Geoscientific Model Development
- Boreal Environment Research
- Journal of Atmospheric and Oceanic Technology

# Acknowledgments

This PhD research would not have been possible without the help and support of many people. But I would like to start thanking my employer, KNMI who has facilitated my research. My superiors Jolle Landman, Albert Kleintank, Gé Verver and Philippe Steeghs gave me time to conduct research and write up results in scientific papers. I have benefited from fruitful interactions with many people. I would like to thank Jan Barkmeijer (RDWK), Ben Wichers Schreur (RDWK), Gert-Jan Marseille (RDSW) and Lotte de Vos (WO) for their help and support. I am especially grateful to my co-promotors, Siebren de Haan and Fred Bosveld, for their invaluable assistance in addressing complex mathematical and physics challenges. Thanks a lot!

The balloonists Willem Hijink, Henri van Bommel and Peter Barlo are acknowledged for providing me with their navigational data during the initial stage of this research, which allowed me to work out my ideas. The pilots Fred Kool, Martijn de Vries and Peter Kelder provided me with data from 2018 for the comparison with the Cabauw tower and hereby I express my gratitude for that.

Chapters 4 and 5 of this work have been partly written during the COVID-19 lockdown period. The locations where I worked on those chapters varied within the borders of De Bilt, namely: KNMI headquarters, my home and the St. Michael church. During warm spells in the summer, I was happy to find refuge in the cooler St. Michael church. I would like to thank the Michael and Martha parish for the hospitality.

For the data analysis, I had to learn Python. I would like to thank Jos de Kloe, Ankie Pipers and Emiel van der Plas for their help and support. Gabriella De Martino (ex-KNMI) and Jessica Strickland are thanked for critical reading of the non-published parts of this work. During the lunch break at KNMI, I have spent many hours in running in the Beerschoten/Houdringe woods with my colleagues Theo Brandsma, Wim de Rooy, Jan Barkmeijer, Isabel Monteiro, Rudolf van

Westrhenen, Hylke de Vries and Thomas Reerink. I have also enjoyed playing badminton with KNMI/IMAU people, like Frank Selten, Richard Bintanja, Erik Tuenter, Michiel Baatsen, and Jan-Fokke Meirink. The sportive activities are a welcome break from brain work at the office.

Wageningen University & Research is thanked for providing staff and equipment which have been crucial for the field experiment with a hot-air balloon. I would like to thank Martin Sikma his valuable contribution to the field work and special thanks are devoted to Bert Heusinkveld, who risked his life while checking the sonic anemometer during the balloon flight (Figure 3.2). For the app development the contribution of the software engineers Jonatan Leloux (RDSW) and Werner Dierssen (ex-KNMI) is very much appreciated. Gert-Jan Steeneveld and Bert Holtslag (WUR) are thanked for encouraging me to write a BAMS paper, which has improved the outreach of my work.

I would like to express my sincere gratitude to my promotor Bert Holtslag, retired professor in meteorology at Wageningen University & Research, for his guidance, support and supervision throughout my PhD study. His stimulating ideas, positive attitude, and diplomatic and tactful approach were instrumental in helping me overcome various hurdles during the course of my research.

At last, I would like to thank my wife Gabriella and my three daughters Francesca, Roberta and Alessandra who have supported me during my PhD research. It all started with a hot-air balloon flight and they had the guts to take part and supported me throughout my research journey. Un grande bacio da papà.



This research was carried out in the framework of my job as a researcher at KNMI, De Bilt, the Netherlands. Financial support from Wageningen University for printing this thesis is gratefully acknowledged.

Cover design by ProefschriftMaken and Lidy Barendregt (photographer)



